



Design of High Speed Permanent Magnet Generator for Solar Co-Generation System Using Motor-CAD

By

Khurram Shahzad

Principal Supervisor: A/Prof. Youguang Guo

Co-Supervisor: Dr LiLi

External Supervisor: Prof. David Dorrell

Thesis submitted as a requirement for the degree of Master

Faculty of Engineering and Information Technology
School of Electrical, Mechanical and Mechatronic Systems

University of Technology Sydney (UTS)

May 2017

Certificate of Original Authorship:

I certify that the work in this thesis has not previously been submitted for a degree nor has it been submitted as part of requirements for a degree except as fully acknowledged within the text.

I also certify that the thesis has been written by me. Any help that I have received in my research work and the preparation of the thesis itself has been acknowledged. In addition, I certify that all information sources and literature used are indicated in the thesis.

Signature of Student:

Date: 13/11/2017

Acknowledgement:

I would first like to thank my thesis supervisors Prof. Dr David Dorrell, A/Prof. Dr Youguang Guo Dr LiLi of the Faculty of Engineering and Information Technology at University of Technology Sydney (UTS). The door to Prof. Dr David Dorrell and A/Prof. Dr Youguang Guo office was always open whenever I ran into a trouble spot or had a question about my research or writing. They consistently allowed this study to be my own work, but steered me in the right direction whenever they thought I needed it.

I would also like to thank the experts who were involved in selecting machine's material for this research project: Special thanks to Mr. Hideki Ichinose from JFE steel corporation Tokyo, Japan. Without their passionate participation and input, the material selection could not have been successfully conducted.

I would also like to acknowledge Mr. Ahmad Salah of the FEIT at UTS as the second reader of this thesis, and I am gratefully indebted to his/her for his/her very valuable comments on this thesis.

Finally, I must express my very profound gratitude to my parents and to my wife for providing me with unfailing support and continuous encouragement throughout my years of study and through the process of researching and writing this thesis. This accomplishment would not have been possible without them. Thank you.

Author

Khurram Shahzad

Table of Contents:

Contents

CERTIFICATE OF ORIGINAL AUTHORSHIP:.....	2
ACKNOWLEDGEMENT:	3
TABLE OF CONTENTS:	4
LIST OF FIGURES.....	6
LIST OF TABLES	7
LIST OF SYMBOLS AND SPECIAL CHARACTERISTICS	8
ABSTRACT:.....	12
CHAPTER 1.....	13
1. INTRODUCTION.....	13
1.1. BACKGROUND.....	13
1.2. CONCEPT OF HIGH-SPEED BPMG.....	14
1.3. MOTIVATION AND OBJECTIVE	16
1.4. ORGANISATION OF THE THESIS	16
CHAPTER 2.....	17
2. LITERATURE REVIEW.....	17
CHAPTER 3.....	24
3. MACHINE DESIGN ANALYSIS.....	24
3.1. MACHINE SELECTION.....	24
3.2. ROTOR SELECTION.....	24
3.2.1. ROTOR MECHANICAL DESIGN.....	26
3.3. STATOR MECHANICAL DESIGN	27
3.4. SELECTION OF POLE NUMBERS.....	29
3.5. MAGNETIC DIMENSIONS	30
3.6. NUMBER OF PHASES.....	30
3.7. SLOTS PER POLE PER PHASE	31
3.8. STATOR WINDINGS	31
3.9. PERMANENT MAGNET MATERIAL SELECTION	35
3.10. STATOR AND ROTOR MATERIAL	37
3.11. MACHINE'S BASIC MODEL	40
3.11.1. WINDING RESISTANCE	40
3.11.2. WINDING AND MAGNET FACTOR.....	41

3.11.3.	VOLTAGE AND FLUX	42
3.11.4.	MACHINE INDUCTANCES	45
3.12.	BASIC LOSSES	47
3.12.1.	STATOR LOSSES	47
3.12.2.	ROTOR EDDY CURRENT LOSSES.....	49
3.12.3.	WINDING LOSSES	50
3.13.	MACHINE SIZING	51
CHAPTER 4.....		56
4.	FINITE ELEMENT ANALYSIS USING MOTOR-CAD	56
4.1.	MACHINE'S GEOMETRY.....	56
4.2.	MACHINE'S WINDING.....	57
4.2.1.	HARMONIC STUDY.....	59
4.3.	MATERIAL INPUT.....	61
4.4.	ELECTROMAGNETIC ANALYSIS OF MACHINE	64
4.4.1.	OPEN CIRCUIT ANALYSIS	66
4.4.2.	ON LOAD ANALYSIS	68
4.5.	HARMONIC ANALYSIS	70
4.6.	THERMAL ANALYSIS OF MACHINE	73
4.6.1.	HOUSING AND END-CAPS	73
4.6.2.	WINDING.....	74
4.6.3.	COOLING METHOD.....	76
4.6.4.	NATURAL CONVECTION.....	76
4.6.5.	LOSSES	76
4.6.6.	STEADY STATE THERMAL ANALYSIS	77
4.6.7.	TRANSIENT DUTY-CYCLE THERMAL ANALYSIS.....	78
4.6.8.	SLOT FINITE ELEMENT ANALYSIS (FEA)	79
4.7.	PERFORMANCE CHARTS.....	81
4.7.1.	FIXED INDUCTANCE MODEL.....	81
4.7.2.	EFFICIENCY MAPS.....	82
CHAPTER 5.....		85
5.1	CONCLUSION	85
5.1	FUTURE WORK	86
6	APPENDIX A.....	88
7	BIBLIOGRAPHY.....	113

List of figures

Figure 1 IPM and SPM.....	25
Figure 2 Radial VS axial flux rotors	25
Figure 3 Slotted vs Slot-less stators	28
Figure 4 stator slot geometry.....	28
Figure 5 winding layout	34
Figure 6 BH curve of different materials	35
Figure 7 6.5% SiFe BH curve	38
Figure 8 per phase model of the machine.....	40
Figure 9 wave symmetry of air-gap flux density	42
Figure 10 speed vs losses	47
Figure 11 vector diagram of voltage	54
Figure 12 radial and axial view of machine	56
Figure 13 3D view of machine	57
Figure 14 winding definition in stator slot.....	58
Figure 15 coil pattern of HSPM	58
Figure 16 winding mechanical harmonics.....	60
Figure 17 winding factor	61
Figure 18 BH curve of 6.5%SiFe	62
Figure 19 steel losses of 6.5% SiFe.....	62
Figure 20 Weight of different materials	63
Figure 21 Terminal voltage of the machine	64
Figure 22 Current of the machine.....	65
Figure 23 O.C flux linkage in machine	65
Figure 24 Cogging torque graph	66
Figure 25 O.C flux density	67
Figure 26 O.C losses in machine.....	67
Figure 27 phasor diagram.....	68
Figure 28 Back EMF	69
Figure 29 on load flux linkage	69
Figure 30 harmonic spectrum of torque	70
Figure 31 harmonic spectrum of cogging torque	71
Figure 32 speed vs torque.....	71

Figure 33 speed vs power	72
Figure 34 Radial & Axial thermal view	74
Figure 35 3D thermal view of the machine	74
Figure 36 thermal design winding.....	75
Figure 37 Steady state temperature	78
Figure 38 Thermal transient graph	78
Figure 39 2D FEA prediction of steady-state temperature in the stator slot.....	79
Figure 40 Axial view of steady-state temperature in the stator slot.....	80
Figure 41 Performance chart: torque vs speed	82
Figure 42 efficiency map of the machine	83
Figure 43 iron losses map.....	83

List of Tables

Table 1 Machines basic requirements	24
Table 2 slotted vs slottless stators	27
Table 3 winding pattern.....	34
Table 4 Magnetic properties of NdFeB and Sm-Co.....	37
Table 5 Features of 6.5SiFe.....	39
Table 6 Basic input parameters of the machine.....	51
Table 7 Basic output parameters of the machine.....	52
Table 8 detailed input parameters of the machine.....	52
Table 9 Detailed sizing parameters of the machine.....	55

List of symbols and special characteristics

V_{tip}	Tip speed
ω_m	Rotational speed
R	Radius
N	Speed (RPM)
p	Number of pole pairs
f	Electrical frequency (Hz)
K_{sn}	Skew factor
θ_s	Skew angle, radE
N	Harmonic number
B_g	Air gap flux density
h_m	Magnet height (mm)
g	Air gap (mm)
B_r	Magnet remnant flux density (T)
P	Real power (W)
Q	Reactive power (VAR)
q	Number of phases
V	RMS phase voltage (V)
I	RMS current (A)
m	Fractional number
($_$)	pitch of the winding
N_s	Number of slots
p	Pole pairs
q	Number of phases
K_d	Distribution factor
N_{spp}	Number of slots per pole per phase
N_m	Number of magnet poles
N_{ph}	Number of phase
R_{ro}	Rotor outside radius
R_{so}	Stator outside radius
Km	Motor constant
α_{sk}	Skew angle

R_a	Winding resistance
l	Length of conductor
σ	Winding conductivity
A_{ac}	Winding cross-sectional area
A_s	Area of slot
N_c	No of turns per coil
K_{wn}	Winding factor
K_{pn}	Pitch factor
K_{bn}	Breadth or distribution factor
n	Harmonic order
m	Slots per pole per phase
γ	Coil electrical angle
K_{gn}	Magnetic gap factor
R_s	Outer magnetic boundary
R_2	Outer boundary of magnet
R_i	Inner magnetic boundary
R_1	Inner boundary of magnet
K_L	Leakage factor
K_r	Reluctance factor
K_c	Carter's coefficient
W_s	Width of slot
W_t	Width of tooth
g_e	Effective air gap
PC	Permanent coefficient
$C\Phi$	Flux concentration factor (A_m/A_g)
μ_{rec}	Recoil permeability
Br	Remnant flux density
θ_m	Magnet physical angle
B_{flux}	Radial flux through coil
L_{ag}	Air gap inductance
Perm	Slot permeance
L_{as}	Slot self-inductance

L_{am}	Slot mutual inductance
L_{slot}	Slot leakage inductance
L_e	End turn inductance
L_s	Total inductance
X_s	Total reactance
ω_0	Angular frequency
P_{cu}	Core losses
m_1	Number of phases
I	Armature current
R	DC armature resistance
δ	Skin depth
ω	Angular frequency
P_{stray}	Stray losses
P_h	Hysteresis losses
η	Material constant
P_e	Eddy current losses
t	Thickness of the material
B	Peak flux density
ρ	Resistivity of the material
β	Geometric structure coefficient
P_{iron}	Iron losses
K_h	Coefficients of hysteresis loss
K_e	Coefficient of excess eddy current loss
E	Electric field
J	Eddy currents density
V	Volume of the material
μ	Kinematic viscosity of cooling media (m ² /s)
r	Radius of the rotor (m)
φ	Radial gap between rotor and stator (m)
λ	Length of the rotor (m)
τ	Shear stress (Psi)
K_z	Surface current density
B_g	Air-gap flux density

L_{st}	Stack length
N_c	Turns per coil
N_a	Assumes each coil has two half coils
ω_m	Mechanical frequency (rad/sec)
V_a	Terminal voltage

Abstract:

Permanent-magnet generators may be the most suitable choice for small co-generation systems due to a variety of merits. For instance, permanent-magnet generators are thermally optimised high-power density systems, which reduce the running costs by their performance and reliability. High-speed generators are currently being used in spindle drives, aircraft, power generation and electric vehicles. Distributed power generation has proven to be very effective and cost efficient in rural or remote areas as compared to building big power plants or long-distance transmission lines. The small distributed power co-generation unit using high speed permanent magnet generator is very efficient and cost-effective project. Moreover, high efficiencies i.e. over 90%, light-weight, low operating temperature, high insulation, no brushes/slip rings and almost negligible cogging torque make PMG's ideal for distributed co-generation systems.

In the past few years, most attention has been paid to “high speed brushless permanent magnet generators (HSBPMGs)”, for their many advantages i.e. substantial reduction in the size of the machine, higher efficiencies and power densities, etc. However, because of very high rotor speed and higher stator frequency, the design of HSBPMG is quite different from a conventional generator with low speed and low frequency. As speed increases, losses and temperature go up, so careful attention is needed while selecting the design parameters and material for the machine.

This study aimed to use basic design process for high speed brushless permanent magnet generators, keeping the losses minimum by using appropriate material and cooling method. All the design parameters calculated analytically, finite element analysis (FEA) is carried by using Motor-Cad simulation software, results obtained are compared and verified, and a prototype modelling of the machine is presented.

Chapter 1

1. Introduction

1.1. Background

Renewable energy is one of the alternative resource which offer the promise of clean, abundant energy gathered from self-renewing resources such as the sun, wind, earth, and plants. A fundamental issue in today's world is the supply of energy needed with shortages of conventional energy, such as coal and oil, predicted shortly in near future. In the same time, reduction of carbon intensity of energy is essential for dealing with climate change in the future. Renewable energy is an appropriate way to satisfy power consumption without environmental degradation.

Cogeneration innovative solar cogeneration technology, which captures and converts sunlight into both electricity and hot water, reduces greenhouse gas (GHG) emissions far faster than conventional solar energy systems, making it the clear choice for customers committed to environmental sustainability. This integration of photovoltaic (PV) and solar hot water (SHW) technology into one system makes solar cogeneration the most cost-effective solar energy solution available for commercial and industrial scale customers. According to 3rd party analysis conducted by Life Cycle Associates, LLC, Cogeneration approach achieves energy payback in less than 6 months, 3X to 4X faster than PV alone. It also delivers the greatest environmental benefits. Cogeneration approach offsets 2.6X more GHG emissions vs. a comparable PV system and at least 1.3X more GHG emissions vs. a comparable SHW system. Solar cogeneration achieves these dramatically higher GHG reductions because it delivers more total renewable energy than PV alone and more valuable renewable energy than SHW alone, from systems of the same area and size.

High cost of renewable power generation technologies is a significant barrier to the uptake of these technologies. Concentrated solar power (CSP) harnesses the sun's thermal energy to produce electricity. It has been deployed globally since the 1980's and is currently undergoing a resurgence, its potential to become a low-cost technology and reduce its levelized cost of electricity (LCOE) from around \$225/MWh currently to \$135/MWh by 2020. Improvements below \$100/MWh are technically feasible by moving to novel high temperature thermodynamic cycles and new low-cost approaches to field design. One effective approach is to reduce the cost of "power block" by designing high speed permanent magnet generator for the system.

As this study aim to reduce the cost as much as possible for a small solar co-generation plant, electrical generator design is needed which offers lower cost, light weight and higher efficiencies. After careful comparison, brushless permanent magnet (PM) generator was chosen as an optimised option as many factors are crucial for such a development for example.

- Cost competitiveness and availability of rare-earth magnets.
- Emergence of efficiency-driven applications.
- High power densities

The virtue of high power density becomes particularly important for applications where low volume/weight and high-speeds are significant. Undoubtedly, permanent magnet (PM) machines dominate the field of a small high-speed machine(Binder & Schneider 2007). This feature can be ascribed to their magnetic excitation—air-gap flux density is determined mainly by the quality of utilised permanent magnets and does not depend on the size of the PM machine. Current-excited machines, on the other hand, lack space for conductors in small volumes and thus have comparatively lower power densities. For the same power requirement, a high-frequency design reduces size and weight of an electrical machine. High-frequency also often means the elimination of power transmission elements. Thus, with downsizing and integration the resulting machinery becomes more efficient, lighter and even portable(Gieras 2008).

1.2. Concept of high-speed BPMG

Companies usually look for competitive designs, and they think it is straightforward and secure to use updated strategy. It should also be viewed that improving the style in this manner might not meet future market demand. End users are actively considering designs that guarantee them the highest production of power. In this situation, the entire converter idea using high-speed as well as using the lowest lifetime expenses permanent magnet machines provides a faster and easier method to enter the market. For example, creating a new high-speed complete converter generator is much simple compared to completely new construction required for the development of low- and medium-speed designs.

A literature review of PMG's shows an important consideration. The concept of smart grid energy system (SGES) is growing from past few years, especially on-site generation. Because of strict rules for environmental protection and higher capital cost due to increased size and fuel, larger power plants are not feasible in many regions of the world. On the contrary, technological development in small generators, power electronics and batteries has given new concepts in distributed energy resources.

Therefore, we need to put more efforts in the development of high-speed PM generators(Keyhani, Marwali & Dai 2009).

HSPMGs give a significant depletion in volume and mass, as compared to the other kind of generators and they have higher power density too. As the rotational speed of generator goes high, its size reduces alternatively for a required output power. As always size, weight and cost are the main factors for a good design. While designing HSPMGs, for an excellent performance and size, permanent magnet material has a vital role, so extra attention needs to be given to the material properties. Another critical parameter is, rotor aspect ratio or sometimes called length-to-diameter ratio is crucial. In case it is comparatively small, then the rotor has higher rigidity and good dynamics, while the diameter will be bigger, the weight goes high and makes magnet retention immensely hard. Moreover, the centre force on the magnets is also directly proportional to the rotor's diameter so rotor radius should not be high. PM machines give resilience in choosing pole sizes which permit for lower diameter size, so PM are ideal for high-speed applications, as they do not have rotor field winding. As a result, they may have a higher length-to-diameter ratio. As speed and frequency are high, stator core losses can be high, and also resistance and winding in the air can result in lower efficiency and heat production. Selecting the number of poles is another important parameter as it affects the electrical, magnetic, and structural performance. For example; electrical frequency, the voltage waveform, the magnetic flux, the magnet volume, the magnet pole pitch, the air gap size, and stator back iron thickness, So all these electromagnetic-design parameters need to be selected very carefully(El Shahat, Keyhani & El Shewy 2010b; Rucker, Kirtley & McCoy 2005).

HSPMGs have much smaller volumes of stator and rotor, because of that power density is much higher. This means that thermal design of PMSGs is also an important task as electromagnetic-design is. At high speed, the temperature is also high close to the critical temperature of some of some components such as permanent magnets, and their excessive heating can cause their demagnetization. And because the carbon fibre sleeve used to retain the magnets against the centrifugal forces is a bad thermal conductor, it makes the cooling even more challenging. The stator winding is also thermally sensitive and it needs careful attention. Concluding, in this study we need to carefully calculate all the required parameters initially, keeping in mind thermal sensitivity we will select an appropriate material for stator and rotor. A good design is not possible by just scaling down the machine and increasing its speed without a suitable cooling method.

1.3. Motivation and objective

Despite a lot of research, models have been developed and tested. Still, much work needs to be done primarily thermal analysis including designing an appropriate cooling system, selecting material, and all the critical parameters. The primary objective of this research is to calculate the design parameters and selection of material for high speed brushless permanent magnet generator keeping the losses minimised. The electromagnetic and thermal analysis will be carried by using Motor-Cad software. This study will put forward the comprehensive design methodology and will present the prototype of high-speed brushless permanent magnet generator suitable for the co-generation system.

1.4. Organisation of the thesis

This thesis is structured as below:

Chapter One: Chapter one provides an introduction to the research and the primary objectives of this research.

Chapter Two: A literature survey of high speed brushless permanent magnet machines is presented.

Chapter Three: Chapter 3 develops the idea for design guidelines and contains device design evaluation.

Chapter Four: This chapter provides Finite element analysis (FEA) using motor-Cad software by motor-design Ltd.

Chapter Five: This chapter presents a conclusion and summary of the thesis and some potential future works for this research.

Chapter 2

2. Literature review

HSPMGs offers light weight, high operational efficiency, lower maintenance costs and a smaller overall package than other counterparts for the same rated power. But, with all these advantages also comes higher power loss density. And a special consideration needed in the selection of lamination material, coil construction and cooling method. For HSPMGs, thermal sensitivity of the magnet material is an important factor. Because of that, samarium cobalt is commonly the better choice for higher temperature design.

2.1. Previous Research

R.A. Ahmed has designed HSPMG driven by a gas turbine, proposed HSPMG design and construction, system topology and evaluation is done. (Ahmad, Pan & Saban 2007).

S. Scridon designed, optimised and tested new generator, good power/volume and superior efficiency (up to 80%) are obtained at costs comparable to those of existing Lundell generator. The generator configuration, principle, equations, finite element, field analysis, design optimisation, performance characteristics and test results, together with the generating system simulations are given(Scridon et al. 2005).

A. Binder investigated that, during the design procedure of high-speed electrical machines, special attention needs to be paid to mechanical design. FE calculations for the mechanical strength of the rotor structure are recommended, for simple but realistic rotor structures, analytical approaches lead to satisfying results. This holds true both for surface mounted and specially selected buried-magnet-type rotors. The fixation of magnets in surface-mounted and buried magnet-type high-speed permanent-magnet machines is compared to the same motor data. Showing that for high-speed operation (e.g., 40,000 r/min, 40 kW), surface-mounted magnets fixed by a Carbon-fibre bandage are the better choice, as they incorporate much higher mechanical strength, allowing higher maximum speed(Binder, Schneider & Klohr 2006).

J.L.F. van der Veen demonstrated that the design of a high-speed 1400 kW synchronous generator with permanent magnet excitation and loaded by a rectifier, it became apparent that rotor losses are a major problem. An approximate solution for the rotor losses caused by the asynchronous field components has been derived. The formulae show the effects of machine dimensions and harmonics and the effect of a conducting shield in the rotor. The primary purpose of the study is to have a tool for making an early choice among several stator winding configurations. Also, verifying that it is possible to reduce the rotor losses to an acceptable level, e.g. 0.1 - 0.2% of the rated power. Consequently, the cooling of the rotor to an acceptable temperature level is feasible (Van der Veen, Offringa & Vandenput 1997).

S. R. Guda introduces modelling and simulation of a microturbine generation system suitable for isolated as well as grid-connected operation. The system comprises a permanent magnet synchronous generator driven by a micro turbine. A description of the overall system is given, and mathematical models for the micro turbine and permanent magnet synchronous generator are presented. Simulation results show that the developed model has can meet the requirements of the load. Simulation studies have been carried out in MATLAB/Simulink under different load conditions (Guda, Wang & Nehrir 2005).

S. M. Hosseini proposed the design, prototyping, and analysis of a relatively small and cheap axial-flux three-phase coreless permanent magnet generator. With the finite-element analysis, the parameters of the generator were calculated. The prototyped generator is relatively small and inexpensive (Hosseini, Agha-Mirsalim & Mirzaei 2008).

P.H. Mellor introduced a good idea about, a permanent machine with a hybrid rotor construction for an aircraft emergency generator application, designed to be capable of generating a constant 20 kW over a wide 3,000 to 36,000 rpm speed range. Initial testing of the prototype machine has indicated a performance close to the design requirements. A maximum generating system efficiency of 84% was obtained at the desired 20 kW output (accounting for the combined mechanical, electrical machine and power electronic losses) (Mellor et al. 2005).

M. Sadeghierad illustrated that, high – speed axial flux machine eligible for distributed generating application due to its compactness and lightness. Also, due to the high rotor speed and high frequency of the stator winding current, the design of a high-speed generator is much complicated and quite different from designing a low-speed conventional generator. The efficiency, total power, with some

critical design parameters, including magnet material (Br), air gap, and outer diameter of the machine were presented (Lesani, Monsef & Darabi 2007).

D. P. Arnold presented the design, fabrication, and characterization of permanent – magnet (PM) generators for use in micro-scale power generation systems. The generators are three phase axial-flux synchronous machines, each consisting of an eight, pole surface, wound stator and PM rotor. At a rotational speed of 120 000 rpm, one generator demonstrates 2.5 W of mechanical to electrical power conversion and, coupled to a transformer and rectifier, delivers 1.1 W of dc electrical power to a resistive load (Arnold et al. 2006).

A. Binder provided that, high–speed applications involve technical and economic advantages because, as direct drives; they avoid the gear as an additional mechanical drive component. Permanent magnet synchronous machines (PMSMs) are attracting growing attention for high-speed drives. The fixation of magnets in surface mounted and buried magnet type high-speed permanent magnet machines is compared to the same motor data. Showing that for high-speed operation (e.g., 40 000 r/min, 40 kW), surface mounted magnets fixed by a carbon-fibre bandage are the better choice, as they incorporate much higher mechanical strength, allowing higher maximum speed (Binder, Schneider & Klohr 2006).

During the design procedure of high-speed electrical machines, particular attention needs to be paid to mechanical design issues. **J. H. Paulides** introduced the influence of the choice of stator lamination material on the iron loss in a high speed, high power permanent magnet generator, which is interfaced to a DC link via a simple bridge rectifier. The potential benefit, regarding reduced iron loss, by employing 6.5% SiFe laminations in a representative high speed, high power permanent magnet generator, whose output is rectified by a simple bridge rectifier, has been quantified. The rating of the generator is representative of machines which would be employed in ‘more – electric’ ships and for embedded power generation (Paulides, Jewell & Howe 2004).

T. S. El – Hasan introduced a design methodology for a modular high-speed PM axial flux generator from first principles is illustrated with a case study on a 50 kVA, 420 V, 3 phase, 50 000 rpm PM generator. Optimisation of the design parameters is shown. In their paper, a good first degree of approximation is achieved by examining the variations of efficiency with different parameters. An efficiency of 92% in this advanced design considerably superior to conventional low-speed generators, has been reached where iron losses have been eliminated, and others have been minimised by proper selection of design parameters (El-Hasan et al. 2000).

S. M. Jang dealt with the rotor losses in the high-speed permanent magnet (PM) synchronous alternator for distributed power generation system. An optimum design of PM machines requires an accurate prediction of these rotor losses. By analytical field analysis and two - dimensional finite element analysis, this study predicts the flux harmonics and rotor losses in the PM alternator considering the rectifier load (Jang, Cho & Jeong 2006).

C. C. Hwang proposed a method effects as a tool in designing a high speed, surface permanent magnet generator with large air gap length. Alnico magnets are used for field excitation. Steady state performance is analysed by finite element (FE) method. Experimental tests are conducted to verify the FEM predictions (Hwang, Tien & Chang 2007).

Z. Kolondzovski purposed the thermal design of high-speed electrical machines because they have a greater challenge in comparison with conventional electrical machines. He deduced that, from the critical thermal operation analysis, it could be concluded that, the magnets cannot be efficiently cooled only by the air flow in the air gap if there is not a shield from eddy currents. Also, he aimed to perform thermal analysis for different rotor types according to the level of a protection from eddy currents to achieve a safe thermal design of the machine. The practical significance of the paper is beneficial for the designers of high-speed PM electrical machines (Wiak et al. 2008).

F. Sahin summarised the critical aspects concerning the design, manufacturing and testing of a high-speed axial flux permanent – magnet machine which will be applied in a hybrid electric vehicle application. Analysis of the losses and the thermal behaviour of the machine are included. Mechanical constraints and the aspects of manufacturing are also summarized (Sahin & Vandenput 2003). The outside diameter, inside-to-outside diameter ratio, the number of slots, magnet span, magnet skewing, and stator offsetting affect the performance of the machine to greater or lesser extents and need to be carefully chosen to obtain an optimal design. These choices are discussed in detail by **Vandenput** (Sahin & Vandenput 1999). **A. S. Nagorny** presented design considerations of a high speed, high efficiency, and permanent magnet synchronous machine for use as a flywheel motor/generator. The surface mounted magnet rotor topology shows a higher output power together with an acceptable back e.m.f total harmonic distortion level. The finite element method allows more detailed examination of the demagnetization of the permanent magnets due to the stator currents and provides more accuracy than the conventional method.

The ability of the SmCo permanent magnets to withstand the high-speed operation can be increased by segmenting the magnet pole. The parallel magnetic field orientation shows lower cogging torque level compared to the radial one (Nagorny et al. 2005). As discussed by several researchers, stator inner and outer diameters are the two most critical design parameters. Hence, for cases where the stator outer diameter is limited or imposed by the rest of the system, the ratio of inner to the outer diameter, K_r is the critical parameter to consider. It has a significant impact on the determination of the machine characteristics, such as torque, torque to weight ratio, iron losses, copper losses, and efficiency.

Caricchi shows the dependency on K_r for designs with various numbers of pole pairs. Other critical design parameters are the pole number, magnet thickness, conductor size, number of turns and material types. On the other hand, every design has its particular constraints, and they differ with the kind of application. One tries to obtain the maximum torque for a given motor diameter at a given speed. Mostly for small machines, the number of poles is limited due to the reduced space available for the windings. Nevertheless, the most restricting limitation for the number of poles is the motor operating speed. If the speed is high, a large number of poles will bring about an increase in the frequency, which directly leads to higher stator core losses and higher converter losses (Caricchi et al. 1996).

The volume, thickness, shape and type of the permanent magnets also affect both the Performance and the cost of the machine. The relationship between magnet volume and torque is explained in detail in (Binns & Shimmin 1996). In reference (Caricchi et al. 1996), a design based on the optimisation of the width of the permanent magnets for a surface-mounted permanent magnet type axial flux machine is explained. The choice of the permanent magnet width to pole pitch ratio is discussed. For higher values of this ratio, 1 for instance, flux linkage is maximum, but also flux leakage due to adjacent permanent magnets is high. By decreasing the permanent magnet width, linkage and leakage fluxes are both reduced though not proportionally.

Since the permanent magnets are the most expensive part of the machine, instead of Ne-Fe-B, ferrite magnets are used in some works. Also, ferrites having small conductivity do not suffer from eddy current problems which emerge in sintered rare-earth magnets (Jensen, Profumo & Lipo 1992). But, of course, ferrite has poor characteristics when compared with Ne-Fe- B, and its usage makes it impossible to obtain high air gap flux densities. Magnet protection must also be considered as a constraint together with the dimensional machine parameters (Slemon 1994).

Additionally, high temperature introduces additional constraints on the choice of the materials. Other limitations to be considered are mainly of mechanical nature. The centrifugal force acting on a rotating mass is proportional to the velocity squared and inversely proportional to the radius of rotation. Consequently, for high-speed applications (speeds more than 10000 rpm) the rotor must be designed with a small diameter to reduce tensile stress and must have a very high mechanical integrity (Gieras 2002).

Pillay presented a literature survey on PM AC motors and drives showing some aspects regarding design and control (Pillay & Freere 1989). A comparative study of different designs regarding dimensions and torque capability is presented in (Binns & Shimmin 1995). A general method for sizing of electric machines that highlights the need of relating the design to the type of converter used is shown in (Huang et al. 1998). Extensive aspects of PM machine technology and design of brushless dc machines are presented in (Hanselman 2003) and (Hendershot & Miller 2010).

El Shahat, introduce high-speed synchronous machine basic neural sizing function for renewable energy applications, and in the aircraft application. Also, he presents high fundamental frequency PM synchronous motor Design general neural regression function and spacecraft flywheel high-speed PM synchronous motor design for both classical sizing and genetic one (El Shahat & El Shewy, 2009b) (El Shahat & El Shewy 2009b) (El Shahat & El Shewy 2009a) (El Shahat & El Shewy 2010).

David Dorrell reviews many design issues and analysis techniques for the brushless permanent-magnet machine. He discusses the basic requirements for the use of both AC and DC machines and issues concerning the selection of pole number, winding layout, rotor topology, drive strategy, field weakening, and cooling. These are key issues in the design of a motor. Leading-edge design techniques are illustrated (Dorrell et al. 2011). Moreover, arrangements and connection requirements for a permanent-magnet generator are discussed. He demonstrates the importance of winding reactance minimization when using a diode bridge rectifier. Uses modern CAD methods to design a small PM generator and verifies the performance using simulation software. The design is modified to improve the generator size. This paper highlights that increasing the electrical loading in an attempt to reduce the generator size can lead to a significant reduction in power factor, where a controlled rectifier would have to be used instead of a diode bridge rectifier (Dorrell 2007).

Finally, extensive research has been done and is ongoing on high-speed technology; a lot of design topologies have been presented. Still, it is challenging to have more efficient and effective design

solution. Appropriate design of high-speed machines requires that multiple design problems be considered simultaneously. The performance of high-speed PM machines may be affected by mechanical and thermal limitations.

Arkkio has presented a design for high-speed permanent magnet synchronous machines in (Arkkio, Jokinen & Lantto 2005), but he has not done the rotor-dynamics analysis. An improved design methodology is given in (Kolondzovski et al. 2011) but lacks in thermal analysis. Although different design methodologies are presented in literature review, no one has given full integrative design process which constitutes electrical, mechanical and thermal analysis.

2.2. Research development

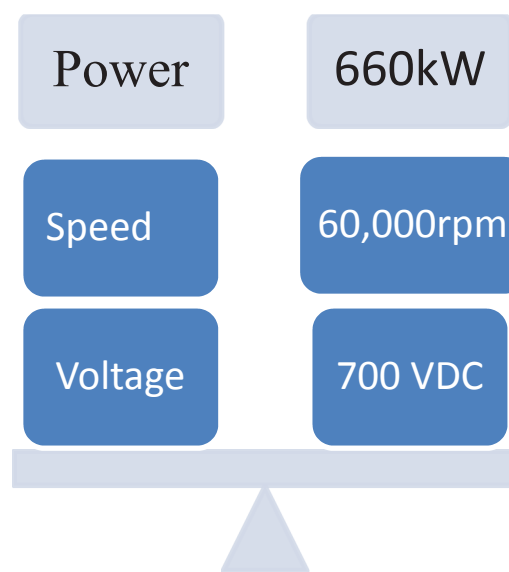
To minimize the different possible design choices, the design approach demonstrated in this study is elaborated for a particular sort of high-speed PM machine. Basic machines specifications are set to required power in 660kW; required speed is 60,000 rpm, and output voltage 700VDC. The geometry of the machine is set to 24 stator slots and two pole pairs, and 3-phase machine. The number of slots per pole per phase ($q = 2$). There are many options we can set for the rotor topology in Motor-CAD; we used U-shaped magnets with circular ducts in this design which helps to reduce the high temperature and losses. Tooth coil winding is used to get the shortest possible length of the machine; winding is set to double layer overlapping, and the number of turns per coil is 8 and 224 conductors per slot. Magnet material used in this design is 6.5%SiFe, which is excellent to reduce the iron losses and has a good operating temperature range. FEA is carried by using motor-CAD. Motor-CAD enables motor designers to optimise their designs for energy efficiency and size and cost reduction, providing the crucial link between the electromagnetic design and thermal analysis of motors. It makes it quick and straightforward for non-heat-transfer-specialists to evaluate different cooling options during the design process for a broad range of machines. Motor-CAD allows fast and easy steady state and transient thermal and e-magnetic analysis of the electric machines numerical and graphical results can be viewed. In thermal analysis, Water jackets are used in the housing for cooling windings are set to self-ventilate. The machine performance calculations and results are given.

Chapter 3

3. Machine Design Analysis

3.1. Machine selection

First, the power requirements need to be identified for a co-generation system, the overall power requirement is 660kW, and 60,000 rpm is selected for high-speed permanent magnet generator. The output voltage will be 700 VDC keeping the losses as minimal as possible. The following table lists the general requirement for the system.



Power	660kW
Speed	60,000rpm
Voltage	700 VDC

Table 1 Machines basic requirements

3.2. Rotor selection

Permanent magnet motors have two rotor PM topologies, namely, Interior permanent magnets (IPM) and surface mount permanent magnets (SPM). Both topologies are shown in the figure below. Comparison of both rotor topologies has been done in (Hwang et al. 2004) which indicates that the air-gap flux density and induced voltages in SPM topology are less sensitive to rotor's irregularity as compared to IPM. Secondly, the cogging torque increases in SPM with the increase of rotors eccentricity while in IPM it decreases; moreover, the peak-to-peak ripple torque is higher in IPM than SPM. Because of the many advantages of IPM over SPM, this topology is selected for HSPMG.

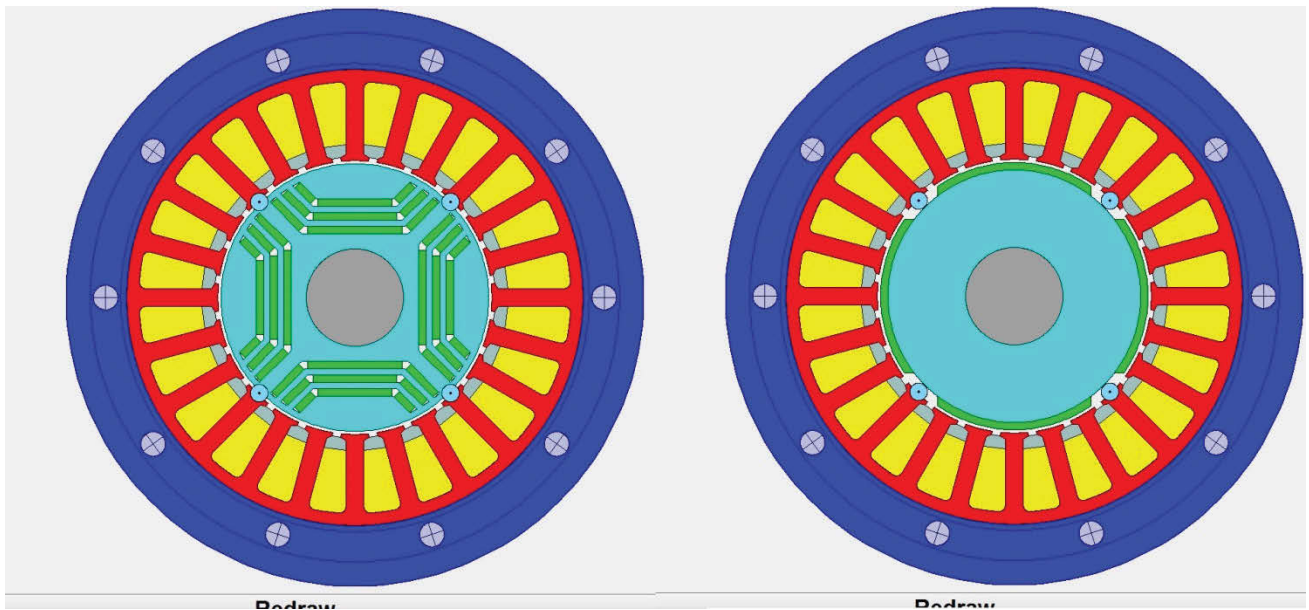


Figure 1 IPM and SPM

PM rotors can be classified by rotation of the flux, radial and axial flux. Axial flux machines have many advantages as they are low cost, flat shape and smooth rotation but at high speed, they have excessive eddy current losses and heating problem, also have complicated stator construction. So the best option is to use radial flux as they are capable of heat removal and proper cooling and high power and speed applicability(Sitapati & Krishnan 2001).

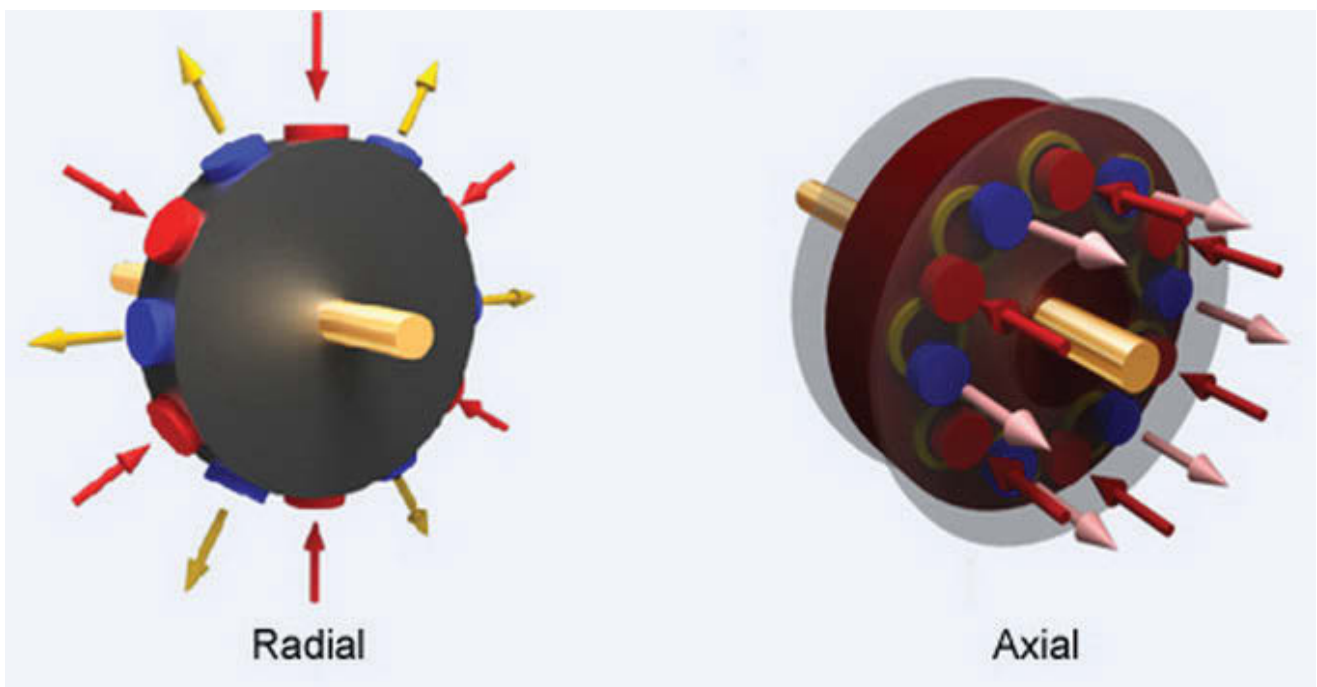


Figure 2 Radial VS axial flux rotors

In this design buried magnet topology or IPM is used rather than surface mounted topology. They have a number of benefits which make them suitable for higher speeds. For instance, in surface mounted flux cannot flow tangentially in magnets to give rotor-to-stator phase advance. In the contrast by using buried magnets topology as flux can flow tangentially significant amount of rotor-to-stator phase advance is achieved, also higher air-gap flux density is achieved which consequently increases the torque of the machine. The torque smoother, and the currents are more sinusoidal as compared to surface mounted topology(Kolehmainen & Ikaheimo 2008; Staunton et al. 2004). Interior U-shaped buried magnets topology is used in this design.

3.2.1. Rotor mechanical design

For high-speed applications, the rotor aspect ratio, defined as length-to-diameter (L/D), is a critical parameter. If it is relatively small, then the rotor has high stiffness and excellent dynamics but a large diameter which increases the weight and makes magnet retention tough. Additionally, the centrifugal force on the surface-mounted magnets is directly proportional to the rotor diameter so the rotor radial size must not be excessive(El Shahat, Keyhani & El Shewy 2010a; Rucker, Kirtley & McCoy 2005).

The PM machines have higher L/D ratio, so they are the best candidates for high-speed applications. The PM machines have a range of selecting the pole sizes, which are suitable for small diameters. A standard L/D ratio for a wound rotor machine is 0.5 – 1.0 compared to 1 – 3 for a PM machine(Bianchi & Lorenzoni 1996; Rucker, Kirtley & McCoy 2005). We will select L/D ratio here to be 2.51 for our design. The tip speed or sometimes called surface velocity of the rotor can be calculated by the rotor radius and the rotational speed as follows.

$$V_{tip} = R\omega_m \quad (3.1)$$

Where ω_m = rotational speed (rad/sec)

R = radius of rotor (m)

The tip speed upper limit lies in 100-250 m/s relying on the design of the machine. The tip speed in this design is taken as 50:200. At high-speed operation, the PM rotors can undergo through the centrifugal forces which may weaken their strength, to avoid the effect of these centrifugal forces, retaining sleeves may be used on the surface of the rotor.

3.3. Stator mechanical design

The stator is the narrative part of the high-speed PM generator as it contains the main structural component of the machine. It constitutes the housing of the machine, main winding and flux path for the magnetic circuit. There are two options to choose the stator, either to make it slotted or slot-less. Both topologies have their advantages and some drawbacks depending on the usage of the machine. The table below details the performance of the slotted and slotless stators.

Motor Size	Slotted design	Slot-less design
Axial length	52.7mm	56.2mm
Outer diameter	16.5mm	16mm
Performance parameters		
Max, No load speed	50,360rpm	45,100
Max, No load current	375 mA	165 mA
Torque constant k	4.63 mN-m/A	7.38 mN-m/A
Motor regulation	6.7 mN-m/sqr W	6.4 mN-m/sqr W
Performance parameters		
Thermal resistance	15.4 °C/W	18.5 °C/W
Thermal time constant	896 s	765 s

Table 2 slotted vs slot-less stators

Figure 3 below shows the slotted PM stator, with the presence of stator teeth which contains the field winding of the machine on the other hand slotless stator with no stator teeth has either skewed or axial winding fixed on the cylindrical stator core and provides the overall reduced size of the machine.

Slotted motors are suitable for high torque density and high acceleration, while slotless motors are optimum for smooth operation and excellent linearity when operating in a servo control system. Cogging torque will vary greatly with different motor designs, and steps are typically taken to minimise its impact, like skewing the magnet or stator laminations. Both technologies offer large through holes and can be designed for low profile direct drive applications. The key performance characteristics of each motor type are summarised in Table below (Celera Motion 2016)

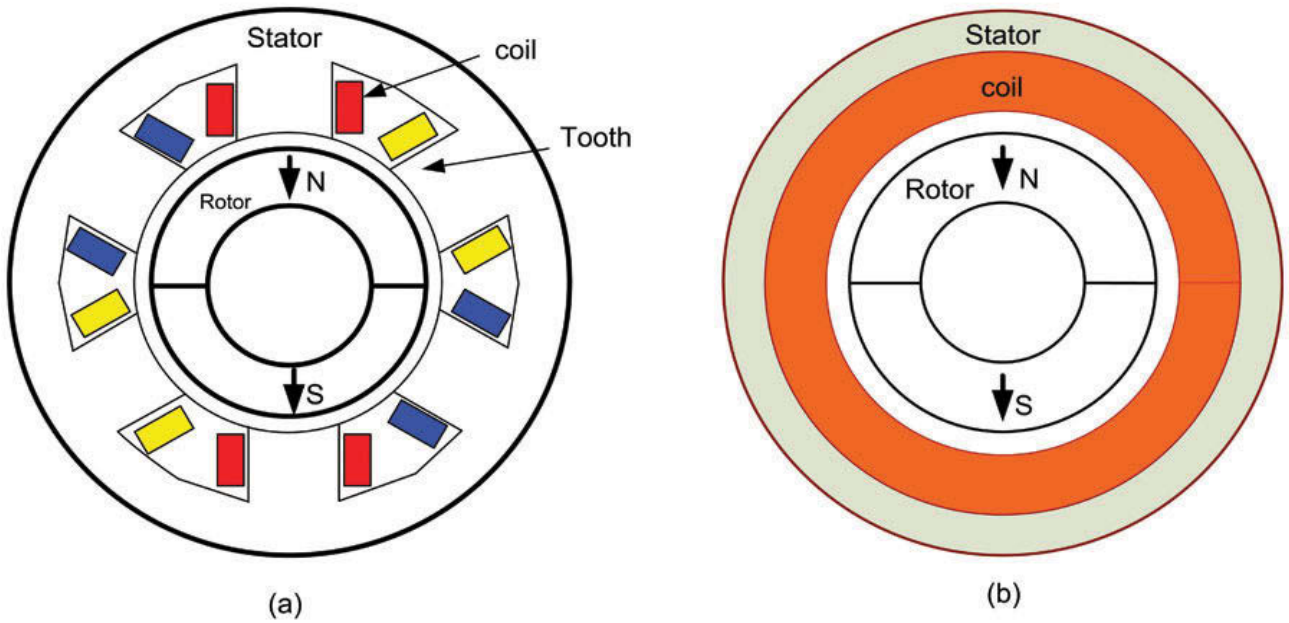


Figure 3 Slotted vs. Slot-less stators

The Stator may have different stator slot shape, which can be rectangular or trapezoidal. In this study, almost rectangular size is assumed as shown in the figure. It contains form-wound windings so that the depression width is same as the slot top width.

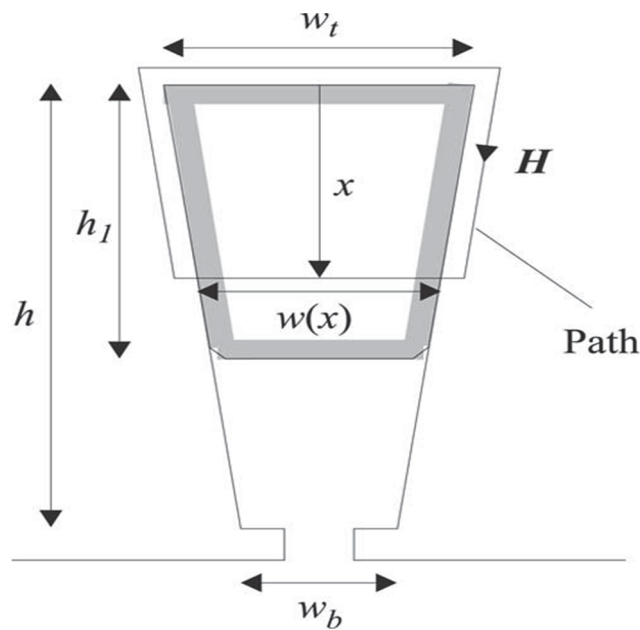


Figure 4 stator slot geometry

In summary, the slotted stators are good at higher acceleration as compared to the slot less stator which is not a good choice for the high-speed applications despite some advantages. Slotting helps to get a

narrow air-gap and keeps the main field winding conductors close to the field magnets to get maximum flux linkage also provides a limited thermal resistance which helps to get proper cooling of field windings. One drawback which slotted topology has, is the cogging torque can be high if the winding distribution is not properly implemented.

The number of phases and windings frequently determines the number of stator slots for a machine and can be different on the basis of the application. Initially, 3-phase and 24 slots machine design have been selected for this design, which can be varied later on depending on the required results.

3.4. Selection of pole numbers

The pole-pair number is a critical factor that affects the structure and performance of the machine. It depends on different parameters. Following equation is used to relate the speed and frequency to number of poles.

$$N \cdot (2p) = 120 \cdot f \quad (3.2)$$

Where N = speed (RPM),

p = number of pole pairs,

f = electrical frequency (Hz).

It can be seen that for higher pole numbers frequency will be high as a result there will be more stator losses. Also, the number of poles can be increased; the number of slots per pole per phase reduces and less sinusoidal voltage waveforms is produced. So the lower pole number is selected for this design. There are two choices either two poles or four poles, in two poles lower frequency is produced i.e. 1000Hz, so stator or copper losses might be reduced. But generator will be longer because of the long endings of the 2-pole stator windings. On contrast, 4 pole designs will be shorter in the axial direction (Fengxiang et al. 2002). For the optimum design, four poles or 2 pole pairs machine is selected for this design. So the frequency will be approx. 2000Hz with the rated speed of 60,000rpm.

Pole arc of the magnets can also be changed. The pole arc is reduced (up to 20 – 30%) and those areas are filled in with soft-iron pieces, the resulting flux waveform is more sinusoidal and has fewer harmonics and therefore lower rotor losses (George P. Gogue & Joseph J. Stupak).

Skewing of magnet poles can be done to reduce the cogging torque and to get off the ripples in air gap reluctance, flux and voltage waveforms. Skewing is done axially along the length of the rotor. A skew factor is used to calculate the effect of skewing which is given as.

$$K_{sn} = \frac{\sin(n\theta_s)}{\frac{\theta_s}{2}} \quad (3.3)$$

Where θ_s = skew angle, radE

N = harmonic number

3.5. Magnetic dimensions

Air gap and magnet height are two main magnetic dimensions which effect HSPMG design. These parameters help to determine the air-gap flux density, air-gap magnetic field and induced voltage of the machine. Air gap flux density can be calculated by the following equation.

$$B_g = \frac{h_m}{h_m + g} \cdot B_r \quad (3.4)$$

Where h_m = magnet height (mm),

g = air gap (mm),

B_r = magnet remnant flux density (T).

Air-gap flux density may be the minimum if the radial air-gap is kept as small as possible. Once the material is selected, using required air-gap flux density and induced voltage the magnet height can be calculated. Magnet losses may be reduced by using smaller magnets, i.e. small magnet height. To keep the magnetic field uniform, magnetic height is greater than the air gap by a ratio 5-10.

3.6. Number of phases

The number of phases can be determined by the following equation, and it affects machine's power, current and voltage ratings.

$$|P + jQ| = q \cdot V \cdot I \quad (3.5)$$

Where P = real power (W)

Q = reactive power (VAR)

q = number of phases

V = RMS phase voltage (V)

I = RMS current (A)

3 phase machine will be used because it is the most common form and mostly used in the industry also balanced torque is achieved in a 3-phase machine. Higher phases can be used if the generator is

connected to a DC bus distribution through power electronics module. But with the higher number of phases we get higher AC line current harmonics.

3.7. Slots per pole per phase

The slots per pole per phase are a very critical parameter and can be calculated by using the following equation. It determines the connection between rotor poles and stator winding also the figure the generated back voltage. When m is a fractional part, the machine is called fractional slot machine and when m is an integer machine is called integral slot machine. In an integral slot machine, winding coils back emf is in phase with each other, and the integer of all individual coil voltage gives the final voltage amplitude. On the other hand, in the fractional slot machine, back emf of all the coils is not in phase, and every coil voltage has the different amplitude.

$$m = \frac{N_s}{2 \cdot p \cdot q} \quad (3.6)$$

Where N_s = number of slots

p = pole pairs

q = number of phases

To get a sinusoidal voltage waveform and reduced machine harmonics the number of slots/pole/phase can be varied accordingly.

3.8. Stator windings

Faraday's law says voltage is induced in stator windings as the flux changes on PM rotor. To get the more sinusoidal voltage waveform winding arrangement is being used. Basically, windings can be distributed in three ways, pitch, skew, and breadth/distribution.

The pitch of the winding is defined as the angular distance (phase angle) between the edges of the coil; it is usually calculated in radians. If the phase angle of induced emf in two coil sides is less than 180 degrees, winding is short pitched. In full pitch winding phase angle is exactly 180 degrees.

We have an option to skew the stator winding along the length of the machine, but it will cause more complication in design, and overall size of the machine will be large. Skewing is not a very effective method to use in high-speed PM generator design.

If all the coil side of any one phase under one pole are bunched in one slot, the winding obtained is known as concentrated winding and the total emf induced is equal to the arithmetic sum of the emf's induced in all the coils of one phase under one pole. But in practical cases, for obtaining smooth sinusoidal voltage waveform, armature winding of alternator is not concentrated but distributed among the different slots to form polar groups under each pole (*Winding Factor | Pitch Factor | Distribution Factor*).

In distributed winding, coil sides per phase are displaced from each other by an angle equal to the angular displacement of the adjacent slots. Hence, the induced emf per coil side is not an angle equal to the angular displacement of the slots. So, the resultant emf of the winding is the phasor sum of the induced emf per coil side. As it is phasor sum, must be less than the arithmetic sum of these induced emf's. Resultant emf would be the arithmetic sum if the winding would have been a concentrated one. As per definition, distribution factor is a measure of resultant emf of a distributed winding in compared to a concentrated winding. It is expressed as the ratio of the phasor sum of the emf's induced in all the coils distributed in a number of slots under one pole to the arithmetic sum of the emf's induced (*concentrated winding*). Distribution factor is calculated as.

$$K_d = \frac{\text{emf induced in distributed winding}}{\text{emf induced if the winding would have been concentrated}} \quad (3.7)$$

$$K_d = \frac{\text{Phasor sum of component emfs}}{\text{Arithmetic sum of component emfs}} \quad (3.8)$$

There may be skin effect issue because of higher frequency, i.e., 2000 Hz. Eddy currents in stator winding cause skin effect which are reduced by using multi-strand wire instead of single conductor and selecting a good material which offers low losses.

There are two possibilities of stator winding pattern wye and delta patterns. The Y-connected pattern is preferred as it is safer and provides low losses. On the other hand in the delta pattern, the back EMFs produces circulating currents which cause losses, increased temperature or damage.

Since there are an infinite number of possibilities for pole and slot count combinations and winding layouts, assumptions are required to focus or limit the scope so that desirable windings can be found. The assumptions considered here are following (Hanselman 2003).

- a) The motor has three phases.
- b) All slots are filled. Therefore, the number of slots is a multiple of the number of phases, i.e., $N_s = kN_p$, so for 3-phase motors, the number of slots is always a multiple of three.
- c) There are two coil sides in each slot. That is, the winding can be classified as a double layer winding.
- d) Only balanced windings are considered. In other words, only pole and slot count combinations that result in the back EMF of phases B and C being 120° offset from the back EMF of phase A are considered.
- e) All coils have the same number of turns and all span the same number of slots. This implies that all coils are the same size and therefore have the same resistance and inductance.

Winding layout

The motor design presented contains the following information.

- The table identifies the number of magnet poles N_m the number of stator slots N_s used in the design, and the number of slots per pole per phase

$$N_{spp} = N_s / N_m / N_{ph} \quad (3.9)$$

- This table also contains important performance data. The ratio of the rotor outside radius to the stator outside radius R_{ro}/R_{so} identifies the rotor radius that maximises motor constant K_m which is calculated as follows.

$$K_m = T / \sqrt{I^2 R} \quad (3.10)$$

- Though not used in the design computations, the minimum skew required to eliminate cogging torque α_{sk} is given in terms of slot pitches.

$$\alpha_{sk} = \frac{N_s}{I_{cm}(N_s, N_m)} \quad (3.11)$$

- Finally, the first or fundamental harmonic index of the cogging torque n_{cog} , given by the smallest value of n that satisfies the following equation, describes the relative harmonic frequency of the cogging torque.

$$n = q \frac{I_{cm}(N_s, N_m)}{N_m} \quad (3.12)$$

We have here

$$N_s = 24, N_m = 4, N_{spp} = 2, Km = 0.7, \alpha_{sk} = 1$$

Coil No.	Coil Angle, °E	Phase A		Phase B		Phase C	
		In	Out	In	Out	In	Out
1	0	1	7	9	15	5	11
2	0	1	19	9	3	5	23
3	30	2	8	10	16	6	12
4	30	2	20	10	4	6	24
5	0	13	7	21	15	17	11
6	0	13	19	21	3	17	23
7	30	14	8	22	16	18	12
8	30	14	20	22	4	18	24

Table 3 winding pattern

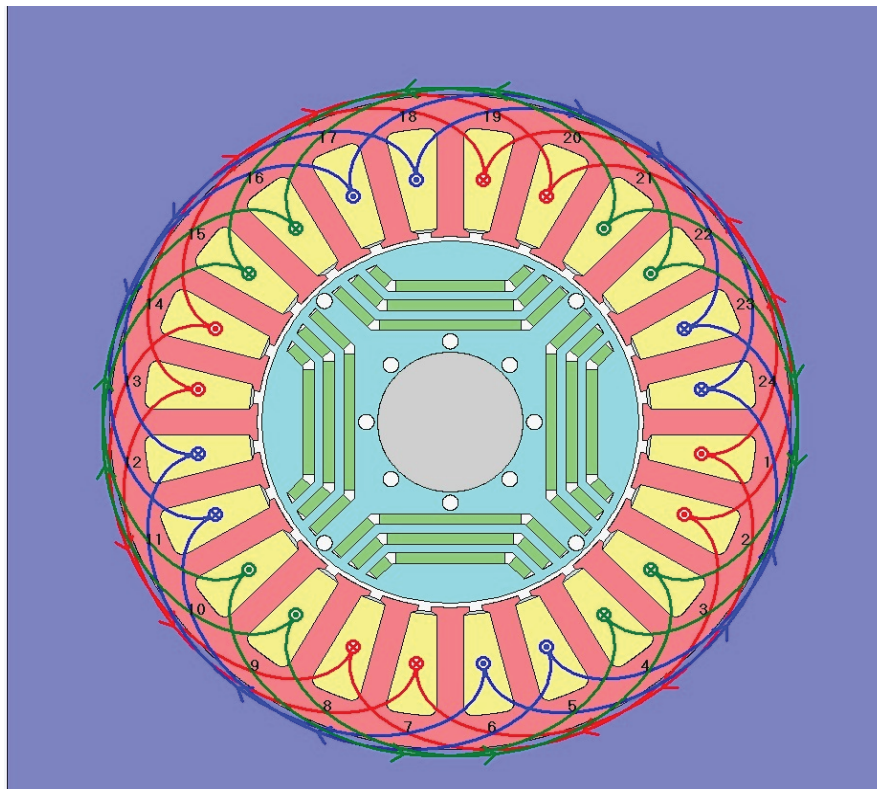


Figure 5 winding layout

3.9. Permanent magnet material selection

One of the primary factor while designing the electromagnetic, structural, and thermal parameters of PM machine is the choice of the magnet, the stator, and the rotor materials (Paulides, Jewell & Howe 2004; Rucker, Kirtley & McCoy 2005). Machine output, heat rise, weight, and cost are a few of the characteristics which are directly influenced by the selection of the machine materials(Rippy 2004; Rucker, Kirtley & McCoy 2005).

PM magnet material properties affect the size and performance of HSBPMG (Fengxiang et al. 2002). The magnets must be selected to provide the necessary air gap magnetic field and ample coercive force to compensate for possible damaging effects while minimising the volume of material because of cost and weight considerations (Pavlik et al. 1988).

Ferromagnetic materials are widely used in machines design, and their properties are described by BH curve and hysteresis loop. BH curve represents the relation between magnetic flux density (B) and magnetic flux strength (H) i.e. non-linear properties of different materials but ignores the multi-valued properties such as temperature, density, resistance, etc. (Hendershot & Miller 1994). BH curve is shown in the following figure.

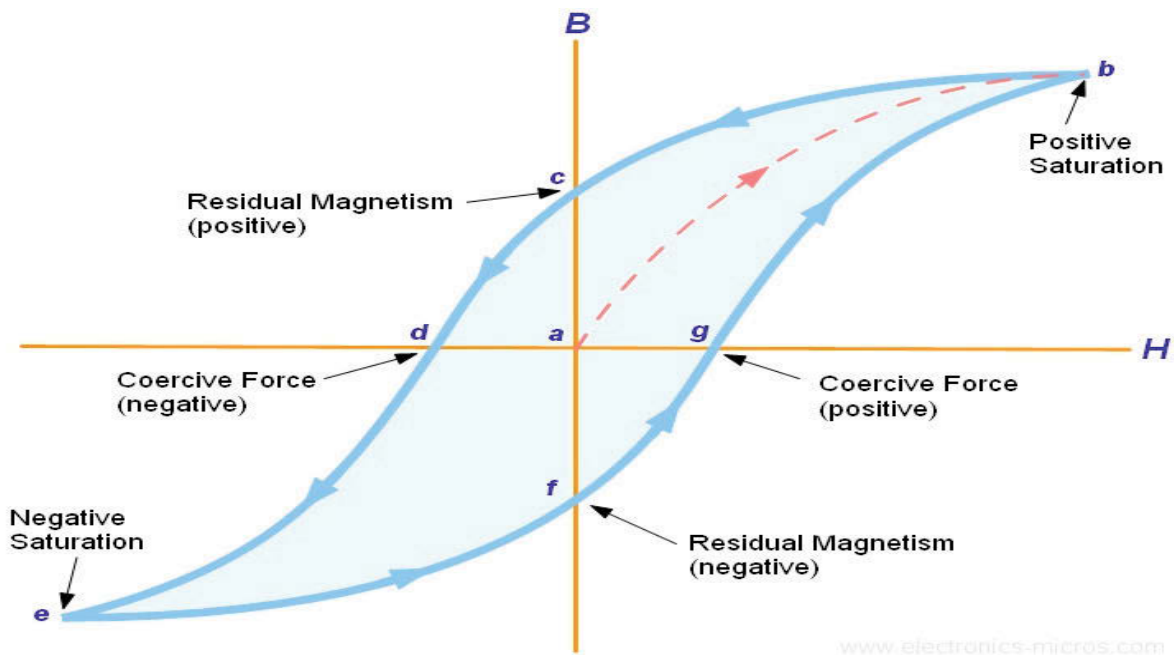
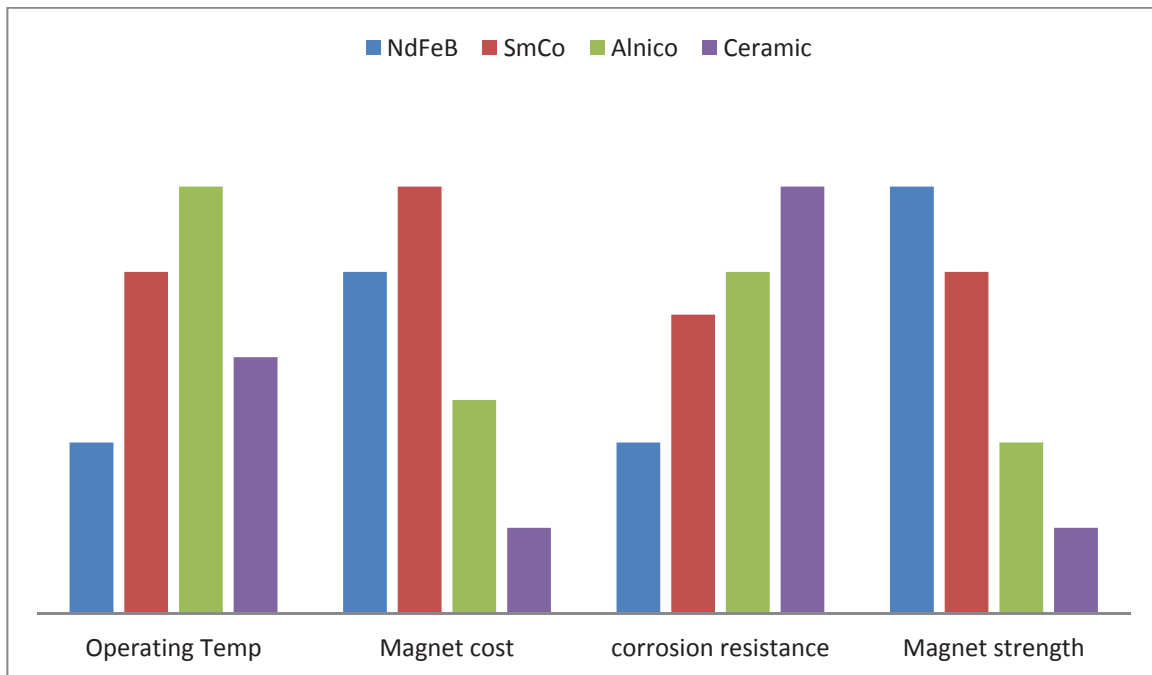


Figure 6 BH curve of different materials

The Chart below compares the various magnetic properties for some common, rare earth permanent magnet materials.



The rare-earth magnets, SmCo and NdFeB, have become more popular for high-performance applications because of their greater power density, high coercivity, high flux densities, and linearity of the demagnetization curves (Curiac, Jeong & Jung 2003; El Shahat, Keyhani & El Shewy 2010a).

Some of the critical properties of magnetic material are defined here

- **Remnant Flux Density (B_r):** It is the measurement of magnetic flux density which remains in magnets after successful magnetisation, and it can affect the air-gap flux and magnet sizes.
- **Coercivity (H_c):** it is the strength of the magnetic field which is required to reduce the magnetisation of the material to zero after the saturation of the magnetisation.
- **Energy Product (BH_{max}):** it is the density of the magnet's energy and is inversely proportional to the total magnet volume required.
- **Recoil Permeability (μ_{rec}):** The recoil permeability describes the steepness of the demagnetization curve in the B (H) description. It is the ability of the magnet to return to its initial state of magnetisation after subjected to different demagnetization forces. If BH value of the magnet goes below H_k , then magnet recoil along a lower line resulting lower flux density.

Property	NdFeB	Sm-Co
Remanence (T)	1–1.3	0.82–1.16
Coercivity (MA/m)	0.875–1.99	0.493–1.59
Relative permeability	1.05	1.05
Temperature coefficient of remanence (%/K)	–0.12	–0.03
Temperature coefficient of coercivity (%/K)	–0.55..–0.65	–0.15..–0.30
Curie temperature (°C)	320	800
Density (g/cm ³)	7.3–7.5	8.2–8.4
CTE, magnetising direction (1/K)	5.2×10^{-6}	5.2×10^{-6}
CTE, normal to magnetising direction (1/K)	-0.8×10^{-6}	11×10^{-6}
Flexural strength (N/mm ²)	250	150
Compressive strength (N/mm ²)	1100	800
Tensile strength (N/mm ²)	75	35
Vickers hardness (HV)	550–650	500–650
Electrical resistivity ($\Omega \cdot \text{cm}$)	$(110–170) \times 10^{-6}$	86×10^{-6}

Table 4 Magnetic properties of NdFeB and Sm-Co

NdFeB is the strongest magnets compared with other materials also lower in price and abundant as well so it is selected from two rare earth materials. It has some disadvantages as modest to corrosion and minor confrontation to effects of temperature; we can overcome this issue by using surface treatments and proper cooling method. In a nutshell, NdFeB is selected for use in high-speed PM generator design.

3.10. Stator and rotor material

Usually, the same material is used for stator and rotor cores, but we can choose any other economical material for both which is suitable for the flux guide minimum absorbance of MMF, so we get maximum flux in air-gap. Kind of material selected for rotor and stator of HSPMG is very critical as it affects the losses and overall efficiency of the machine. Selection of the material depends on the application of the machine plus cost, saturation flux, permeability and core losses. We need the material which offers minimum losses at high-speed operation to be selected for this design.

There are four main material types used to form high quality, non-oriented, electrical grade lamination steel for HSPMG i.e.

1. Low carbon steels
2. Silicon (Si) steels
3. Nickel (Ni) alloy steels
4. Cobalt (Co) alloy steels

Conventional silicon steel sheets have a Si (silicon) content of 3.5% or less. It has long been known that the magnetic characteristics of a silicon steel sheet improve as the Si content increases, peaking at 6.5%. However, it has been impractical to produce thin steel sheets with a Si content of over 3.5% because the steel tends to harden and become brittle. In 1993 JFE Steel solved this production problem through the adoption of a process called the CVD process and successfully introduced the first 6.5% Si steel sheets (JNEX-Core) to the world. To meet new demands, this technology has continued to be developed, leading to the commercial production of gradient high-silicon steel sheets with superior high-frequency characteristics (JNHF-Core) (Corporation). B/H curve of 6.5%SiFe is shown below in figure 7.

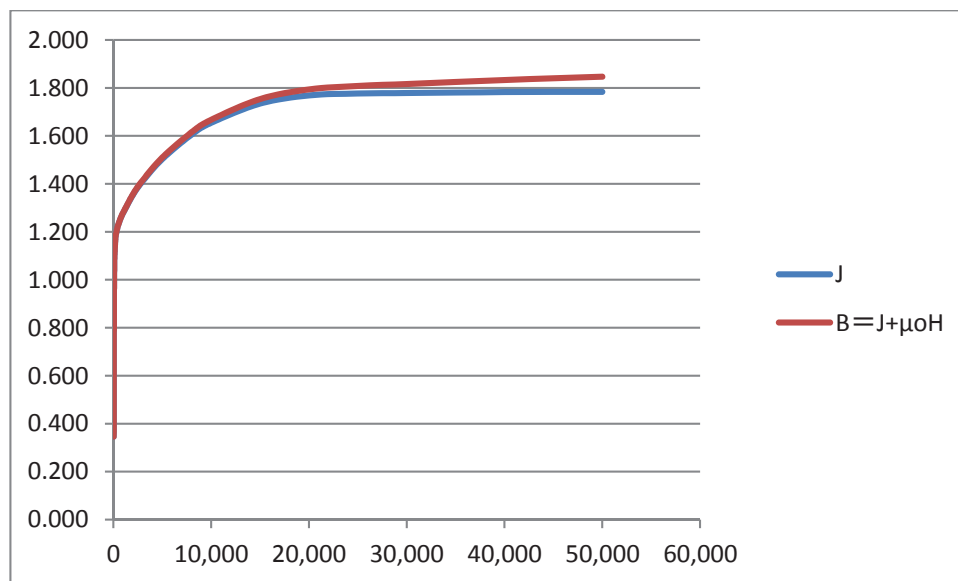


Figure 7 6.5% SiFe BH curve

JNEX-Core is the highest-grade non-oriented magnetic steel sheets manufactured with a production method (CVD process) that is completely different from that for conventional silicon steel sheets, allowing a previously impossible Si content of 6.5%. Potential benefits of using this material are discussed below. Some of the operating features are given in Table 5.

- **Low Core Loss**

Core loss in high-frequency ranges is extremely low. This allows for low heat generation and size reductions for magnetic components such as high-frequency reactors and transformers.

- **Magnetostriction Low Magnetostriction**

Magnetostriction which causes noise and vibration is nearly zero. This enables significant noise reductions for magnetic components such as reactors and transformers.

- **High Permeability**

The permeability is extremely high across a wide range of frequencies, making it highly suitable for use in shield applications and CT.

- **Stable Quality**

The high-temperature processing provides thermal stability. Since there is minimal deterioration of the properties due to machining, so stress-relieving anneals are not required.

- **Non-oriented**

There is virtually no difference in the characteristics between the rolling direction (L-direction) and the transverse (C-direction). Therefore, this can be used in a wide range of applications, from stationary machines to rolling machines.

Saturation flux density	1.6 Tesla.
Typical core loss	(50kHz, 100mT) 650 mW/cm ³ .
Curie temperature	700°C.
Operating temperature range	-30°C to 200°C.

Table 5 Features of 6.5SiFe

In summary, the potential benefit, in terms of reduced iron loss, by employing 6.5% SiFe laminations in a representative high speed, high power permanent magnet generator, whose output is rectified by a simple bridge rectifier, has been quantified. While it is shown that reducing the thickness of 3% SiFe laminations is highly beneficial, the adoption of 6.5% SiFe laminations results in a significant reduction in the iron loss as well (Paulides, Jewell & Howe 2004). Manufacturing process and other properties can be found in an appendix.

3.11. Machine's basic model

We can model our machine as a phasor circuit as follows. As the machine is assumed to be balanced so we can determine the parameters for one phase and apply to other two phases. The phasor diagram of the machine is shown in figure 8

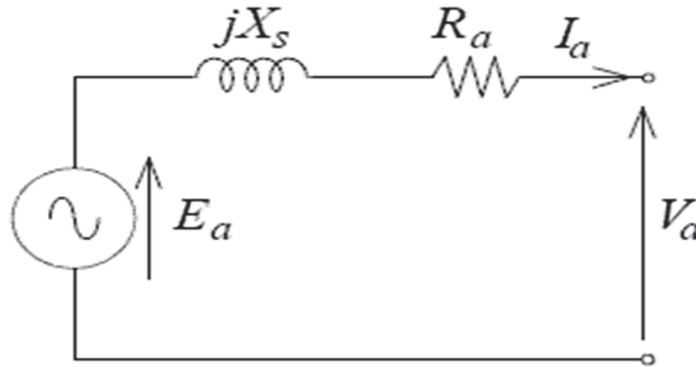


Figure 8 per phase model of the machine

Where R_a the winding's resistance which is usually very low, X_s is the inductance of winding includes slot leakage inductance, end turn inductance and air-gap inductance. E_a Is the back electromotive force (emf) produced because of flux linkage in the stator windings of the machine, and V_a is the terminal voltage of the machine; we need to calculate all these basic parameters.

3.11.1. Winding resistance

Winding resistance is caused by the copper material used for stator coils in the stator winding. Winding resistance can be calculated by using the following equation.

$$R_a = \frac{L}{\sigma A} \quad (3.13)$$

Where l = length of conductor

σ = winding conductivity

A = winding cross-sectional area

The length of the conductor is defined as the coil travels two times across the length of the machine and around the end turns. Here assumption has been made that end turns travel a circular path whose radius is almost equal to one-half the stator slot height.

The cross-sectional area of the winding is calculated through slot area, and slot fill factor and is shown in the following equation.

$$A_{ac} = \frac{A_s \cdot \lambda_s}{2 \cdot N_c} \quad (3.14)$$

Where A_s = area of slot

N_c = no of turns per coil

3.11.2. Winding and magnet factor

As ideally winding should be full pitch and concentrated but actually, this is not the case winding is short pitch instead and have breadth connected to it. This phenomenon is well described with the help of winding factor which is the ratio of flux linkage in a nutshell pitch (actual) winding, and full pitch concentrated winding. Winding factor is calculated as below.

$$K_{wn} = K_{pn} \cdot K_{bn} \quad (3.15)$$

Where K_{pn} = Pitch factor

K_{bn} = breadth or distribution factor

Pitch factor is defined as the ratio of flux produced by full pitch coil to the flux generated by the short pitch coil. The advantages of short pitch are reduced harmonics and improved power quality of the HSPMG. The formula of flux caused by the short pitch coil and full pitch coil determined the pitch factor and given as.

$$K_{pn} = \text{Sin} \left(\frac{n \cdot \alpha}{2} \right) \cdot \text{Sin} \left(\frac{n \cdot \pi}{2} \right) \quad (3.16)$$

Where n = harmonic order

As discussed earlier in section 3.8 the breadth factor is defined as it is the ratio of actual voltage gained if all the coils are under same phase belt to the possible voltage induced in distributed winding. Breadth factor can be calculated as below.

$$K_{bn} = \frac{\text{Sin} \left(\frac{n \cdot m \cdot \gamma}{2} \right)}{m \cdot \text{Sin} \left(\frac{n \cdot \gamma}{2} \right)} \quad (3.17)$$

Where n = harmonic number

m = slots per pole per phase

γ = coil electrical angle

Moreover, the geometry of the magnetic air gap is crucial along with other winding effects. The geometry of magnetic air gap can be expressed in terms of magnetic gap factor (K_{gn}). The equation of magnetic gap factor for the slotted stator, buried magnets configuration is shown in the equation below.

$$K_{gn} = \frac{R_i^{np-1}}{R_s^{2np} - R_i^{2np}} \cdot \left[\left(\frac{np}{np+1} \right) \cdot (R_2^{np+1} - R_1^{np+1}) + \frac{np}{np-1} \cdot R_s^{2np} \cdot (R_1^{1-np} - R_2^{1-np}) \right] \quad (3.18)$$

Where R_s = outer magnetic boundary

R_2 = outer boundary of magnet

R_i = inner magnetic boundary

R_1 = inner boundary of magnet

3.11.3. Voltage and flux

According to Faraday's law changing flux in machines winding induces significant voltages. To calculate the correct induced voltages, the air-gap flux density needs to be calculated in 1st step. There is a leakage flux in the machine which accounted as a leakage factor ($K_L \sim 0.95$). There is a small effect of the reluctance of the stator steel on air-gap which is accounted in terms of reluctance factor ($K_r \sim 1.05$). Carter's coefficient (K_c) is used to account the effect of the difference of permeance caused by the stator slots. As discussed earlier in equation 3.15 the geometry of magnetic air gap affects the air-gap flux density. As magnet poles are rotating north/south, air-gap flux density can be expressed in terms of Fourier series, considering only odd components because of half-wave symmetry shown in figure9 and calculated in equation 3.16 and 3.17.

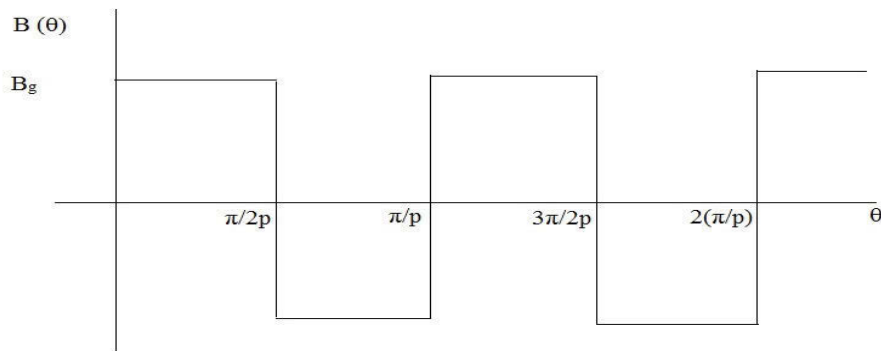


Figure 9 wave symmetry of air-gap flux density

$$K_c = \left[1 - \frac{1}{\frac{\tau_s}{W_s} \cdot \left(5 \cdot \frac{g}{W_s} + 1 \right)} \right]^{-1} \quad (3.19)$$

Where W_s = width of slot

W_t = width of tooth

$$\tau_s = W_s + W_t$$

$$g_e = K_c \cdot g \quad (3.20)$$

Where g_e = effective air gap

$$PC = \frac{h_m}{g_e \cdot C_\phi} \quad (3.21)$$

Where

PC = permanent coefficient

$C\Phi$ = flux concentration factor (Am/Ag)

$$B_g = \frac{K_1 \cdot C_\phi}{1 + K_r \cdot \frac{\mu_{rec}}{PC}} \cdot B_r \quad (3.22)$$

Where μ_{rec} = recoil permeability

B_r = remnant flux density

$$B(\theta) = \sum_{n=1}^{\infty} B_n \cdot \sin(np\theta) \quad (3.23)$$

Where

$$B_n = \frac{4}{n\pi} \cdot B_g \cdot k_{gn} \cdot \sin\left(\frac{np\theta_m}{2}\right) \cdot \sin\left(\frac{n\pi}{2}\right)$$

θ_m = Magnet physical angel

n = harmonic number

Once the flux density is calculated, the flux can be calculated in equation 3.24 for a full pitched coil which runs by an angle from 0 to π/p .

$$\phi = \int_0^{\frac{\pi}{p}} B_{flux} \cdot R_s \cdot L_{st} d\theta \quad (3.24)$$

Where B_{flux} = radial flux through coil

$$\phi_{pk} = \frac{2 \cdot R_s \cdot L_{st} \cdot B_{flux}}{p} \quad (3.25)$$

Back EMF is determined by using Faraday's law

$$\lambda(\theta) = \sum_{n=1}^{\infty} \lambda_n \cdot \sin(np\theta) \quad (3.26)$$

Where

$$\lambda_n = \frac{2 \cdot R_s \cdot L_{st} \cdot N_a \cdot B_n \cdot K_{wn} \cdot K_{sn}}{p}$$

$$Ea = \sum_{n=1}^{\infty} V_n \cdot \sin(np\theta) \quad (3.27)$$

Where

$$V_n = \frac{d}{dt} \lambda_n = \omega_0 \cdot \lambda_n$$

Here we need to choose the number of turns in stator winding very wisely so that the EMF obtained closely matches the nominal system voltage. We can use power electronics to get the system nominal voltage as well.

3.11.4. Machine inductances

There are mainly three types of inductances in machine given below.

- Air gap inductance,
- Slot leakage inductance,
- End-turn inductance.

These are accurately calculated by FEA; we will also have a look at analytical method to calculate them as given below.

Air-gap inductance constitutes the major portion of the machine inductances and is because of the correspondence of the air-gap flux linkage and stator windings. To calculate the air-gap inductance, air-gap flux density needs to be calculated firstly. Air gap flux density due to full pitch, concentrated winding carrying the current I , is given as.

$$B_{flux} = \sum_{n=1}^{\infty} B_n \cdot \sin(np\theta) \quad (3.28)$$

Where

$$B_n = \frac{4}{n\pi} \cdot \frac{\mu_0}{g+h_m} \cdot \frac{N_a \cdot I}{2p}$$

And for polyphase winding with balanced operation is given by

$$B_{flux} = \sum_{n=1}^{\infty} B_n \cdot \sin(np\theta) \quad (3.29)$$

Where

$$B_n = \frac{q}{2} \cdot \frac{4}{n\pi} \cdot \frac{\mu_0}{g+h_m} \cdot \frac{N_a \cdot I}{2p}$$

Considering all real winding affects, the air gap inductance is calculated as below.

$$L_{ag} = \frac{\lambda}{i} = \frac{q}{2} \cdot \frac{4}{n\pi} \cdot \frac{\mu_0 \cdot R_s \cdot L_{st} \cdot N_a^2 \cdot k_{wn}^2}{n^2 \cdot p^2 \cdot (g+h_m)} \quad (3.30)$$

Due to the magnetic field generated by coil currents, crosses one side of the slot to the other, there is slot leakage inductance. We consider rectangular slot with slot depression which results in slot permeance per unit length.

$$Perm = \frac{1}{3} \cdot \frac{h_s}{w_{st}} + \frac{h_d}{w_d} \quad (3.31)$$

For m slots/pole/phase and standard double layer winding, slot leakage inductance is given as below.

$$L_{as} = 2 \cdot p \cdot L_{st} \cdot perm \left[4 \cdot N_c^2 (m - N_{sp}) + 2 \cdot N_{sp} \cdot N_c^2 \right] (self) \quad (3.32)$$

$$L_{am} = 2 \cdot p \cdot L_{st} \cdot perm \cdot N_{sp} \cdot N_c^2 (mutual) \quad (3.33)$$

$$L_{slot} = L_{as} - L_{am} (3phase)$$

$$L_{slot} = L_{as} - 2 \cdot L_{am} \cdot \cos\left(\frac{2\pi}{q}\right) (higher\ odd\ phases) \quad (3.34)$$

The end turn inductance per phase which is the smallest portion of the machine inductance is very complicated to be calculated. It is because of the very small magnetic field around the coil just before it enters another slot. Approximation has been used to calculate this inductance assuming that end turns are semi-circular having a radius of one-half the mean coil pitch. By using the method explained in (Hanselman 2003)

$$L_e = \frac{\mu_0 \cdot N_c \cdot N_a^2 \cdot \tau_s}{2} \cdot \ln\left(\frac{\tau_s \cdot \pi}{\sqrt{2} \cdot A_s}\right) \quad (3.35)$$

The total inductance is the sum of three inductances

$$L_s = L_{ag} + L_{slot} + L_e \quad X_s = \omega_0 \cdot L_s \quad (3.36)$$

3.12. Basic Losses

Losses increase as the speed increase; it can be seen in the graph below.

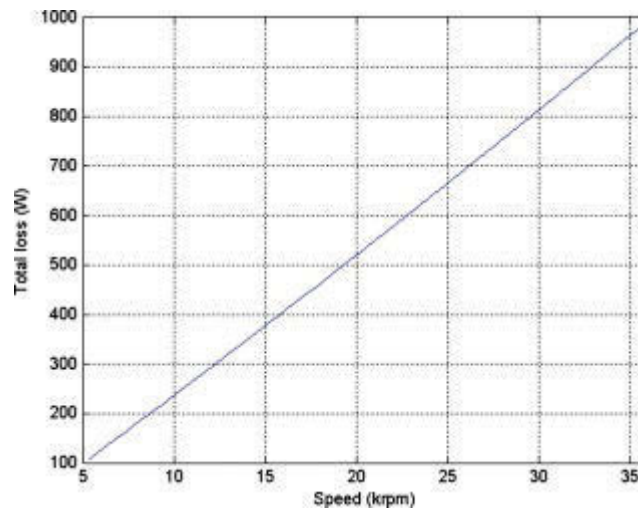


Figure 10 speed vs losses

Basic losses in HSPMG can be categorised as follows as discussed in (Huynh, Zheng & Acharya 2009)

- Stator losses
- Rotor eddy current losses
- Winding losses

All the losses are analysed in depth by FEA. Analytical assumptions can be made as well, as given below.

3.12.1. Stator losses

Stator losses made up of copper losses and iron losses. Copper losses consist of conventional I^2R loss and stray losses which are due to the skin effect and proximity effect. These losses can be analysed in depth in FEA or analytically. Stator iron loss is further divided into hysteresis losses and classical eddy current loss and excess eddy current loss as discussed in (Huynh, Zheng & Acharya 2009). I^2R losses can be calculated by equation 3.37.

$$P_{cu} = m_1 I^2 R \quad (3.37)$$

Where m_1 = number of phases

I = armature current

R = DC armature resistance

Stray losses consist of (a) skin effect causing because of the same source conductors and (b) proximity effect which is because of the electromagnetic field induced in two adjacent conductors sharing the one slot. Electromagnetic induction caused by skin effect opposes the main E-field. The intensity of skin effect can be analysed by skin depth which is a measure of a distance of a current flow along the surface of the material and reduces in amplitude by a factor $1/e$, where $e = 2.71828$. Skin depth can be calculated by the formula given below.

$$\delta = \sqrt{\frac{2}{\omega\mu_0\sigma}} \quad (3.38)$$

Where ω = angular frequency

σ = electrical conductivity

Losses because of proximity effects of the conductor can be estimated based on the equation 3.39 as given below.

$$P_{stray} = P_{cu}(K_d - 1) \quad (3.39)$$

Where K_d = average resistance coefficient

Iron losses include hysteresis and eddy current losses, if the magnetic material selected does not change its state, it causes hysteresis losses. Hysteresis losses increase when the magnetic field intensity is at peak it can be seen in B-H curve. As discussed in (Hamdi 1994) hysteresis loss per unit volume in terms of maximum flux density and frequency can be analysed by the following formula.

$$P_h = \eta B^n f \quad (3.40)$$

Where η = material constant

N = exponent (1.8-2.2)

Change in the flux density also causes the eddy current loss in the core as current is induced in the ferromagnetic material which dissipates power due to the resistivity of the material. The eddy current loss per unit volume at lower frequencies is given by the following equation.

$$P_e = \frac{\pi^2 B^2 t^2 f^2}{\rho\beta} \quad (3.41)$$

Where t = thickness of the material

B = peak flux density

ρ = resistivity of the material

β = geometric structure coefficient

Eddy current loss is further divided into two classes (a) classical eddy current and (b) excess eddy current for more accurate calculation. So, for a given frequency, the iron losses of the machine are calculated as below.

$$P_{iron} = K_h B^2 f + K_c (Bf)^2 + K_e (Bf)^{\frac{3}{2}} \quad (3.42)$$

Where K_h = coefficients of hysteresis loss

K_c = coefficient of classical eddy current loss

K_e = coefficient of excess eddy current loss

3.12.2. Rotor eddy current losses

Rotor losses produced by eddy currents do not have significant value in machines total losses. Nevertheless, heat removal from rotor section is much more complicated as compared to the stator. To get reasonable operating temperature, losses prophecy is very important to high-speed operation. Eddy current losses can be divided into three categories as below. (a) No-load rotor eddy current losses caused by the presence of stator slots, (b) On-load rotor eddy current losses caused by winding's harmonics (space harmonics), (c) On-load rotor eddy current loss induced by the time harmonics of the phase currents (PWM). Generally, following relationship can be used to calculate the eddy current losses.

$$\int_v \sigma E^2 dV = \int_v J^2 / \sigma dV \quad (3.43)$$

Where σ = material conductivity

E = electric field

J = eddy currents density

V = volume of the material

More precise analysis of rotor losses can be done through FEA in transient solver mode which will be discussed later in FEA section in depth.

There are several methods to reduce rotor eddy current losses. Reducing the slot opening and increasing the magnetic gap between rotor and stator can reduce no-load rotor loss. Increasing the number of slots

per pole and using fractional winding can reduce rotor loss caused by the space harmonics of the armature winding. Increasing the switching frequency and using external line inductors can reduce rotor loss caused by time harmonics of the phase currents. Since rotor loss caused by time harmonics is dominant in most applications, increasing the switching frequency and using external line inductance to reduce current THD is a very effective way to reduce rotor loss (Huynh, Zheng & Acharya 2009).

3.12.3. Winding losses

Winding in air cause losses as well, and power is needed to control the drag resistance of rotor cylinder. Different gases or fluids are also used in between rotor and stator, so winding losses is a function different operating conditions such as temperature, density, the pressure of these fluids/gases and the rotational speed of the shaft. Winding loss can be estimated by the following equation.

Shaft rotational speed:

$$\omega = \frac{2\pi N}{60} \quad (3.44)$$

Reynolds number:

$$R_e = \omega r \frac{\rho}{\mu} \varphi \quad (3.45)$$

Skin friction coefficient (C_d):

$$\frac{1}{\sqrt{C_d}} = 2.04 + 1.768 \ln(R_e \sqrt{C_d}) \quad (3.46)$$

Windage:

$$W = C_d \pi \rho \omega^3 r^4 \lambda \quad (3.47)$$

Where N = rotational speed of rotor (rpm)

ρ = density of fluid (kg/m³)

μ = kinematic viscosity of cooling media (m²/s)

r = radius of rotor (m)

φ = radial gap between rotor and stator (m)

λ = length of the rotor (m)

There are frictional losses as well because of surface roughness of rotor and stator should also be taken into account for the more precise calculation of overall losses.

3.13. Machine Sizing

Machines are sized for rated torque capability rather than power. Output torque is proportional to the product of rotor volume and shear stress, air-gap shear stress is proportional to the product of air-gap electrical and magnetic loading. The best sizing parameter for PMSMs is probably air-gap stress. Shear stress is calculated as

$$\tau \propto K_z \cdot B_g \quad (3.48)$$

Where τ = shear stress (Psi)

K_z = surface current density

B_g = air-gap flux density

Typically for liquid cooled machine the value of shear stress is 10-20Psi, we will use 15Psi for this design. The tip speed has been discussed previously, with the assumed value of 200m/s. The following fundamental power equation can be used to find out the stack length and rotor radius.

$$P = 2 \cdot \pi \cdot R \cdot L_{st} \cdot \tau \cdot v_{tip} \quad (3.49)$$

Where R = rotor radius

L_{st} = stack length

With L/D ratio assumed to be 2.5, air-gap flux density to be 0.8T, slot height 15mm and slot fill fraction to be 0.5, basic parameters like frequency and the current density of the machine are found. The Appendix contains the MATLAB code for input parameters calculation and results are shown below.

❖ Basic Design parameters of the machine:

Input Parameters of machine			
Shear Stress	15.0 psi	Power requirement	660.0 kW
B_g	0.8 T	Pole Pairs	2.0
v_{tip}	200.0 m/s	L.D Ratio	2.51

Table 6 Basic input parameters of the machine

Output parameters of the machine			
Stack Length	0.160 m	Rotor Radius	0.032 m
Frequency	2001.9 Hz	Speed	60000 RPM
J_a	1757.67 A/cm ²		

Table 7 Basic output parameters of the machine

❖ **Detailed sizing of the machine:**

Once the basic parameters are known in depth analysis is done. To get a better understanding pre-existing database of the same kind of machines need to have a look. These data bases are helpful to choose input parameters. This data can be collected from several firms including ATE in Germany, Rueland electric in the USA and E und A in Switzerland given in the appendix, from all these databases and analysing different machines the following input parameters are developed.

Parameter	Value	Parameter	Value
Rotational Speed	60,000RPM	Required Power	660.0 KW
Number of Phases	3	Rotor Radius	0.032 m
Turns per Coil	1	Slots Short-pitched	1
Number of Slots	24	Magnet Height	20 mm
Peripheral Tooth Fraction	0.5	Slot Depth	25 mm
Winding Conductivity	6.0x10 ⁷ s/m	Magnet B_r	1.2 T
Pole Pairs (p)	2	Slot Depression Width	N/A
Slot Depression Depth	0.5 mm	Stator Back Iron Ratio	0.7
Magnet Angle	50 ⁰ deg	Power Factor Angle	0 deg
Magnet Skew Angle	10 ⁰ deg	M Slot Fill Fraction	0.5
Air Gap	2 mm	Stack Length	0.160 m
Steel Density	7700 kg/m ³	Conductor Density	8900kg/m ³
Magnet Density	7400 kg/m ³	Avg Slot Width (W_s)	16.0 mm

Table 8 detailed input parameters of the machine

After entering the input parameters second step is to generate the geometry of the machine. In geometry number of slots/pole/phase (Eqn 3.6), tooth width, stator back iron dimensions, winding end turn geometry, the number of armature turns, slot dimensions, and coil pitch are determined.

$$N_a = 2 \cdot p \cdot m \cdot N_c \quad (3.50)$$

Where N_c = Turns per coil

N_a = assumes each coil has two half coils

Rotor surface speed and electrical frequency are determined by the following equation.

$$f = \frac{p \cdot N}{60} \quad (3.51)$$

$$\omega = 2 \cdot \pi \cdot f$$

$$\omega = p \cdot \omega_m$$

Where ω = electrical frequency (rad/sec)

ω_m = mechanical frequency (rad/sec)

Winding skew, magnetic gap factor air-gap flux density (B_g), and flux leakage are calculated as per the equations discussed in earlier sections.

By utilising equation 3.26 and 3.27 internal voltage of the generator is calculated shown in equations below.

$$B_1 = \frac{4}{\pi} \cdot B_g \cdot K_g \cdot \sin\left(\frac{p\theta_m}{2}\right) \quad (3.52)$$

$$\lambda = \frac{2 \cdot R_s \cdot L_{st} \cdot N_a \cdot K_w \cdot K_s \cdot B_1}{p} \quad (3.53)$$

$$E_a = \omega_o \cdot \lambda$$

Machines inductances and reactances are determined by using the formulas from section 3.11.4. By using the basic geometric calculations, volumes, length and mass of the machine are calculated. In the large liquid cool machine 15% service mass fraction is added to total mass of the machine as

discussed in (Rahman & Slemon 1985). Once the mass is known all the losses are calculated by using the equations from section 3.12.

The phasor relationship between internal voltages (E_a), terminal voltage (V_a) and the synchronous voltage drop is used to get the terminal voltage and current of the machine as shown below.

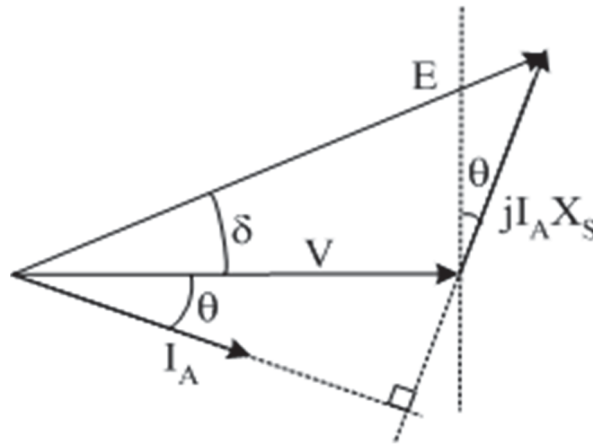


Figure 11 vector diagram of voltage

$$V_a = \sqrt{E_a^2 - (X_s \cdot I_a \cdot \cos\theta)^2} - X_s \cdot I_a \cdot \sin\theta \quad (3.54)$$

All the results by MATLAB coding are shown below.

Machine Size:			
Machine Length	0.257 m	Machine Diameter	0.195 m
Tooth Width	8.050 mm	Slot Avg Width	8.050 mm
Active length	0.160 m	Slot Height	25.000 mm
Back Iron Thick	11.200 mm	Rotor radius	0.032 m
Machine Rating:			
Power Rating	660.0 kW	Speed	60000 RPM
V_a (RMS)	417 V	Current	527.9 A
E_a (RMS)	430 V	Arm Resistance	0.00246 ohm
Synch Reactance	0.194 ohm	Synch Induct	0.015 mH
Stator Cur Den	1049.3 A/cm ²	Tip Speed	201 m/s
Efficiency	0.993	Power Factor	1.000
Phases	3	Frequency	2000.0 Hz

Stator Parameters:			
Number of Slots	24	No of arm Turns	8
Breadth Factor	0.966	Pitch Factor	0.966
Tooth Flux Den	1.14 T	Back Iron	0.81 T
Slots/pole/phase	2.00		
Rotor Parameters:			
Magnet Height	25.00 mm	Magnet Angle	50.0 degm
Air gap	4.00 mm	Pole Pairs	2
Magnet Remanence	1.20 T	Air Gap Bg	0.57 T
Magnet Factor	1.203	Skew Factor	0.995
Machine Losses:			
Core Loss	1.5 kW	Armature Loss	2.1 kW
Windage Loss	1.3 kW	Rotor Loss	TBD kW
Machine Weights:			
Core	14.06 kg	Shaft	3.96 kg
Magnet	2.30 kg	Armature	9.98 kg
Services	4.55 kg	Total	34.85 kg

Table 9 Detailed sizing parameters of the machine

Chapter 4

4. Finite Element Analysis using Motor-CAD

4.1. Machine's geometry

Setting up machines geometry is most critical step in Motor-CAD, it gives us the number of options to set the desired geometry of the machine, from the menu bar motor type is set to the brushless permanent magnet (BPM) and model is set as E-magnet.

Housing is set as round, and slot type parallels tooth in the stator. Rotor topology is configured to u-shaped inner magnets with circular rotor ducts for ventilation. Now the stator and rotor dimensions need to be set in radial view as calculated in MATLAB.

Axial and 3-D view of the machine geometry can be analysed as well. Front and rear shaft diameter and front and rear end-cap thickness in axial view need to be set; all other parameters remain same.

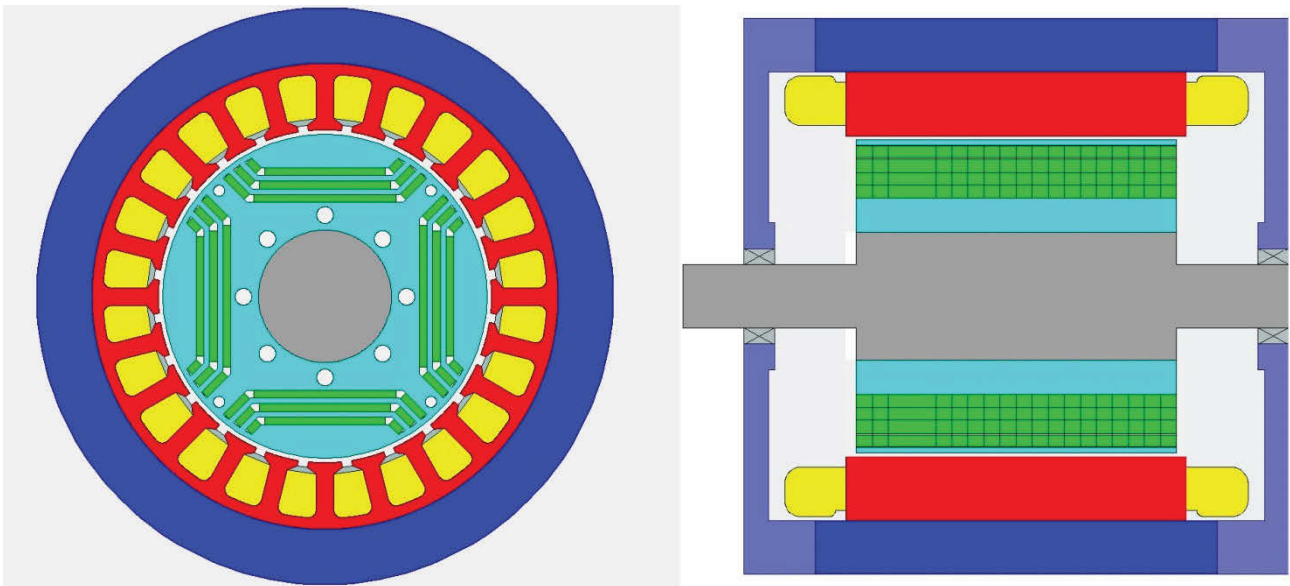


Figure 12 radial and axial view of machine

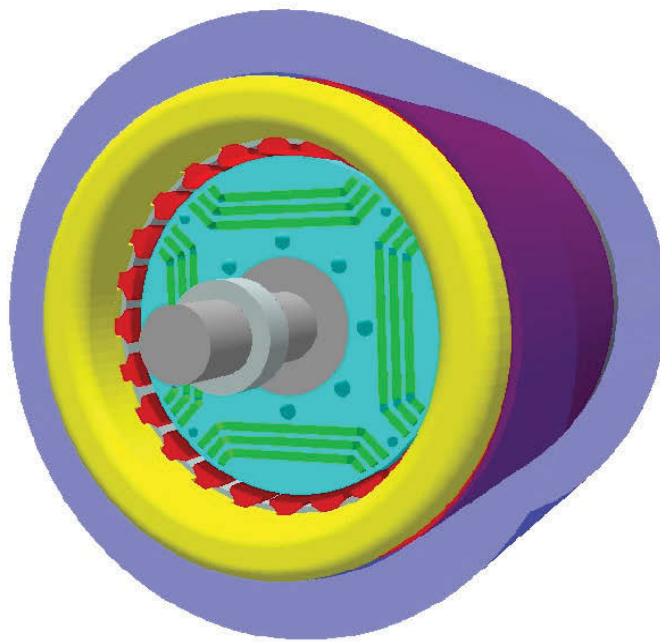


Figure 13 3D view of machine

4.2. Machine's winding

The second step is to setup the windings of the machine. In winding definition, the winding type is selected as overlapping; the wedge definition is defined by wire size, which is set to be 0.885mm and 0.800mm from the metric table, and the material between the liner and lamination is set as air as shown in the picture. The number of strands in hand is set to 14 and conductor separation is 0.025mm. Conductor/ slot and conductor/ slot drawn should be same. In pattern tab the coil is configured with eight turns, the coil throw is six slots, coil connected in 2 parallel paths and the double layer winding, as shown in figure 14. Coil pattern and phasor diagram are analysed as shown in figure 15.

There were already defined 24 slots and four poles. Therefore the number of slots/pole/phase is equal to 2. As the first attempt, it's considered coils per pole equal to 1, as usual in fractional slot type. Having four poles in the winding, it means that eight coil sides per phase are present, to distribute along 24 slots. So for 3-phases, it gives 48 coil sides, which is exactly the double of slots number. It means that a double layered winding was guaranteed. As it's not possible to have a non-overlapping one, the coils span chosen is equal to 6 forming an overlapping winding. However is important to the point that span is higher than pole pitch, which means that coils are not short-pitched or chorded. As a consequence,

no filtering effect will happen in the harmonic content of air gap flux density distribution. This is not necessary a problem because it was already discussed that skewing the stator is an acceptable solution regarding the design options taken (Marques).

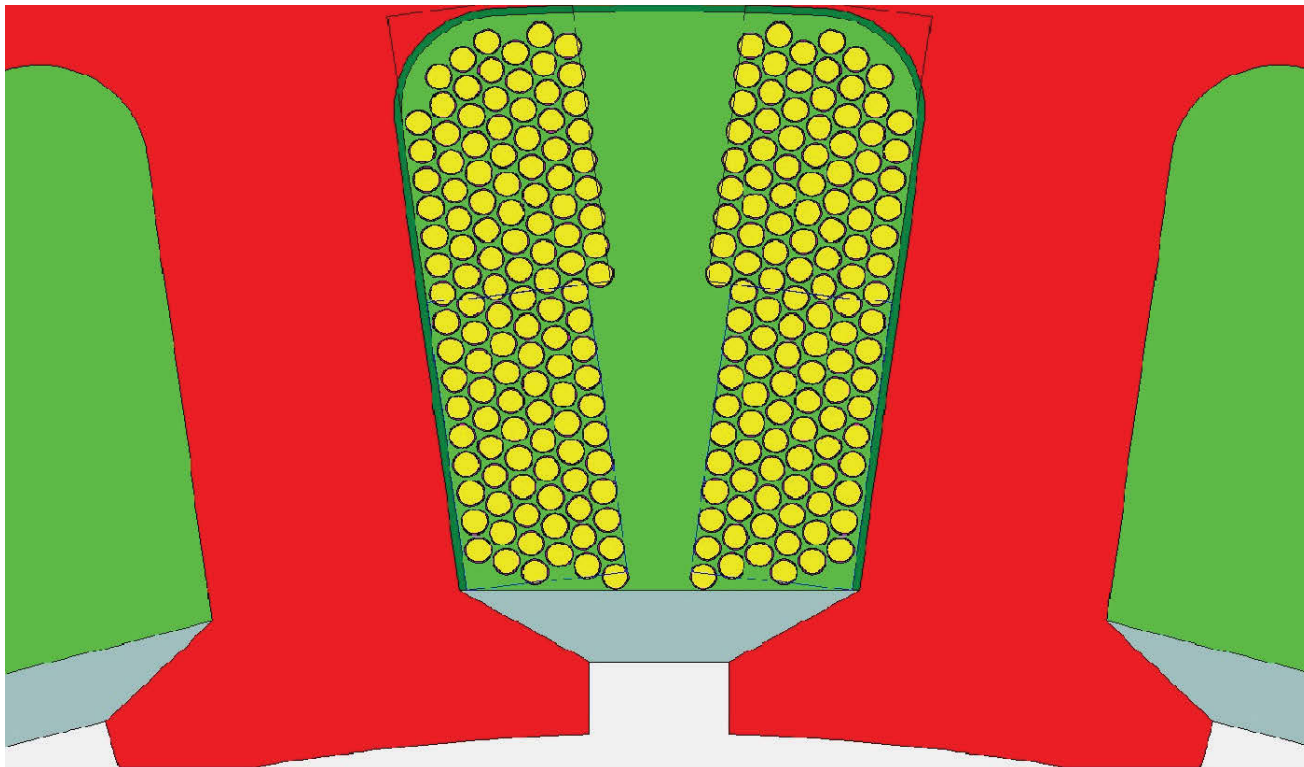


Figure 14 winding definition in stator slot

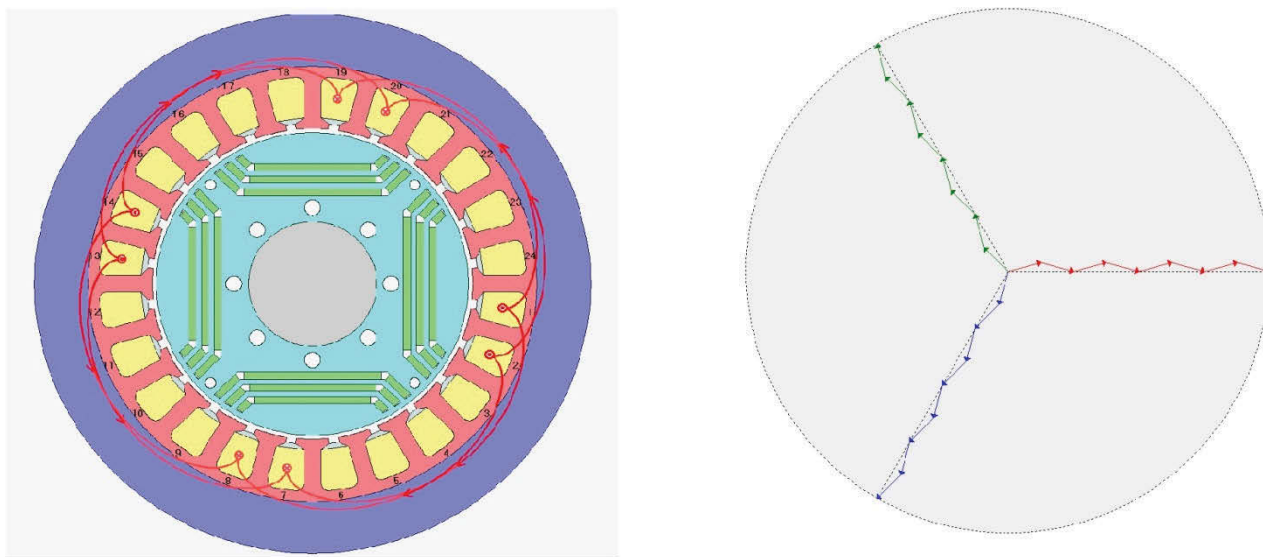


Figure 15 coil pattern of HSPM

4.2.1. Harmonic study

Eddy-current losses in the rotor are caused by three main sources:

- Winding harmonics: the asynchronous harmonics concerning the rotor due to spatial distribution of the linear current density induce eddy current losses;
- Permeance variation: slot openings change the permanent magnet working points, depending on the rotor position. Thus, there is a flux density variation that induces eddy currents in the permanent magnet and other solid conductors;
- PWM harmonics: frequency-converter-caused time harmonics in the stator current waveform cause additional losses in the rotor.

Various slot/pole combinations which have a proper number of slots and winding factor could be selected in a design of fractional-slot concentrated winding. However, the MMF harmonics of fractional winding induce eddy-current losses in the rotor, and this effect could not be studied individually by using time-stepping FEA since effects of slot opening could not be separated. In this study, a semi-analytical method is proposed to investigate the effects of MMF harmonics on the eddy-current losses and to find the particular order of harmonic which contribute the majority of losses. This method first examines MMF harmonics of candidate winding designs, and then each order of harmonics are applied to a simplified FEA model which is treated as the time-harmonic magnetic problem as discussed in (Li et al. 2012).

The individual harmonic components are multiplied by a function to account for the modulating effect of the slot openings (Miller 2002). It can be verified in harmonic spectrum that there is no odd harmonics available. In this 24/4 machine, lowest MMF harmonics is too working harmonics, which implies that either 1st electrical harmonics or 6th mechanical harmonics, it can be seen in mechanical MMF harmonic spectrum that first lower harmonic have appeared is the 6th one. It has benefits in electrical point of view because differential inductance leakage is increased when sub-harmonics appear.

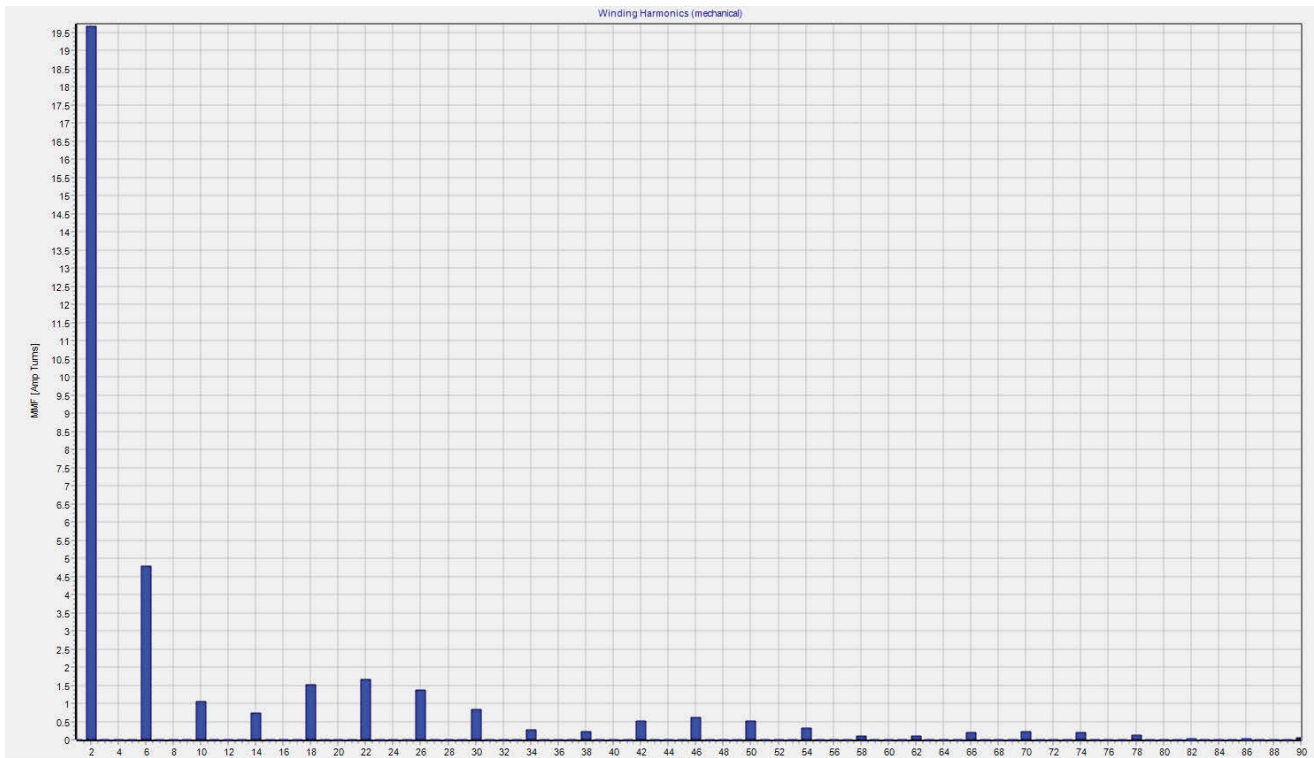


Figure 16 winding mechanical harmonics

Recently, the industry is more and more interested in fractional-slot concentrated windings (FSCW). Especially their use of permanent magnet (PM) brushless machines profits from the advantages such as a high winding factor of the working harmonic, efficiency, slot filling factor and fault tolerance, short, less sophisticated and profitable end-windings. These characteristics contribute to an increase of the machine power density and make a reduction of material and manufacturing costs possible. Because of the almost sinusoidal counter-electromotive force (CEMF), the PM machines work very well with distorted stator magnetomotive force (MMF), where the high winding factor is of most top priority (Moros & Gerling 2015).

Figure 17 shows the winding factor as a bar chart which is calculated from the Fourier analysis of winding distribution. It can be verified that we are getting 0.96 value of winding factor which is good to maximise the torque, avoid unbalanced magnetic pull and to minimise the rotor losses. As winding is connected in the star connection, odd harmonics will be subtracted other two phases as well.

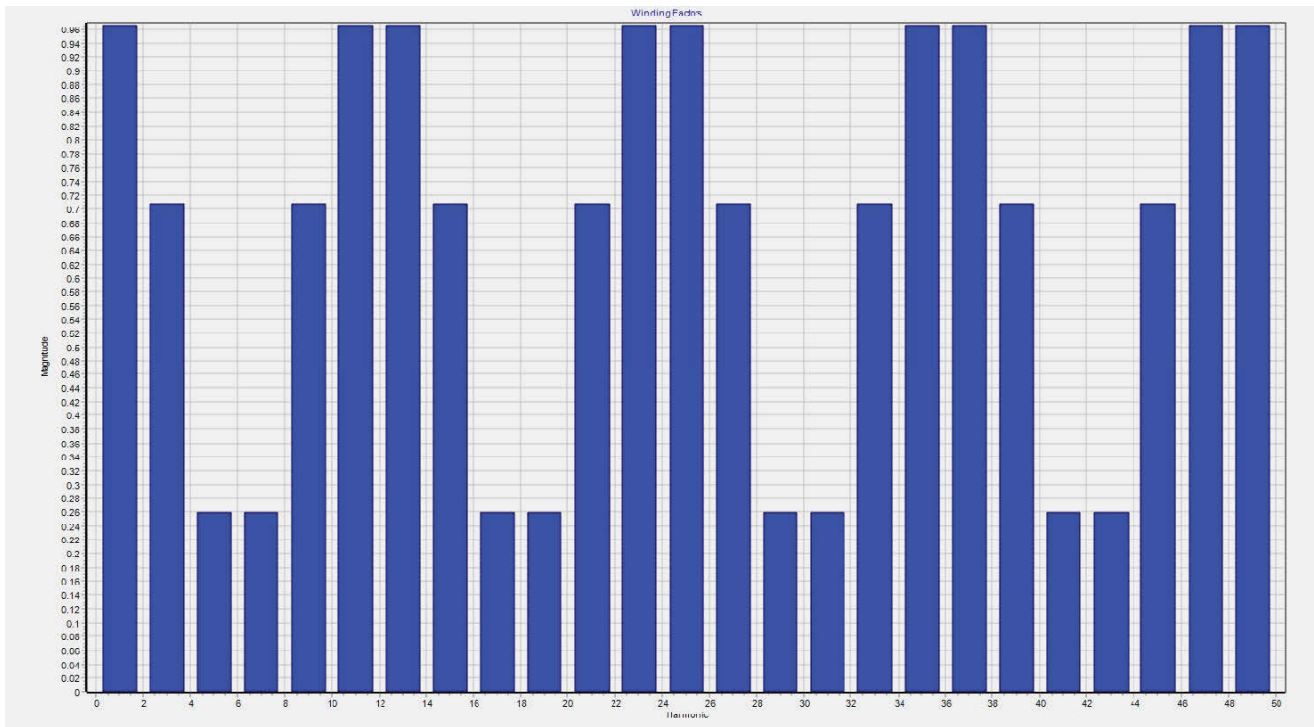


Figure 17 winding factor

4.3. Material input

As discussed earlier 6.5%FeSi will be used in this design, alloy of iron and silicon is also known as JFE_10JNEX900, as this material is excellent to minimise the iron losses due to high speed (Paulides, Jewell & Howe 2004). Non-oriented electrical steels with silicon content up to 6.5% (weight) opened the way to a new application such as high-frequency applications. It is well known that the silicon content reduces the eddy current and excess losses. Although the material is brittle, a steel manufacturer has developed a patented process that uses chemical vapour deposition (CVD) to improve the workability of the 6.5% silicon non-oriented electrical steel(Leicht et al. 2008). This material is in Motor-Cad database highlighted as steel for HSPMG.

Magnetic properties of JNEX material are given in BH curve. It can be seen that this material offers high saturation values which give the advantage where inductance under load is critical and where medium range frequencies have to deal with. BH curve for JFE_10JNEX900 is shown in figure 18 below.

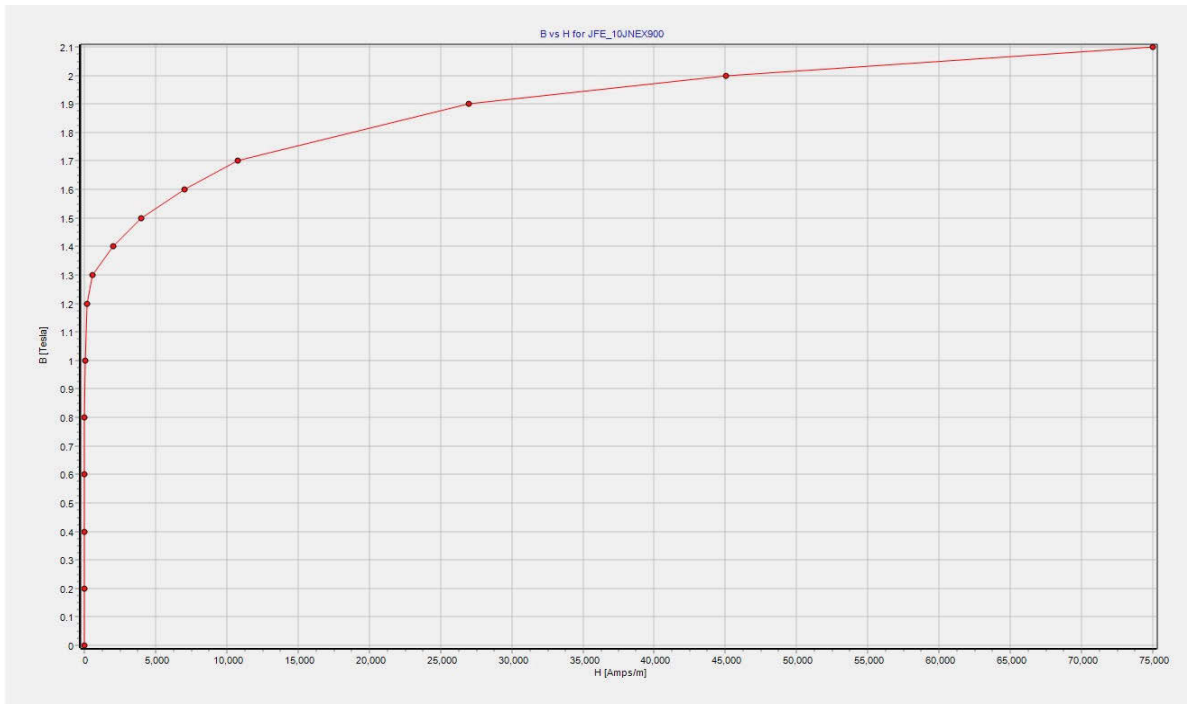


Figure 18 BH curve of 6.5%SiFe

The graph of loss density (W/Kg) and flux density (T) to get overall power loss for the given frequency can be analysed in the figure below. Total loss while using 6.5% SiFe is nearly 40% lower than the sample with 5.5% silicon.

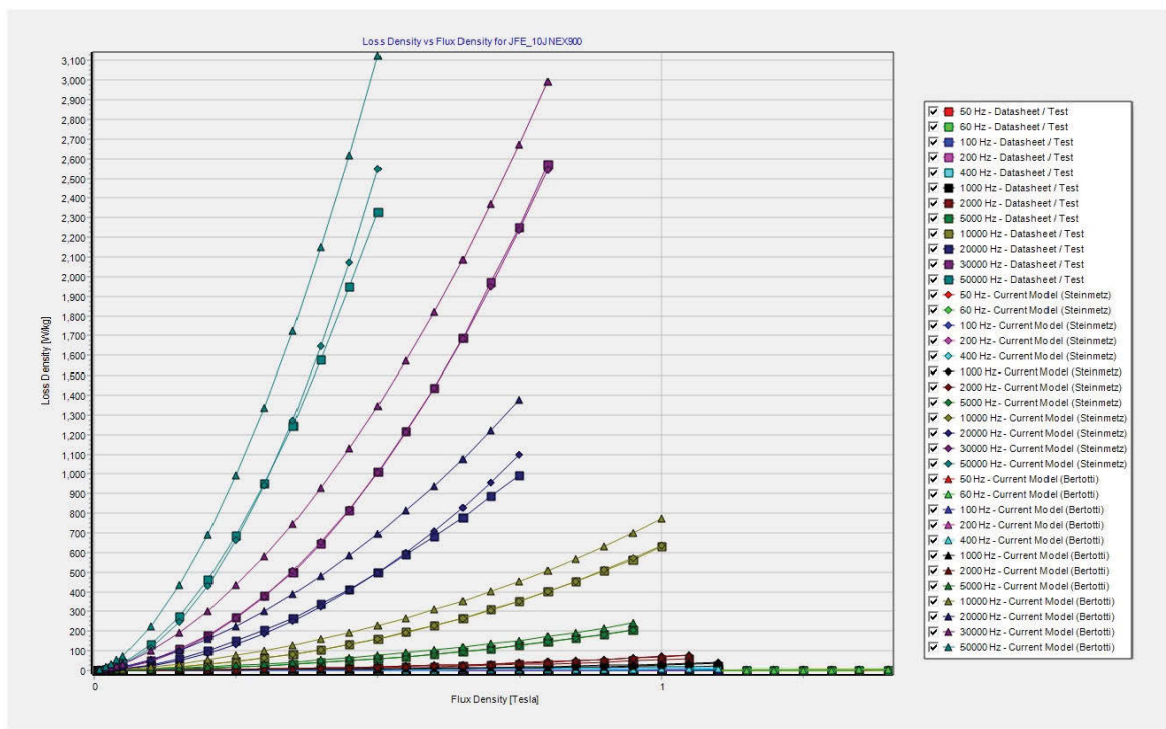


Figure 19 steel losses of 6.5% SiFe

The materials are configured in the Materials tab. This tab also provides the weight of the different materials comprising the machine as shown in the following figure.

Component	Material from Database	Electrical Resistivity	Temp Coef Electrical Resistivity	Magnet Br at 20C	Magnet Relative Permeability	Temp Coef Br	Density	Weight	
Units		Ohm.m		Tesla			kg/m3	kg	
Stator Lam (Back Iron)	JFE_10JNEX900	5.9E-07	1.3				7490	4.028	
Stator Lam (Tooth)	JFE_10JNEX900	5.9E-07	1.3				7490	7.087	
Stator Lamination								11.12	
Winding [Active]	Copper (Pure)	1.68E-08	0.003862				8933	4.319	
Winding [Front End-Wdg]	Copper (Pure)	1.68E-08	0.003862				8933	2.581	
Winding [Rear End-Wdg]	Copper (Pure)	1.68E-08	0.003862				8933	2.581	
Winding [Total]								9.482	
Slot Wedge		0	0				1000	0.08482	
Magnet	N30UH	1.4E-06	0	1.105	1.1	-0.12	7650	3.94	
Rotor Lam (Back Iron)	JFE_10JNEX900	5.9E-07	1.3				7490	4.535	
IPM Magnet Pole	JFE_10JNEX900	5.9E-07	1.3				7490	6.191	
Rotor Lamination [Total]								11.64	
Shaft [Active]		0	0				7800	3.683	
Shaft [Front]		0	0				7800	0.4686	
Shaft [Rear]		0	0				7800	0.3032	
Shaft [Total]								4.455	
Total								40.63	Weight [Total]

Figure 20 Weight of different materials

4.4. Electromagnetic analysis of machine

After finalising main design parameters and variables, open circuit calculation can be performed in which model calibration of analytical calculations and FEA calculations can be done. Terminal voltage, back EMF, current, flux linkage, torque and cogging torque are analysed in the resulting graphs shown below in figure, 21-27.

The terminal voltage waveform is close to sinusoidal, although some torque ripples can be observed because of harmonic contents of line-line voltage and skew effect in air-gap flux density, it shows a good agreement between analytical and FEA result. However, the reduction of torque ripples is important to enhance the machine life and to get good behaviour towards noise cancellation and reduced vibration. The current waveform is ideal sinusoidal and closely match with the back EMF waveform.

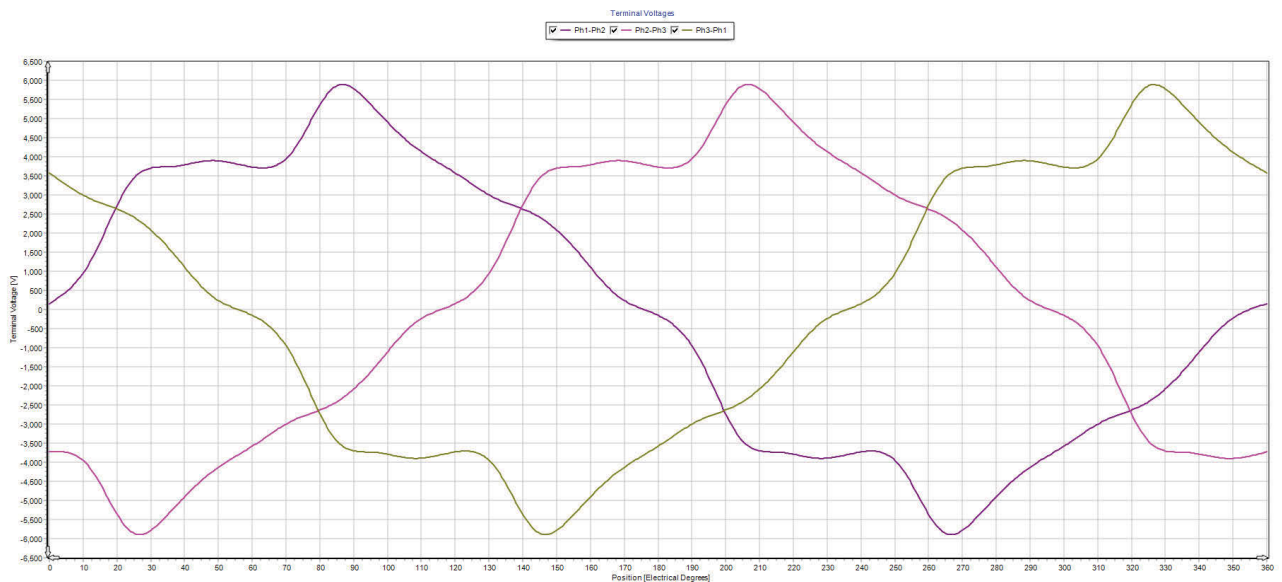


Figure 21 Terminal voltage of the machine

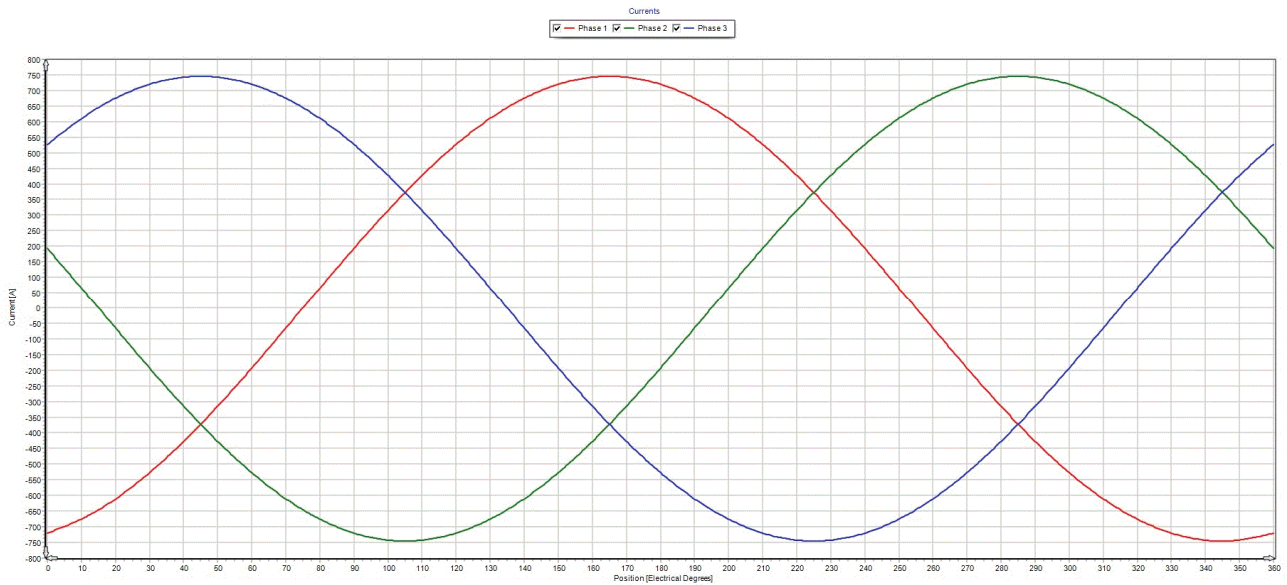


Figure 22 Current of the machine

The flux linkage waveform is not sinusoidal as the current waveform is which justifies i - ψ wave-shape; it indicates a good match with analytical calculations.

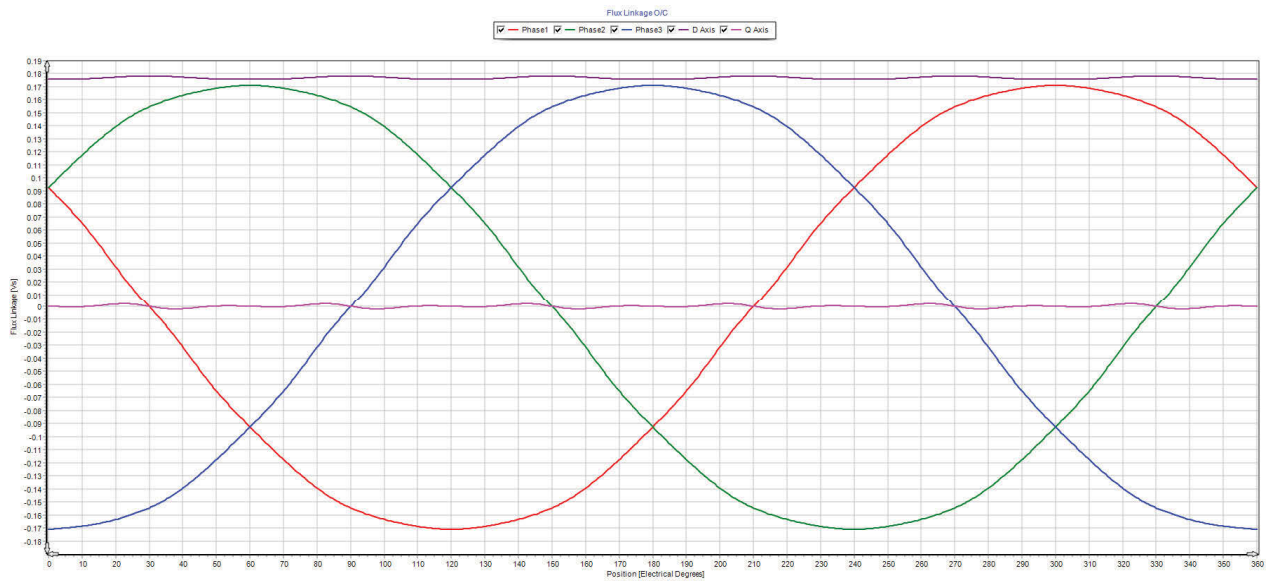


Figure 23 O.C flux linkage in machine

The cogging torque which is due to the alignment of magnet poles and the edges of the stator teeth, it changes with the position of the rotor; it can be reduced by selecting an appropriate skewing angle. When the skew value is about half of the slot pitch, cogging torque can be eliminated.

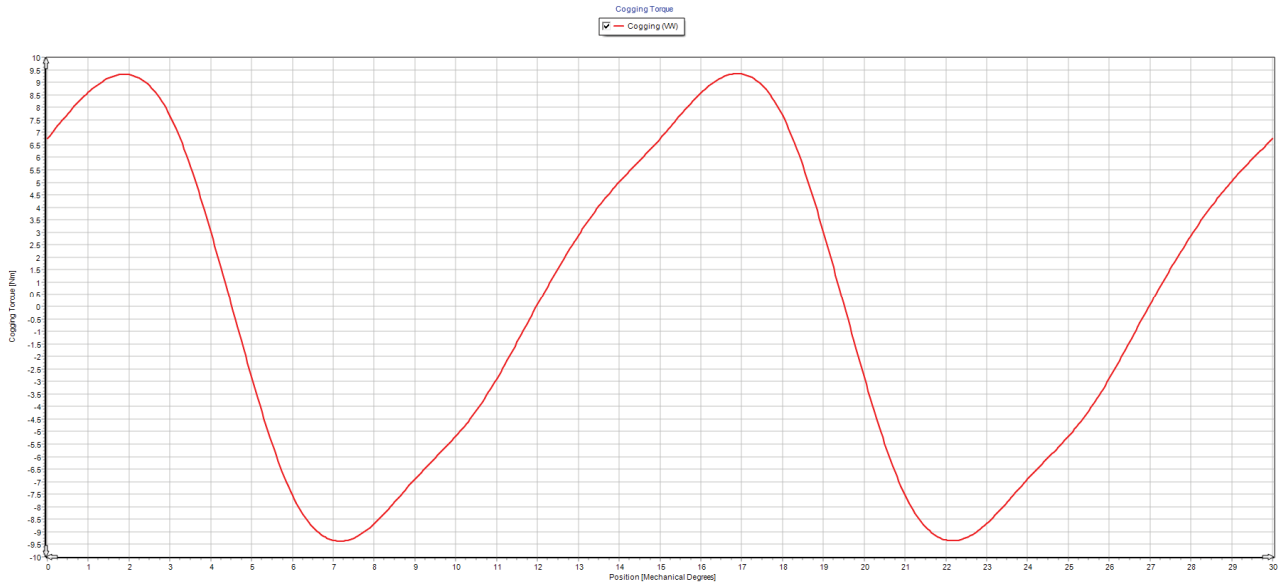


Figure 24 Cogging torque graph

4.4.1. Open circuit analysis

By solving the e-magnetic model, the flux distribution in rotor and stator of the machine can be analysed. It is verified that flux lines are leaving the rotor polar piece nearly perpendicularly which means that the main field components are radial and tangential are neglected. Tooth and stator yoke have the flux density value within the calculated range which is 1.8T. Also tooth and stator yoke dimensions are good to get the design objectives. As it can be seen that all the flux from rotor can easily enter into the stator tooth, indicates that flux distribution is good and calibration process is succeeded. Open circuit losses can be analysed in figure 25, as we can verify that the losses in rotor and stator teeth are well below within the calculated range. Higher losses can be observed in stator yoke due to some harmonics present in current going through the armature winding, another cause of these losses may be the skin effect resulting from the same source conductors. In (Sarumol & Reeba 2015) it is suggested Core loss can be reduced by replacing core material with an amorphous alloy.

Moreover, in (Mlot, Lukaniszyn & Korkosz 2015) some methods of rotor and stator geometry modification are discussed to reduce the losses. In (Huynh, Zheng & Acharya 2009) losses in high-speed PM machines used in micro-turbine are discussed in detail, Various loss verification methods are also discussed. (Zarei, Abbaszadeh & Safari 2012) has discussed the three most important main parameters have the most influence on the core losses of the PM machines.

Motor-CAD

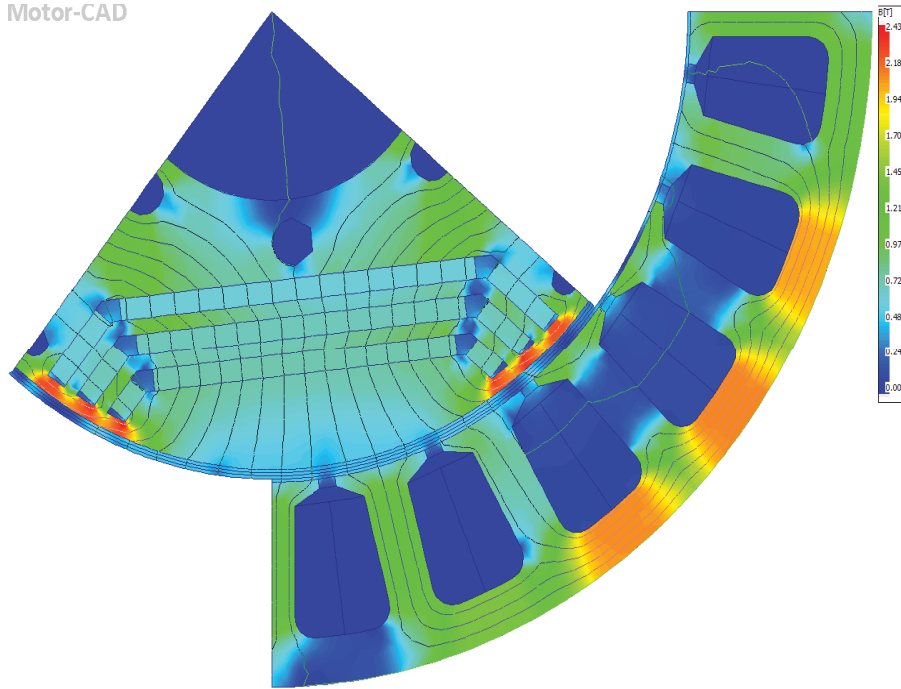


Figure 25 O.C flux density

Motor-CAD

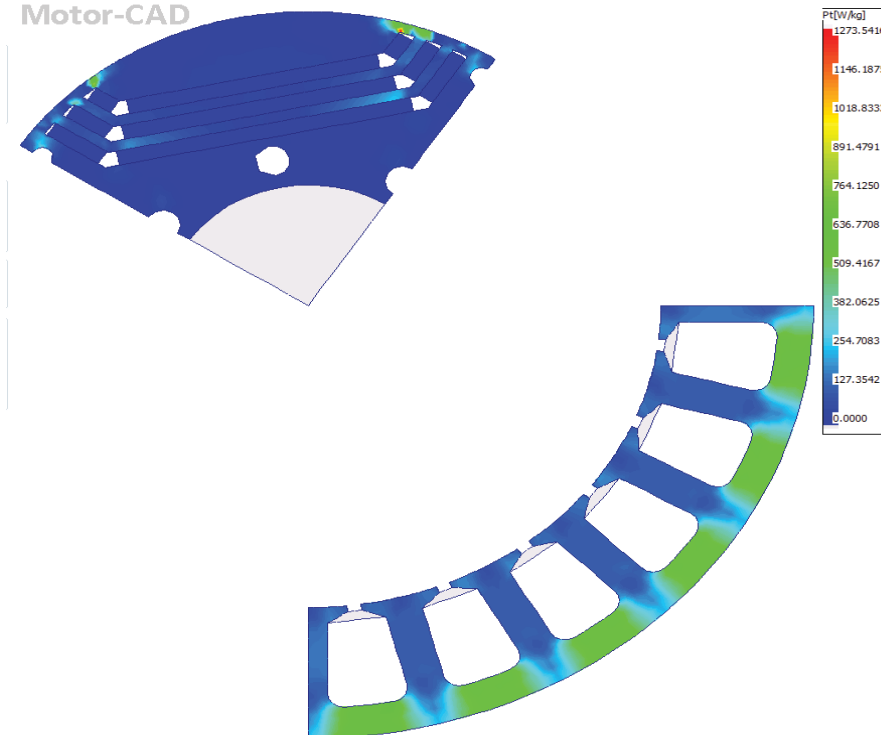


Figure 26 O.C losses in machine

4.4.2. On load analysis

A 3-phase balanced current is injected in armature winding to get a sine-wave drive. Phasor diagram in figure 27 is used here to calculate the required terminal voltage. It can be seen that by knowing the value of impedance and current voltage can be calculated which has a sinusoidal waveform which verifies the analytical results. Flux linkage and symmetry of the back EMF also verify the calculated results.

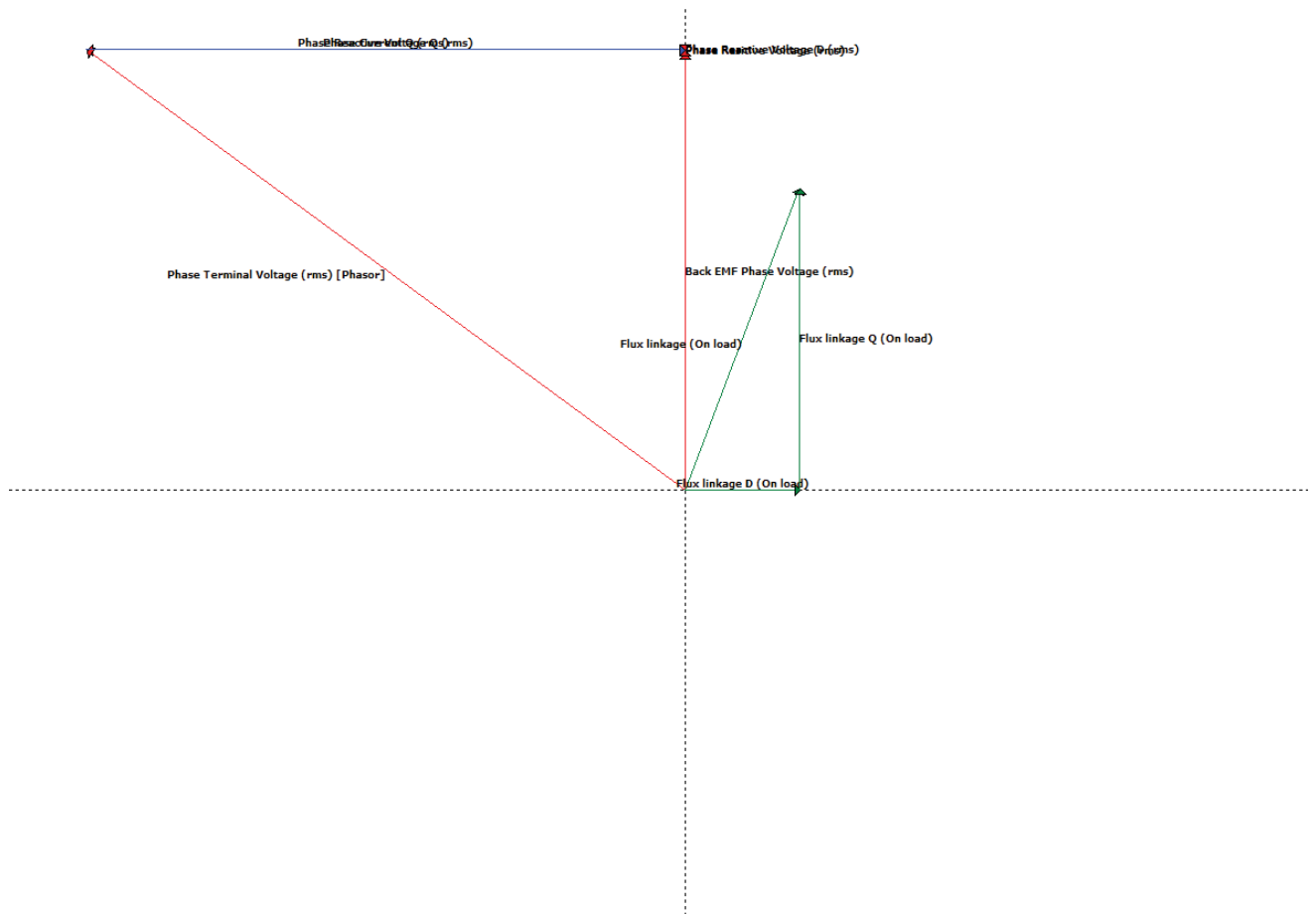


Figure 27 phasor diagram

Flux linkage and symmetry of the back EMF also verify the calculated results.

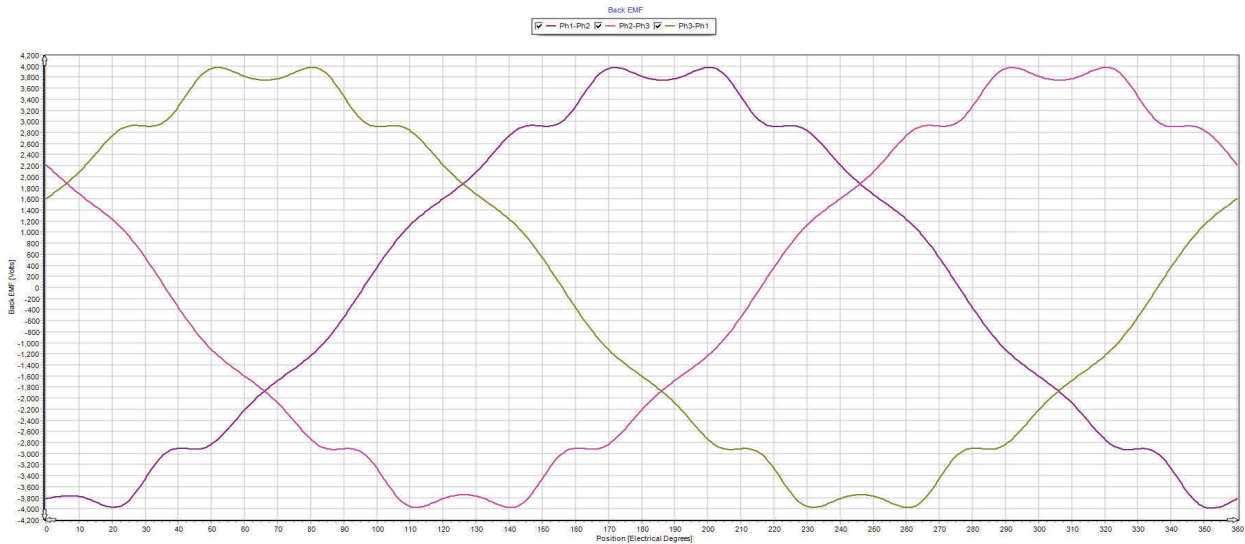


Figure 28 Back EMF

In on-load flux distribution, it can be verified that machine is highly saturated, the value of flux density is about 2.2T as can be seen in the figure below. It confirms that the dimensions of tooth width and stator yoke are good. Losses are also within the calculated range.

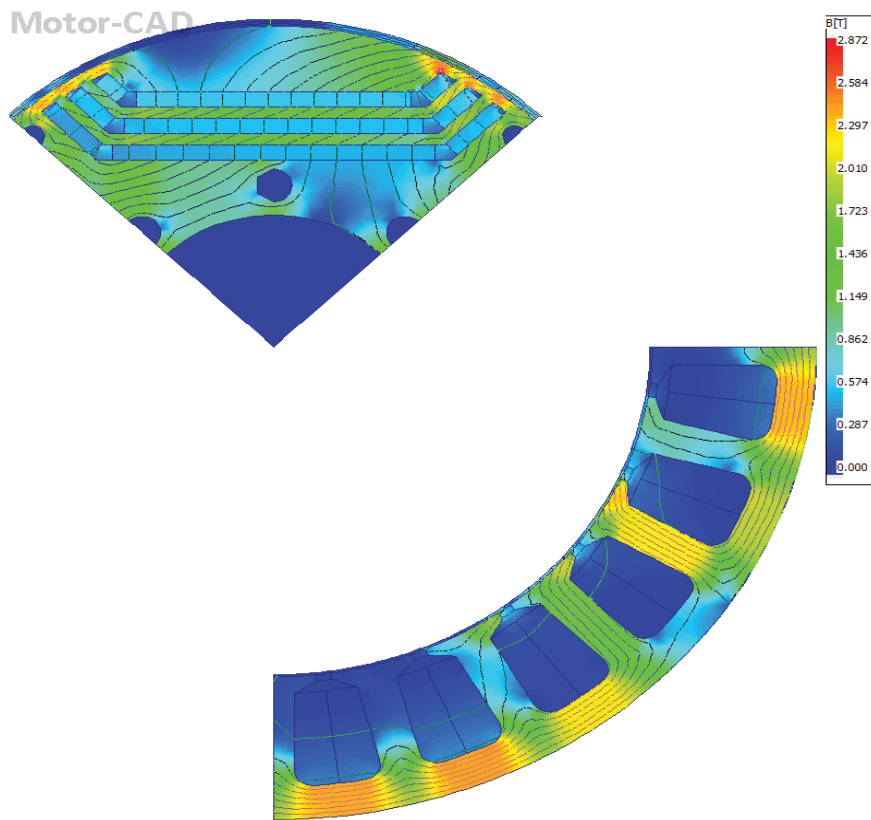


Figure 29 on load flux linkage

4.5. Harmonic Analysis

The harmonics spectrum of torque can be seen in figure 30. From the harmonic spectrum, it can be seen that harmonic torque is distributed in the vicinity of 0, 6, and 12 mainly around 0, higher harmonics can easily be filtered.

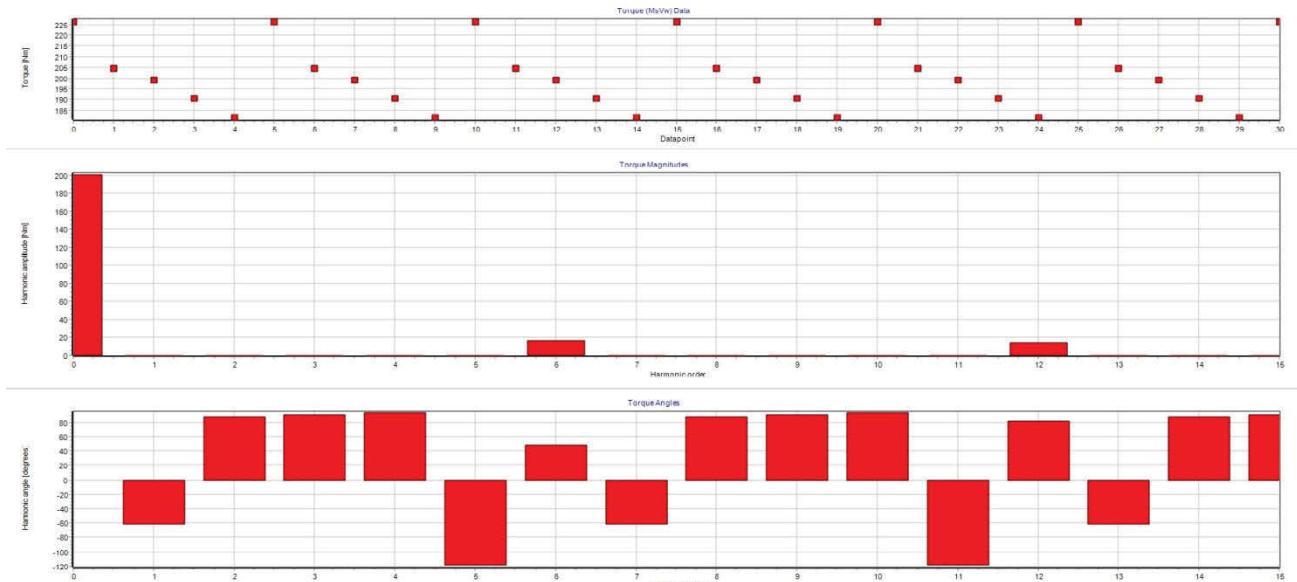


Figure 30 harmonic spectrum of torque

Cogging torque and harmonic spectrum analysis are also analysed in detail in figure 28. High-performance drives in co-generation applications require permanent magnet motors that produce smooth torque with a very low component of cogging torque. This is not easy to attain as improper designs of PMs which has the cogging torque that may be inadmissibly high regarding the rated torque. In lower cost machines, it has typical value around 5 % of the rated torque. As nowadays a number of high-performance applications necessitate cogging torque not to exceed 1 % of the rated torque, effective methods for its analysis and computation are required to design machines that meet such specifications. Minimization of cogging torque frequently becomes a challenging task, since it is composed of numerous harmonic components, which originate in combination of many design parameters and material or assembly imperfections such as combination of rotor and stator technique. Control method used for the drive and substantial differences between calculated and measured cogging torque (GAŠPARIN & FIŠER 2013). Dominant harmonics are 48, 96 and then 144 which are well below 1 % of the rated torque. As we are getting very low cogging torque still there is a possibility to reduce cogging torque by changing the width of stator slot opening and to skew stator slot.

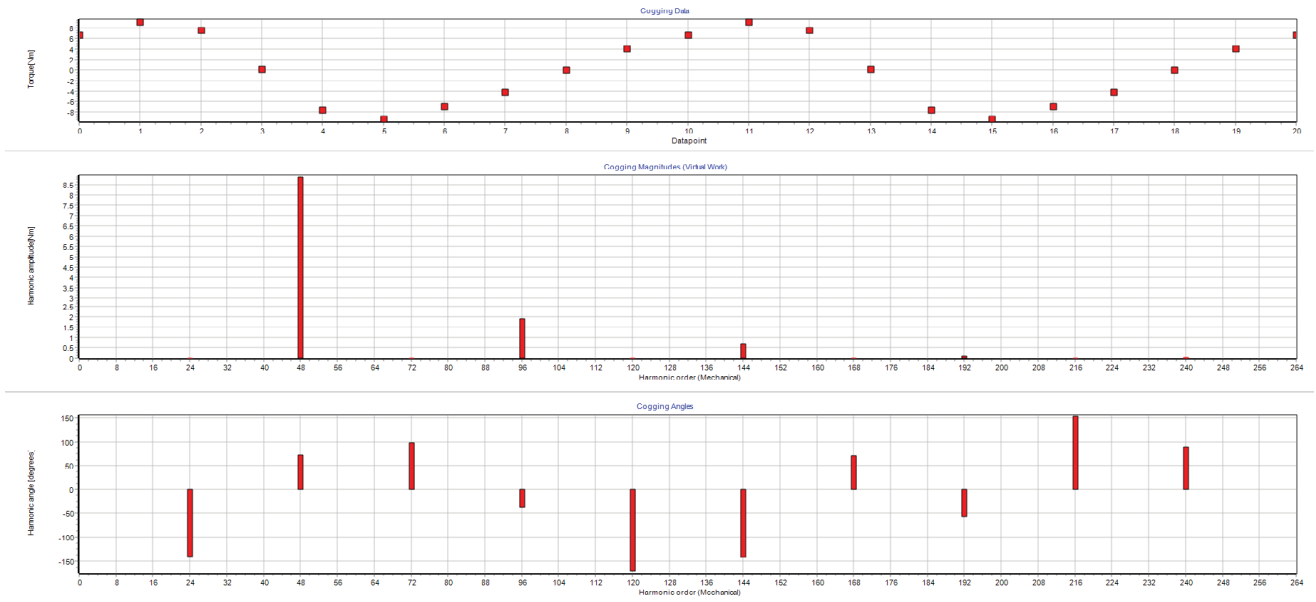


Figure 31 harmonic spectrum of cogging torque

Finally, the torque and power are plotted against the speed for different phase advance values. It can be seen that torque remains constant at lower speed and reduces gradually as the speed increases, whereas power increases with the speed (rpm). The torque peak will occur at a substantially lower RPM than the power peak. The reason is that, in general, the torque curve does not drop off (%-wise) as rapidly as the RPM is increasing (%-wise). That positioning of the torque curve would allow the engine to produce significantly more power if it could operate at a higher RPM, but the goal is to optimise the performance within the operating range.

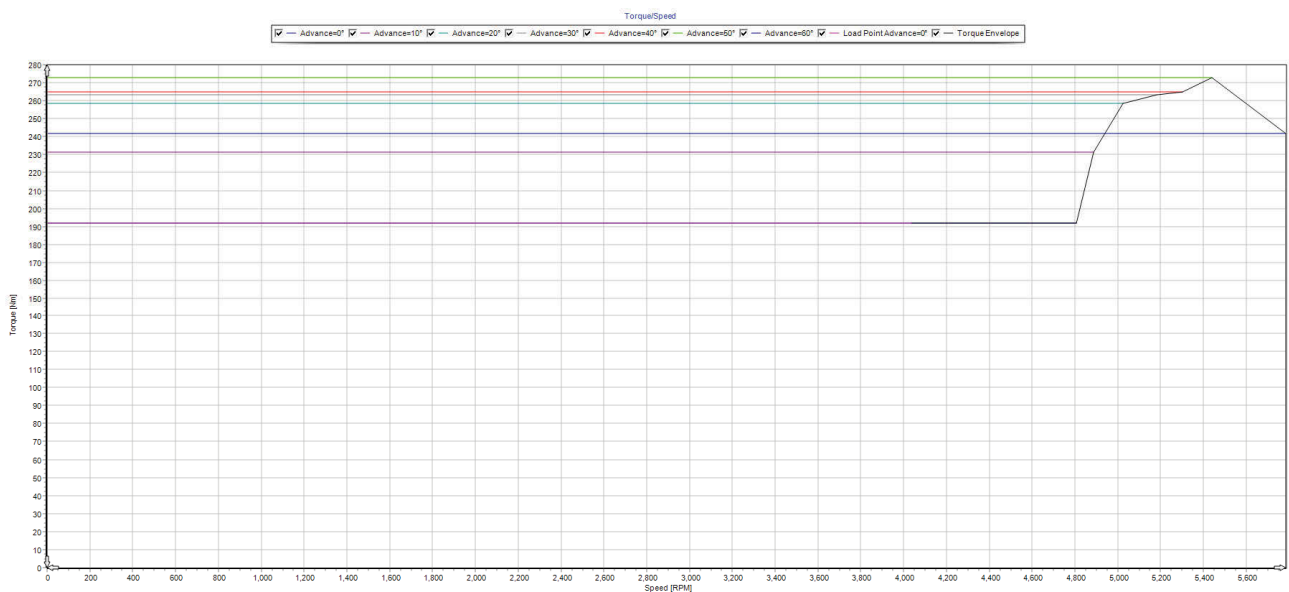


Figure 32 speed vs. torque

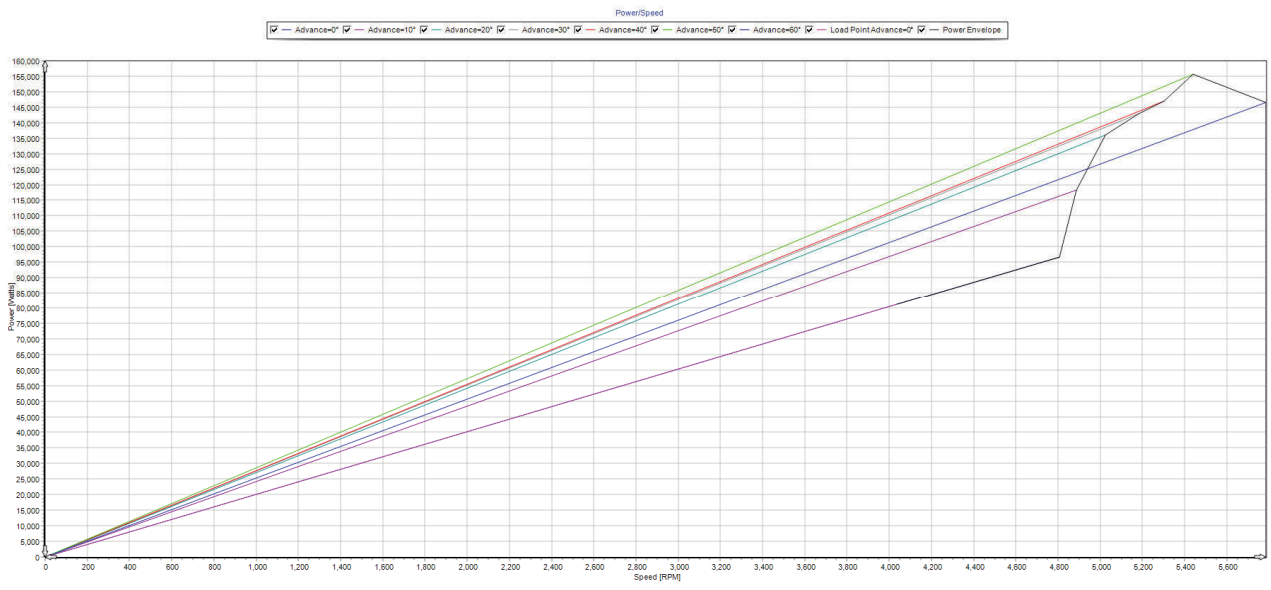


Figure 33 speed vs. power

4.6. Thermal analysis of machine

Compared with the conventional permanent magnet (PM) machine, the high-speed PM machine has smaller size and larger power density. However, owing to high-speed high frequency and low volume, the PM rotor is more easily to become overheated so that irreversible demagnetization of the PM is induced. Traditional cooling methods of the machine directly cool the machine stator; the temperature rise of the rotor is reduced through heat exchange among stator, air gap and rotor. Owing to rapid temperature rise of the high speed PM machine rotor, the method of indirect cooling rotor does not adequately protect the PM rotor from overheating (Xing et al. 2012). To directly reduce the temperature increase in the winding and the rotor of the machine we will use self-ventilated with the water jacket as the main cooling method to control the temperature.

In thermal the main cooling options are defined, and the final results are obtained using the lumped thermal circuit at steady state. Duty cycle operation is a specific feature, directed to analyse specific exploration regimes. To perform the necessary sensitivity analyses and check the critical cooling paths is more easy and quick to look at steady state operation. Then, since the cooling is defined, the duty cycle analysis can be performed

4.6.1. Housing and end-caps

Machine's overall weight is an essential requirement in this design, light weight and smoother material should be used for housing of the machine. Aluminium is the best candidate which is smoother and lighter in weight so we can use it for the housing and end-cap material. Another important issue to be considered is winding impregnation. Its main function is to improve the thermal conductivity of the winding and to reduce the hot-spot value. Also provides the reinforcement, protecting the machine from moisture, dirt and chemicals.

Motor-CAD offers different options in liquid cooling. For instance, rotor water jackets may be the option, but its implementation is very costly. Another option is to use slot water jackets but again the mechanical manufacturing becomes complicated and expensive. One possibility is to use the wet rotor and spray cooling; both have a more fluid concentration in the rotor parts and end windings rather than stator parts. The optimum method is to use water jackets in housing which can extract heat from active windings and end windings in the end space region as well. Moreover, by using the water jackets in the housing cooling process turns more standard and cheaper to implement as well.

The geometry of the machine after setting up the cooling method can be viewed in radial axial and 3D view below.

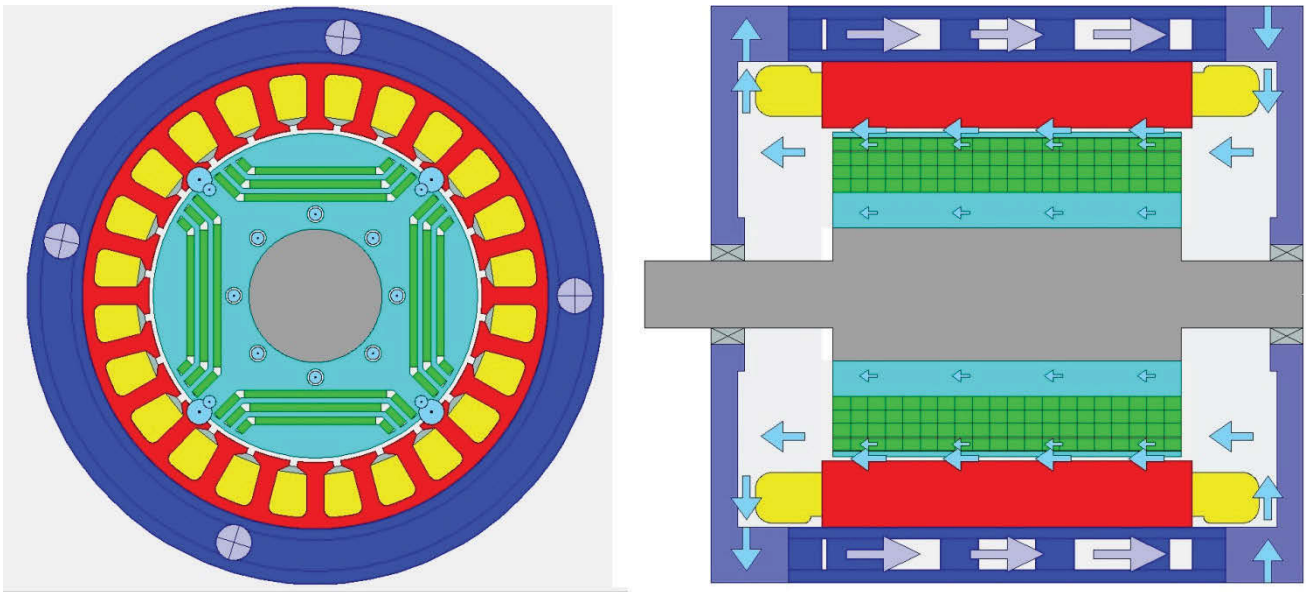


Figure 34 Radial & Axial thermal view

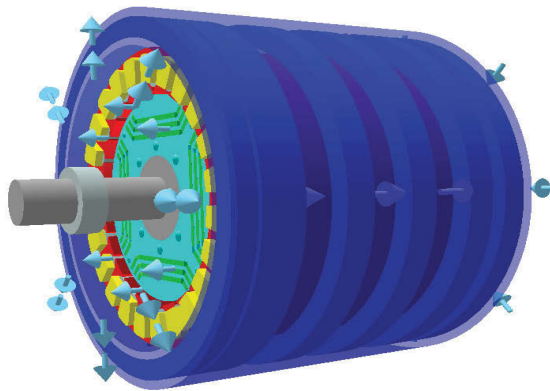


Figure 35 3D thermal view of the machine

4.6.2. Winding

Before the configuration of the water jackets, it is important to define the winding layout model. Generally, the windings stay same as in e-magnetic model just one change has been done, and the winding view has been changed to cuboids. Possible placement of the conductors in the slot needs to be checked. Winding editor can be used to modify the position of conductors, liner thickness, and

impregnation goodness, etc. here multiple strands in hand will be utilized; the larger number of strands will not affect the temperature rise if the same slot-fill is used.

Motor-CAD calculates slot temperature rise using the 3-D network of thermal resistance. Cube size and effective thermal conductivity automatically calculated from conductor positions, slot fill and materials used. These cuboids are drawn within the slot in the Winding tab and as part of the thermal network in the Circuit Editor.

Cooling options are set in input data tab. The cooling system is set as water jacket and self-ventilated. The ambient temperature for convection and radiation is set to 65 °C. The material, interface, radiation material convection values remain the same as default. Only the unit of volume flow rate is changed l/min. The fluid flow in water jacket is configured as constant flow and set to 5 l/min. in cooling options; fluid flow is set up to active cooling with non-spiral ducts.

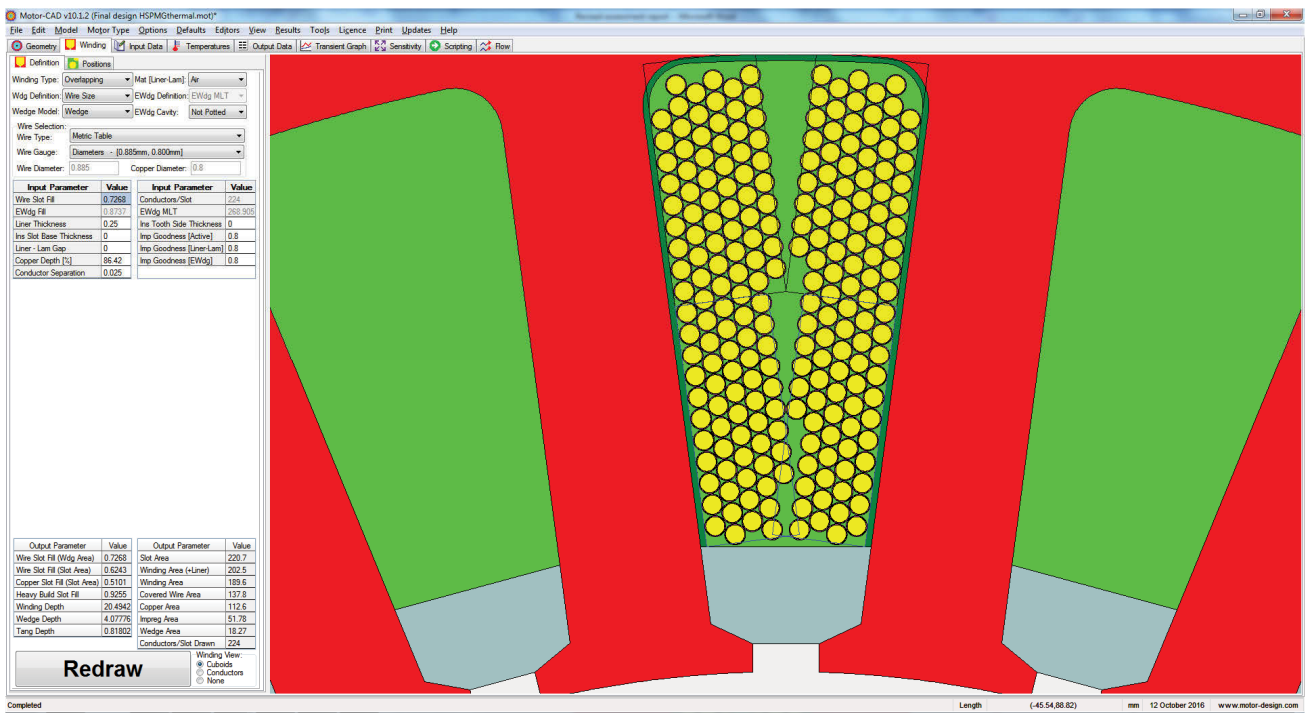


Figure 36 thermal design winding

4.6.3. Cooling method

There are two cooling methods which are used primarily in this design.

1. Liquid cooling
2. Self-ventilated

Liquid cooling which is used as the primary cooling method in this model is useful to meet the high torque densities and desired overload capabilities. However, a liquid jacket alone is often inadequate to remove the heat from the stator windings and the rotor, because of the high thermal resistivity between the heat source and the coolant. The thermal resistance of the stator yoke, the contact thermal resistances, and the low thermal conductivities of the insulated stator winds and the internal air together cause a significant temperature difference between the coolant and the stator winding. In addition to liquid cooling, forced air flow to cool the rotor structure of a dual mechanical port machine, as the liquid jacket has only a minor influence on the rotor temperatures (Polikarpova et al. 2015).

4.6.4. Natural convection

This process defines heat transfer between housing and ambient. Convection Correlations based on Simonson's formula is applied to different machine parts, depending on their geometry. For housing and radial area of end-caps are used the correlation to a horizontal cylinder, and for the end cap axial area is applied the correlation to a vertical flat plate. In rigour, could be considered a forced convection cooling between the housing and ambient based on-air displacement due to the car moving, which defines a blown over the system. However, since the main cooling path is the liquid cooling, that modulation is not expected to affect too much the final result. Besides that, it introduces more complexity in the modulation process (Marques).

4.6.5. Losses

Losses and temperature in PM machines have interrelationship, and they are dependent on each other, so their relationship must be defined. Lumped thermal circuit can describe both components by two nodes.

Iron losses are divided between the losses developed in the teeth and yoke. To give a more physical meaning of temperature gradient along the teeth, it is represented by three nodes, this means that total teeth losses are divided by 3 and applied in each node, while the yoke losses are inputted directly in the stator yoke node. Rotor iron losses are applied to the rotor node and the same with the magnet losses. Copper losses are split between active and end windings according to formulations based on the winding layered model. There are two nodes for each end winding, front and rear and losses are divided

between them according to their volumes. The first calculation to define the cooling system is done at steady state operation. The best approach is to consider that machine has to develop constant torque at steady state and the loss variation takes into account the temperature and load, according to explanations and formulations referred in earlier sections (Marques).

4.6.6. Steady state thermal analysis

In Motor-CAD, we can put together to represent the heat transfer in the machine. This is then solved to calculate the steady state or transient thermal performance. A set of non-linear simultaneous equations are solved for the steady state, and an integration technique is used to solve the transient. The temperature at all nodes in the thermal network is calculated together with the power through all the thermal resistances (Tassi, Zanolchi & Staton 2006).

The thermal network for Motor-CAD is quite sophisticated with 32 nodes. This is shown in Fig. 37; the five nodes below represent the nodes closest to the measured nodes and were chosen as being suitable for comparison (Dorrell et al. 2006).

- Winding Layer – winding slot
- Housing (active) – frame
- Stator Tooth – tooth
- End Space (Rear) – end winding
- End Cap (Rear) – end cap
- Shaft (front) – shaft at standstill

The figure below shows the temperature-schematic with steady state temperatures. The predicted average winding temperature is 112 °C. The predicted magnet temperature is 107 °C. These values are below the initial estimated values of temperatures.

4.6.8. Slot finite element analysis (FEA)

In motor-CAD conduction heat transfer in the stator slot can be calibrated. The figure below shows the result with minimum, average and maximum winding temperature of 105°C, 107°C, and 112°C respectively. Good match of temperatures in the slot with minimum, average and maximum winding temperature can be verified in the figure below after solving the slot FEA.

Slightly different results may come if the distribution of the conductors is different in the slots. Large average and maximum temperature giving a closer match to the analytical solution as the conductor touching the slot liner move towards the slot centre.

Motor-CAD

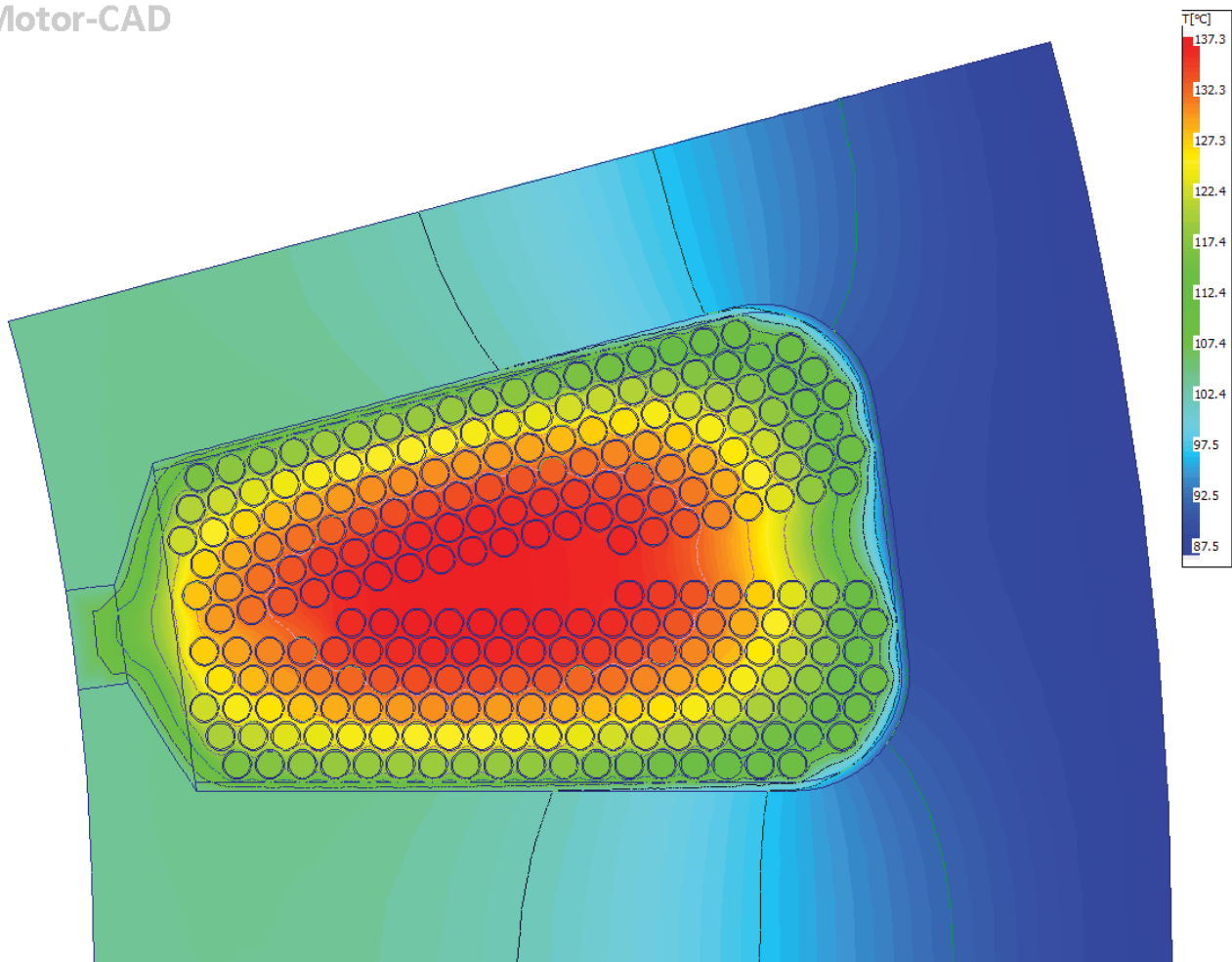


Figure 39 2D FEA prediction of steady-state temperature in the stator slot

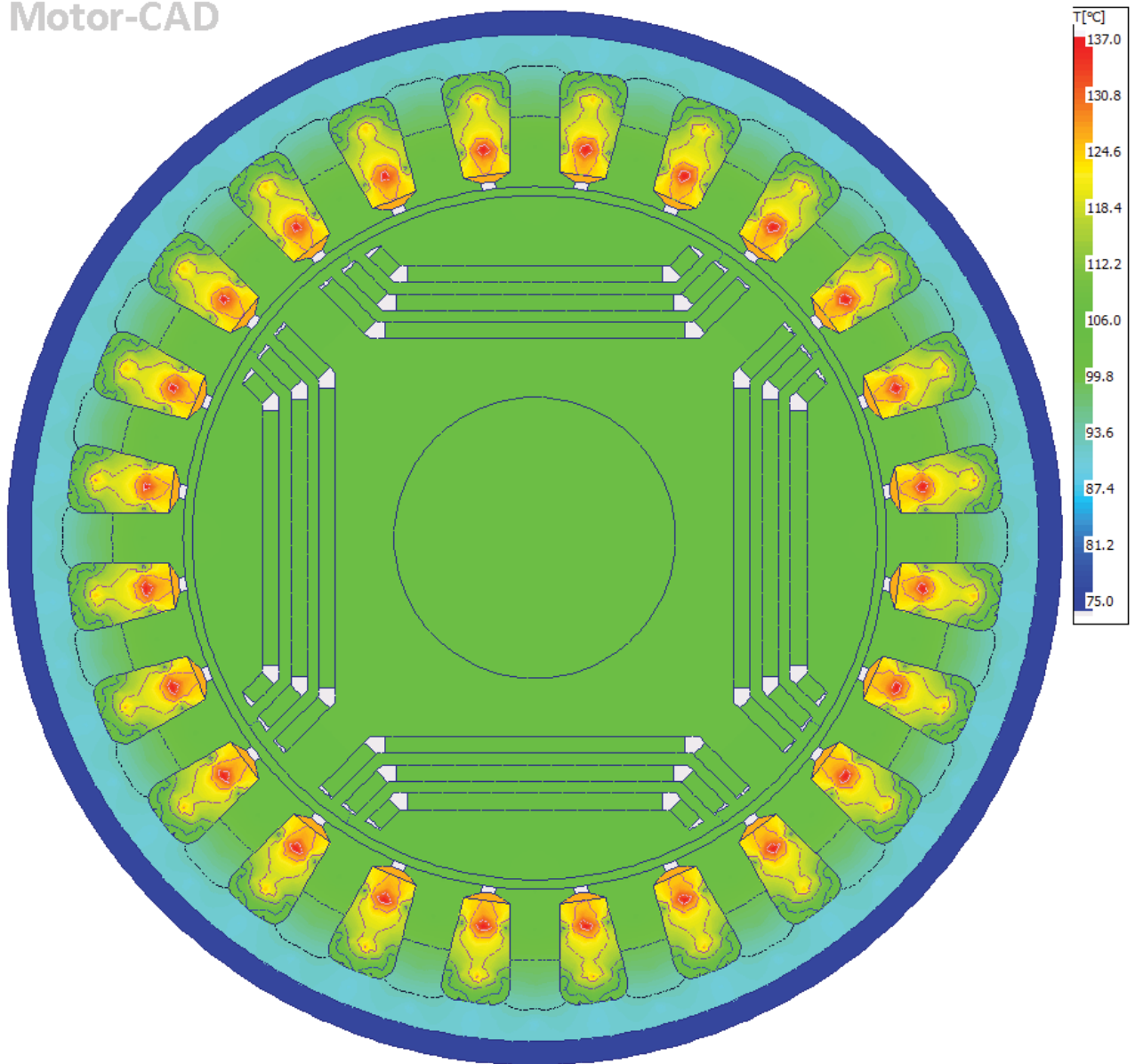


Figure 40 Axial view of steady-state temperature in the stator slot

4.7. Performance Charts

In a machine design, it is important to appraise machine performance across the entire torque-speed envelope that can include a field weakening region. Design optimisation of this performance is challenging as all CAD tools available, like PC-BDC, only provide analysis at individual working points. It's, therefore, useful a computationally efficient technique that allows for rapid and accurate modelling of the entire operational envelope of any HSBPM machine. Such solution was found with Motor LAB software from Motor Design Ltd©, a software package that takes advantage of Windows ® Active X to connect PC-BDC and Motor-CAD. It performs the calculation of torque-speed characteristics, loss and efficiency maps that can be used in an iterative design process.

4.7.1. Fixed inductance model

In fixed induction model is possible to calculate the torque-speed characteristic constrained by maximum voltage available from the inverter and considering a linear inductance approximation to describe flux linkage. It's a computationally efficient calculation that provides accurate iron loss prediction at any operating point from only two time-stepping FEA calculations: at a short circuit and open circuit. This avoids the typical computationally intensive methods to calculate iron losses at single points, even more, when a large number of operating points are needed for entire envelope. This method simplifies that procedure with exquisite improved results. More details can be consulted in (Goss et al. 2012; Mellor, Wrobel & Holliday 2009).

Performance graph obtained in fixed inductance model are considering the maximum speed of 60,000 RPM; the current varies in 4 steps until it reaches its maximum value. The result is shown below in the figure.

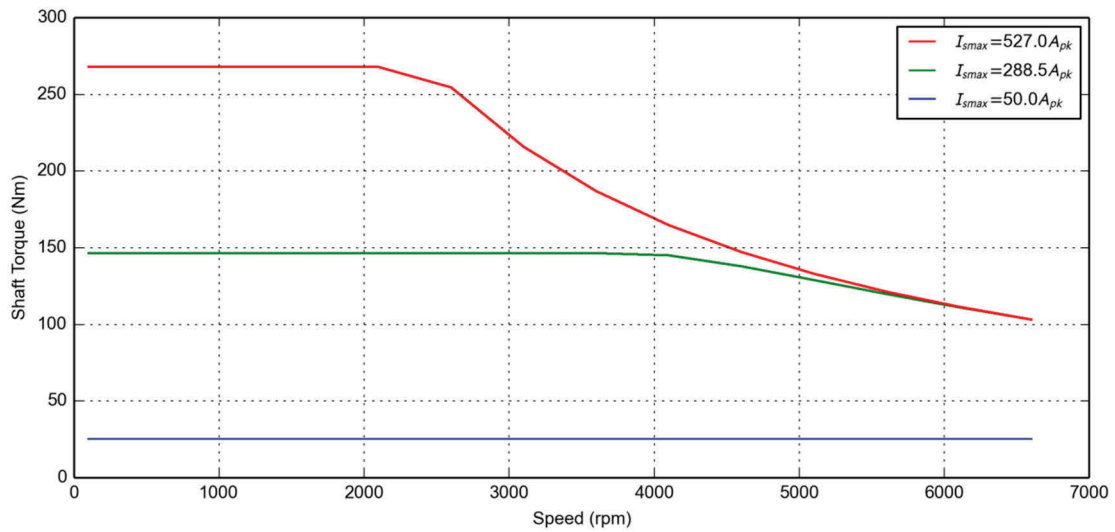


Figure 41 Performance chart: torque vs. speed

It's seen that around of corner speed the maximum torque developed with peak current is 250 Nm, much higher than expected. Comparing these results with saturation and cross coupling modelling could be useful to understand its viability.

4.7.2. Efficiency Maps

In motor-lab it is possible to plot the efficiency characteristics against the full torque speed, we will get efficiency map. Efficiency map is very useful to get the ideal region of efficiency where the design is laying. At high speeds operations, we may get a larger spectrum of efficiency. This is because of copper losses are higher at lower speeds. Therefore, at high speeds, the losses are decreased and efficiency increases, as can be seen in losses map in the figure below. It can be seen that efficiency of 94% can be achieved in a larger spectrum between the speed of 30,000rpm and 60,000rpm.

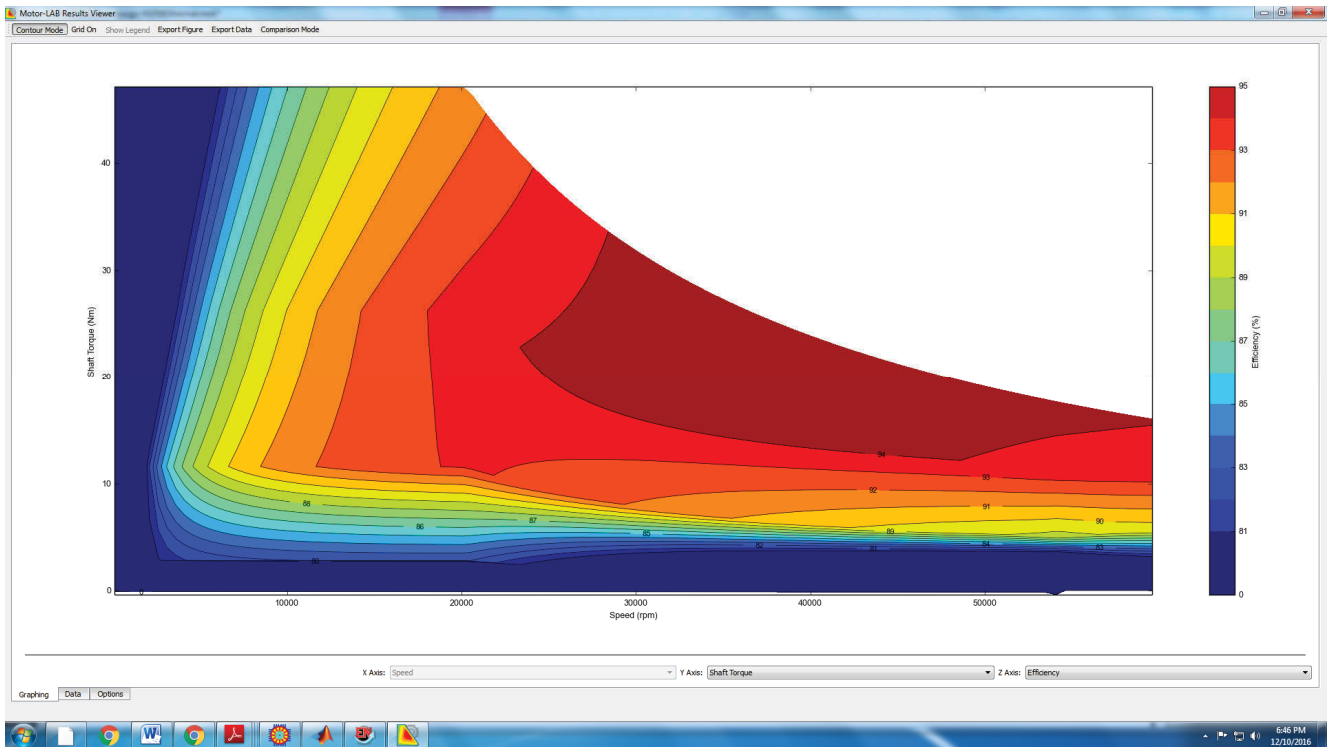


Figure 42 efficiency map of the machine

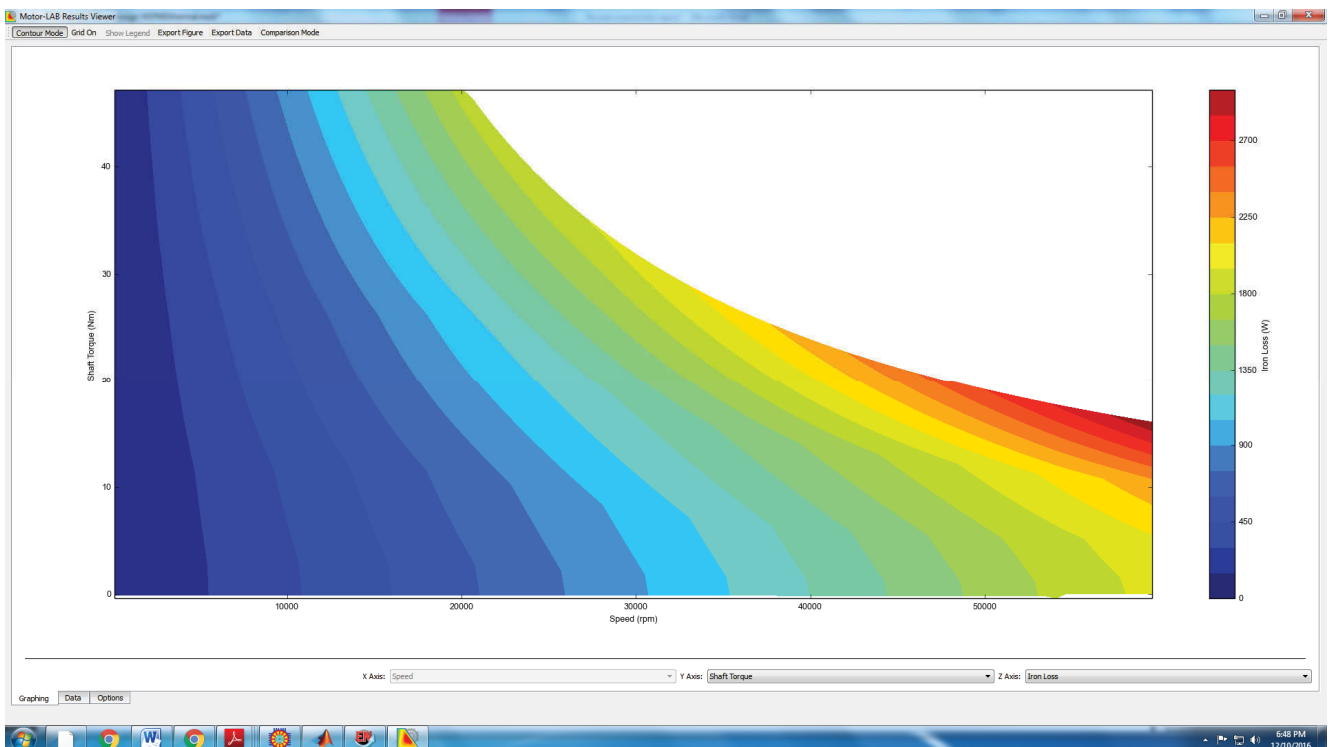


Figure 43 iron losses map

The contour plot shows a big area between 90 and 95% of efficiency which is a very good result; mainly in peak power at corner speed where machine attains approximately 91%. In autocross competition, the average power is 16 kW, and contour plot shows that is possible to attain such result with efficiency superior to 90% between 50,000 RPM and 60,000 RPM. This is a very comfortable margin and gives good perspective for fuel economy competition.

Chapter 5

5.1 Conclusion

This work presents the complete virtual prototyping of a brushless high-speed PM machine with interior magnets. This design was made after an intensive research in the last six months to achieve the necessary knowledge and tools to fulfil the team requirements in the project after a first approach not so well succeeded.

This prototype meets all the specification requirements given, in the peak power and weight. It has the power density very close to the other machines already constructed by another formula student teams. It was possible to check the advantage of use this cylinder rotor type, mostly regarding weight because with this geometry it's possible to avoid a rotor with a massive iron. In the electromagnetic point of view, the torque ripple attained could be considered acceptable for this application. Although electromagnetic noise and vibrations can result, this kind of subject isn't as important as with servomotors design or other applications where high position precision is required.

To eliminate the cogging torque, a skew angle was needed, and the results were good not only in the cogging cross off but also in the filtering effect of the harmonic content relative to the air gap field. This enables a sinusoidal flux linkage and a better EMF waveform, reducing the initial torque ripple. Another important issue about the fractional slot winding was the guarantee of an unbalanced magnetic pull in the rotor to avoid mechanical problems, which was achieved in the final design.

In the cooling system, the sensitivity analysis performed let concluded not only about the ideal dimensions of water jackets channels but also to the main constraints in the machine construction. The robust analysis made indicate a significant dependence on the winding temperature of interface gap between housing and stator lamination. This effect can be mitigated using heat sink paste to reduce this interface. In the ducting system, the water velocity and the pressure drops across the housing channels have very good values, according to the average duct wall roughness considered in the aluminium alloy used. So, there is no problem with particles in the fluid to wear away the surface. The intensive cooling strategy and the thermal class of the machine, improved with self-ventilation, allowed achieving the high-power density. A great behaviour in the thermal limits was proven.

The superior limit peak performance is 6.5kW @ 600000 RPM for 80 seconds, which is a superb result for a machine with 42 kg. It's important to note that such accomplishment is only possible due to the

iron-silicon alloy used in the project and sintered NdFeB magnets. Such high-power densities in small machines require low loss irons as well as high saturation polarisation. At the same time, big values of B_r are needed to attain high values of open circuit field in the air gap and with it. The sintered NdFeB magnets are the strongest and should be used to accomplish these goals.

5.1 Future work

The presented design is based on simple electromagnetic and thermal assumptions, developed sophisticated tools and tested with software already used in other motoring applications in the industry. Nevertheless, more work can be done in this subject but with a different approach.

Different ways of investigating optimum design is being developed all around. One good example is BCS software from SPIN Company at Italy. They use SPEED software to achieve the optimum electromagnetic design, based on the definition of design variables, constraints and objectives.

It's possible to avail some of the benefits in the software used, mainly with Active X interface, to make some scripting in order to integrate the thermal and electromagnetic design together, working with SPEED and MOTOR CAD as a black box using MATLAB® or Microsoft® Excel. The FEA calibration could be done using PC-FEA embedded solver which permits to calibrate the SPEED analytical models in EM design, constrained to one or more objective functions. At the same time, MOTOR-CAD updates the SPEED thermal model and with this became possible to automate the iterative design.

Such application could boost the machine project, exploring other solutions to the team in less time. For example, another interior magnet machine like V-shaped magnet or the classical IPM with slits used to buried the magnets in rotor slots and protect them better against magnet losses. The goal is to find the best configuration with less weight, given some initial constants, constraints and define the objective function to achieve the goal established. Comparing the final results, it could be interesting to check what the best machine is: the one with non-massive rotor steel like used in this design or other IPM with high saliency and slits? In the answer might be the next machine development.

6 Appendix A

ate

Antriebstechnik und Entwicklungs GmbH
 Brandenburger Str. 10
 D-88299 Leutkirch im Allgäu

Torque Motoren *direct drives*

MS

Innenläufer <i>internal rotor</i>		Kundenspezifisch projektierte Motoren <i>customized projected motors</i>		
Drehmoment - max. Drehzahl / <i>torque - max. speed</i>				
Typ / type D1/L _{FE} /Polzahl D1/L _{FE} /number of poles	Nenn Drehmoment rated torque S1 [Nm]	max. Drehzahl max. speed [min ⁻¹ /rpm]		Bemerkungen remarks
MS 30 / 50 / 8	0,223	1.000		Höhere Drehzahlen und Drehmomente auf Anfrage <i>higher speed and torque to be inquired</i>
MS 35 / 50 / 8	0,5	1.000		
MS 42 / 180 / 6	2,5	26.000		
MS 60 / 60 / 8	2,8	12.000		
MS 60 / 30 / 22	1,75	2.000		
MS 80 / 80 / 8	9	5.000		
MS 100 / 95 / 22	29	2.000		
MS 140 / 22 / 44	12	1.500		
MS 140 / 100 / 22	51	1.200		
MS 210 / 70 / 38	150	3.000		
MS 210 / 70 / 44	175	480		
MS 220 / 290 / 38	600	2.000		
MS 340 / 100 / 66	620	800		
MS 370 / 450 / 38	2.400	800		
MS 450 / 200 / 38	2.000	1.500		
MS 520 / 150 / 88	2.000	500		
MS 580 / 300 / 38	5.000	2.000		

Hauptabmessungen / <i>main dimensions</i> [mm]							
Typ / type	Statorabmessungen <i>stator dimensions</i>				Rotorabmessungen <i>rotor dimensions</i>		Bemerkungen <i>remarks</i>
	D1	D2	WK1	WK2	d6		
MS 30 / 50 / 8	30	16	12	10	12		
MS 35 / 50 / 8	35	20	13	11	16		
MS 42 / 180 / 6	42	28	12	10	17		
MS 60 / 60 / 8	60	41	15	14	32		
MS 60 / 30 / 22	60	44	12	10	38		
MS 80 / 80 / 8	80	55	18	14	45		
MS 100 / 95 / 22	100	65	19	16	56		
MS 140 / 22 / 44	140	100	17	13	77		
MS 140 / 100 / 22	140	90	20	18	60		
MS 210 / 70 / 38	210	170	21	19	140		
MS 210 / 70 / 44	210	170	21	19	140		
MS 220 / 290 / 38	220	170	35	19	140		
MS 340 / 100 / 66	340	280	35	25	240		
MS 370 / 450 / 38	370	280	50	35	220		
MS 450 / 200 / 38	450	346	45	35	300		
MS 520 / 150 / 88	520	450	40	30	400		
MS 580 / 300 / 38	580	446	50	50	380		

Die angegebenen Werte sind Richtwerte und basieren auf Wasserkühlung. Abweichende Baulängen sind möglich. Das Drehmoment ändert sich entsprechend zur Baulänge.
 Nennleistung / Nenn Drehzahl und Arbeitspunkt werden kundenspezifisch angepaßt und in Datenblättern definiert.
 Values are approximated values and are based on water cooling. Different lamination lengths are possible. The torque will change according to the lamination lengths. Rated power / rated speed and operating point to be customer specified in the technical datasheet.

Technische Änderungen vorbehalten *Subject to technical change without notice*

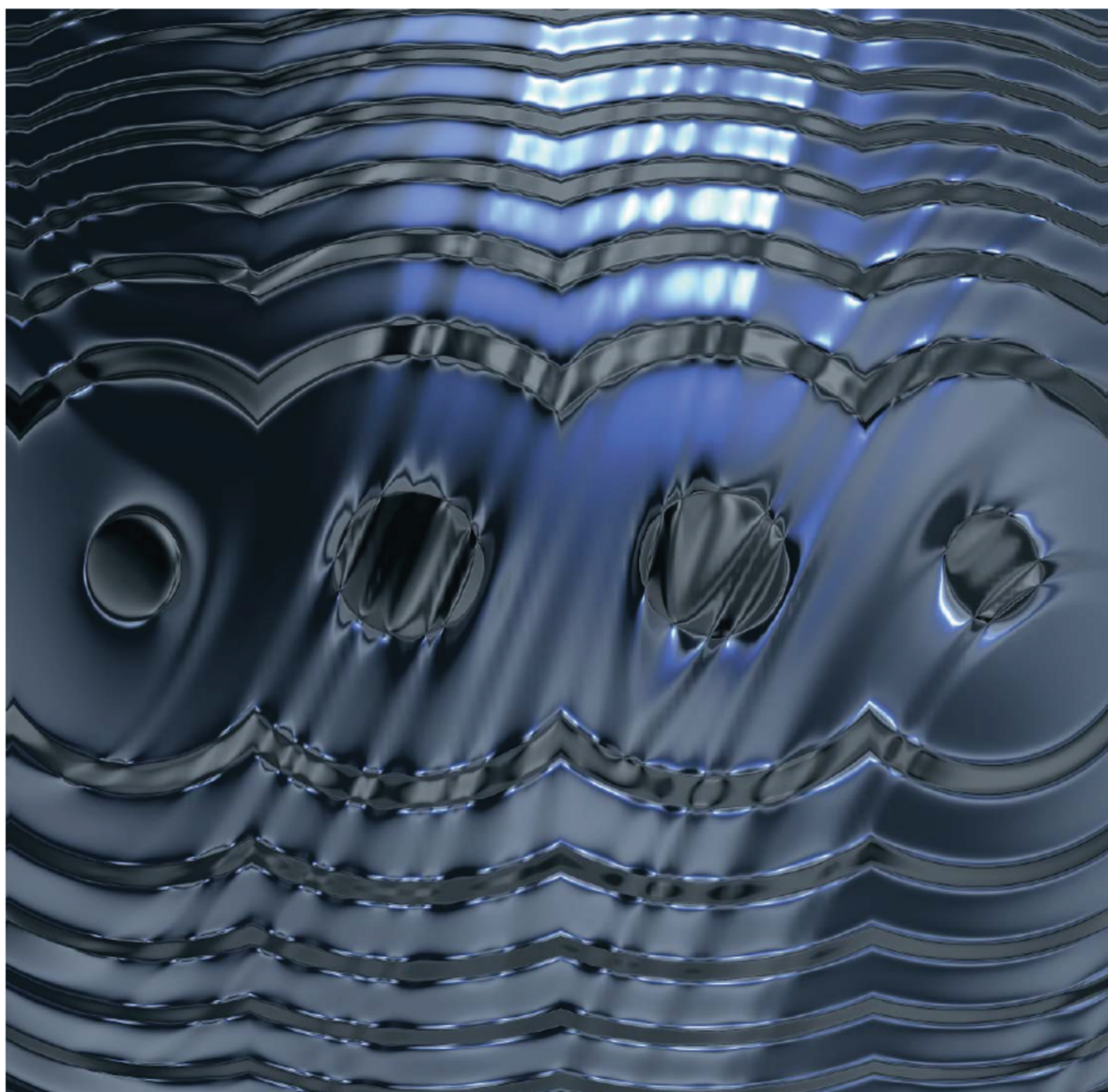
November 2007

1



Super Core™

Electrical steel sheets for high-frequency application



JFE Steel Corporation



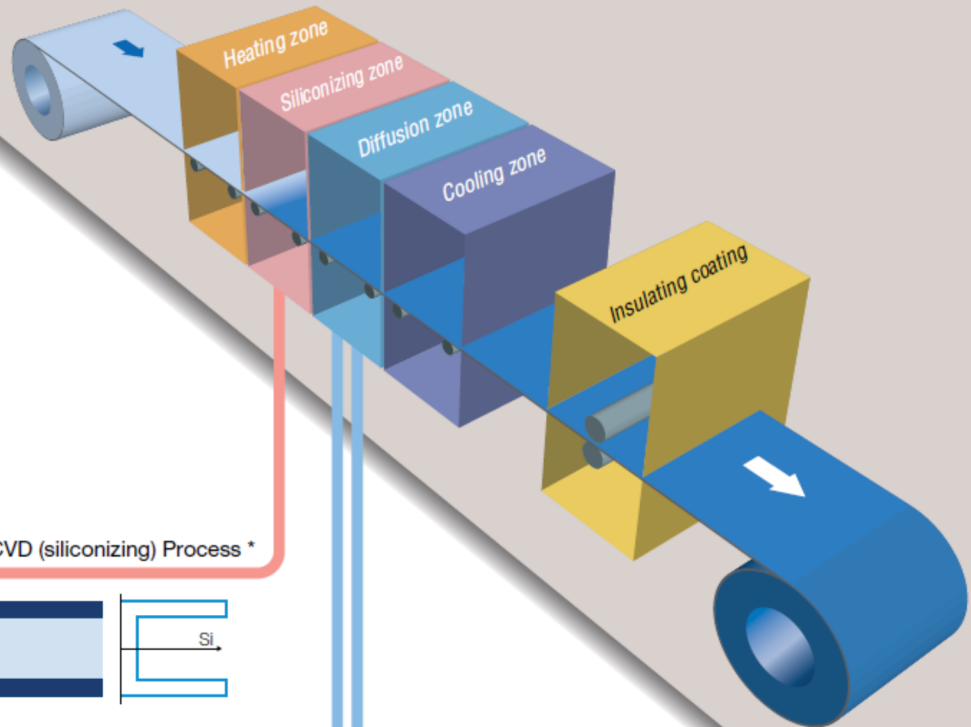
Super Core™

Super Core™ is manufactured using an innovative process that is completely different from that for conventional silicon steel sheets. These are the highest grade, non-oriented magnetic steel sheets available.

Conventional silicon steel sheets have a Si (silicon) content of 3.5% or less. It has long been known that the magnetic characteristics of a silicon steel sheet improve as the Si content increases, peaking at 6.5%. However, it has been impractical to produce thin steel sheets with a Si content of over 3.5% because the steel tends to harden and become brittle. In 1993 JFE Steel solved this production problem through the adoption of a process called the CVD process, and successfully introduced the first 6.5% Si steel sheets (JNEX-Core) to the world.

In order to meet new demands, this technology has continued to be developed, leading to the commercial production of gradient high-silicon steel sheets with superior high-frequency characteristics (JNHF-Core).

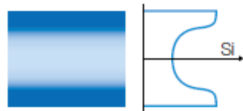
Super Core™ Production Process



CVD (siliconizing) Process *



Concentration distribution control diffusion process



JNHF-Core

Gradient high-silicon steel sheet with low silicon content at the center portion and 6.5% silicon near the outer surface areas

Uniform diffusion process



JNEX-Core

6.5% silicon steel sheet. (A high-silicon steel sheet with a uniform silicon content of 6.5% throughout the sheet)

* CVD Chemical Vapor Deposition

• Super Core is a registered trademark or trademark of JFE Steel Corporation in the United States and other countries.



JNEX-Core

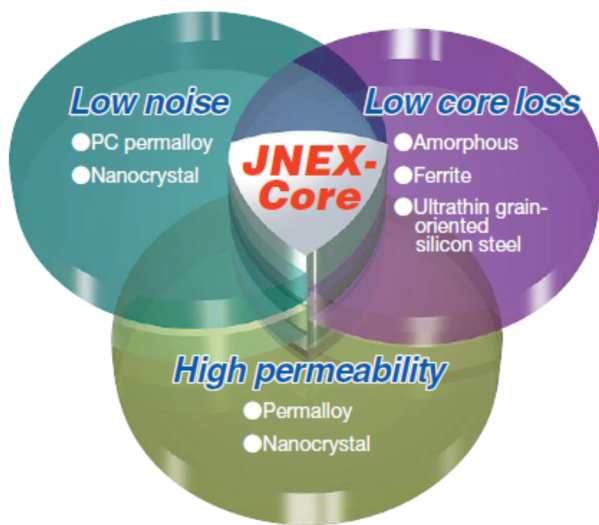
JNEX-Core is the highest-grade non-oriented magnetic steel sheets manufactured with a production method (CVD process) that is completely different from that for conventional silicon steel sheets, allowing a previously impossible Si content of 6.5%.

Low Core Loss

Core loss in high-frequency ranges is extremely low. This allows for low heat generation and size reductions for magnetic components such as high-frequency reactors and transformers.

Low Magnetostriction

Magnetostriction which causes noise and vibration is nearly zero. This enables significant noise reductions for magnetic components such as reactors and transformers.



High Permeability

The permeability is extremely high across a wide range of frequencies, making it highly suitable for use in shield applications and CT.

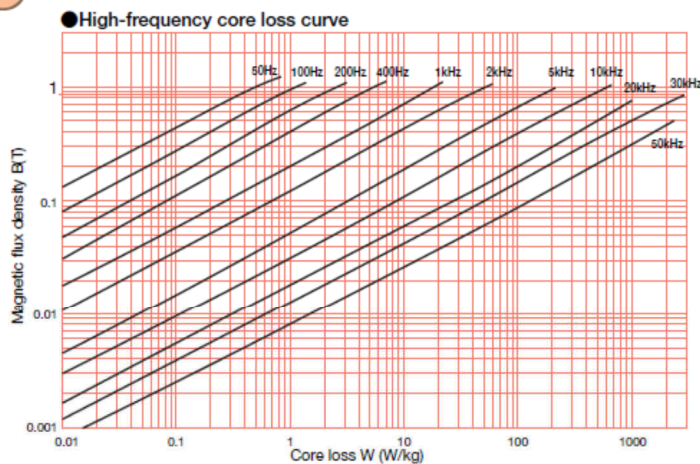
Stable Quality

The high-temperature processing provides thermal stability. Since there is minimal deterioration of the properties due to machining, so stress-relieving anneals are not required.

Non-oriented

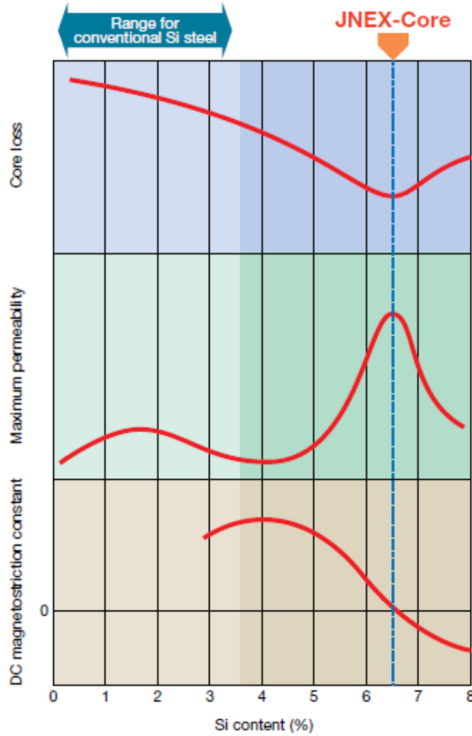
There is virtually no difference in the characteristics between the rolling direction (L-direction) and the transverse (C-direction). Therefore, this can be used in a wide range of applications, from stationary machines to rolling machines.

10JNEX900



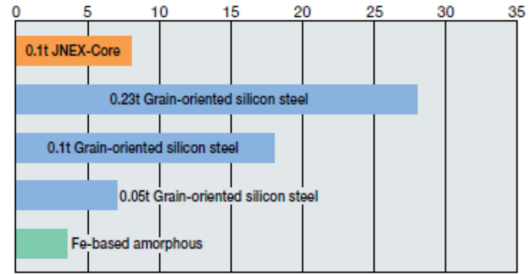
Measurement : 25 cm Epstein test
Rolling direction, shear cross-section

Variation in magnetic properties of silicon steel by Si content

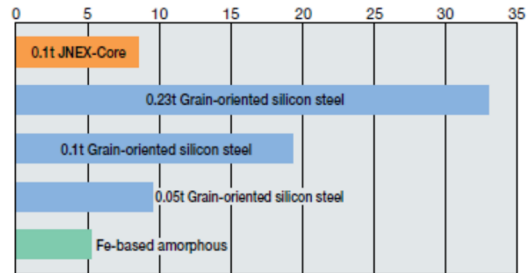


Characteristics

Material core loss W1/10k (W/kg)* (in-house data)



Cut core (CS500 core loss W1/10k (W/kg)* (in-house data)



* W1/10k is the core loss at 10kHz, 0.1T(=1kG) when the magnetic flux sine wave is excited.

Sample Characteristics Table

Comparison of magnetic characteristics (JFE in-house data) : Rolling direction, shear cross-section

Material	Thickness (mm)	Specific resistance ($\mu\Omega\cdot m$)	DC max relative permeability	Saturation magnetization (T)	Magnetic flux density B_8 (T)	Magnetic flux density B_{25} (T)	Magnetostriction $\lambda_{10/400}$ ($\times 10^{-6}$)	Core loss (W/kg)						
								W10/50	W10/400	W10/1k	W5/2k	W2/5k	W1/10k	W0.5/20k
JNEX-Core	0.10	0.82	23,000	1.80	1.29	1.40	0.1	0.5	5.7	18.7	13.7	11.3	8.3	6.9
Grain-oriented silicon steel	0.05	0.48	—	2.03	1.75	—	-0.8	0.8	6.4	17.2	13.5	9.2	7.1	5.2
	0.10		24,000		1.84	1.91		0.7	6.0	22.7	22.0	20.0	18.0	14.0
	0.23		92,000		1.92	1.96		0.3	7.8	35.0	33.0	33.0	30.0	32.0
	0.35		94,000		1.92	1.96		0.4	12.2	55.0	49.5	49.5	47.0	49.0
Non-oriented silicon steel	0.10	0.57	12,500	2.05	1.58	—	7.8	0.8	8.5	27.1	22.4	16.5	13.3	—
	0.20		15,000	2.03	1.44	1.53		0.7	11.0	38.5	33.2	26.2	23.0	—
	0.35		18,000	1.96	1.45	1.56		0.7	14.4	62.0	50.2	38.0	33.0	—
Fe-based amorphous	0.025	1.30	300,000	1.50	1.38	—	27.0	0.1	1.5	5.5	8.1	4.0	3.6	3.3
Ferrite	Bulk	—	3,500	—	0.37	—	21.0	—	—	—	—	2.2	2.0	1.8

* W10/50 is the core loss at 50Hz, 1T(=10kG) when the magnetic flux sine wave is excited.

* B_8 is the magnetic flux density at 800A/m.

* $\lambda_{10/400}$ is the magnetostriction at 400Hz, 1T when the magnetic flux sine wave is excited.

JNHF-Core

For the JNHF-Core, the siliconization technology (CVD process) used for JNEX-Core has been further developed, leading to even greater lower core loss in the high-frequency ranges.

Low Core Loss

For high-frequencies in excess of 5 kHz, outshines even JNEX-Core for low core loss.

Highly Workable

Excellent workability for pressing, bending, stamping, etc.

Non-oriented

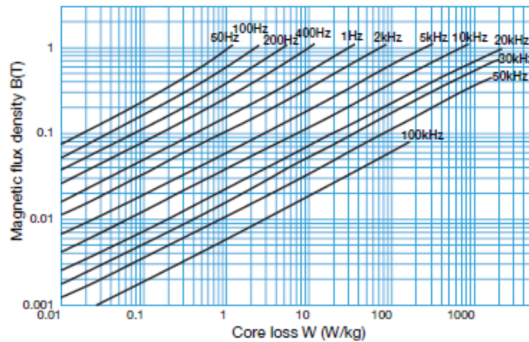
There is virtually no difference in the characteristics between the rolling direction (L-direction) and the transverse direction (C direction). Therefore, this can be used in a wide range of applications, from stationary machines to rolling machines.

High-saturation magnetic flux density

Has a high saturation magnetic flux density of 1.85 ~ 1.94 T Using this material in a reactor takes full advantage of the superior DC superimposition characteristics.

10JNHF600

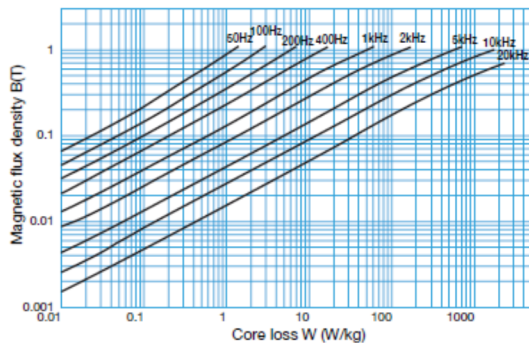
High-frequency core loss curve



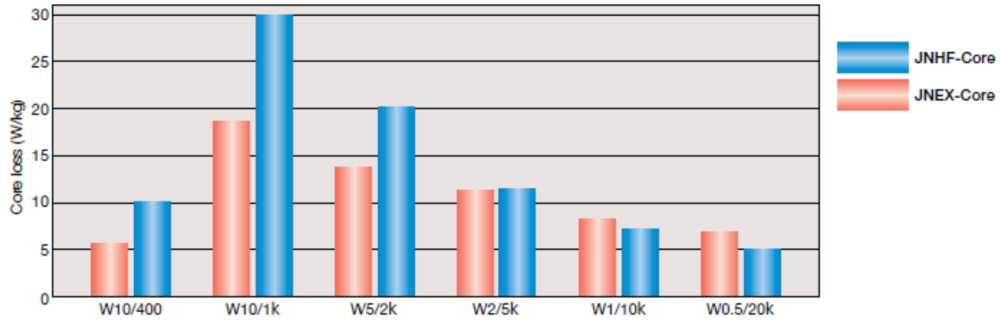
Measurement: 25 cm Epstein test
Rolling direction, shear cross-section

20JNHF1300

High-frequency core loss curve

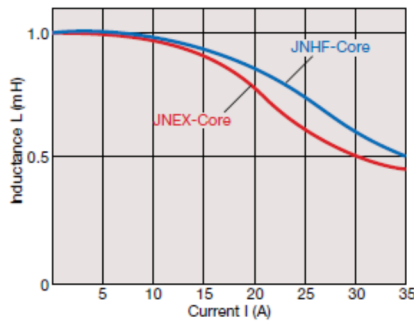


Core Loss Comparison between JNHF-Core and JNEX-Core (0.10 mm thick)



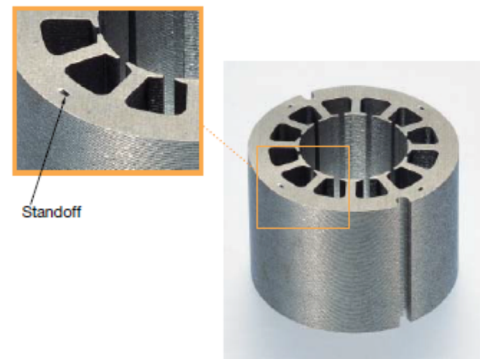
* W10/400 is the core loss at 400Hz, 1T(=10kG) when the magnetic flux sine wave is excited.

Comparison of reactor DC superimposition characteristics



* Using a multi-layer block core (sheet thickness 0.1 mm)
 * 20 kHz, 0.05 T equivalent ripple current applied

Press machined sample (0.2 mm thick)



Sample Characteristics Table

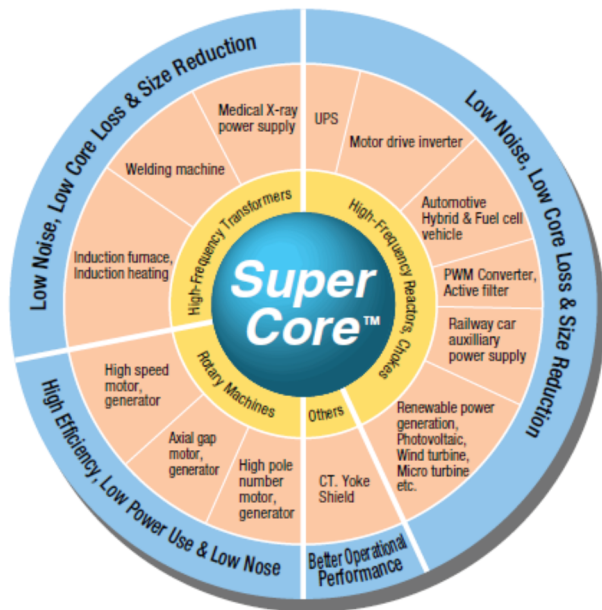
Comparison of magnetic characteristics (JFE in-house data) : Rolling direction, shear cross-section

Material	Thickness (mm)	DC max relative permeability	Saturation magnetization (T)	Magnetic flux density Bs(T)	Magnetic flux density Bcs(T)	Core loss (W/kg)						
						W10/50	W10/400	W10/1k	W5/2k	W2/5k	W1/10k	W0.5/20k
JNHF-Core	0.10	4,100	1.88	1.15	1.44	1.1	10.1	30.0	20.2	11.5	7.1	5.0
	0.20	3,900	1.94	1.09	1.47	1.2	14.5	51.6	29.1	17.9	12.7	9.5
JNEX-Core	0.10	23,000	1.80	1.29	1.40	0.5	5.7	18.7	13.7	11.3	8.3	6.9
Grain-oriented silicon steel	0.10	24,000	2.03	1.84	1.91	0.7	6.0	22.7	22.0	20.0	18.0	14.0
Non-oriented silicon steel	0.35	18,000	1.96	1.45	1.56	0.7	14.4	62.0	50.2	38.0	33.0	—
Amorphous	0.025	300,000	1.50	—	—	0.1	1.5	5.5	8.1	4.0	3.6	3.3

* W10/50 is the core loss at 50 Hz, 1 T (=10kG) when the magnetic flux sine wave is excited
 * Bs is the magnetic flux density at 800A/m.

Uses for Super Core™

Super Core™ Applications



JNEX-Core

Reduced noise and low core loss for high-frequency magnetic components

JNHF-Core

Further core loss reduction in high frequency ranges beyond 5 kHz



High-frequency transformer

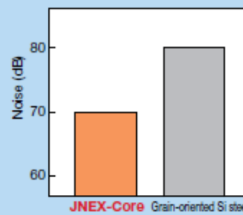
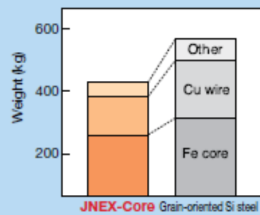
Transformers

The low core loss characteristics at high-frequency of Super Core™ allow it to be effectively used for a wide range of transformers, driven from several hundred Hz to several tens of kHz.

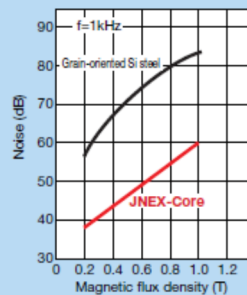
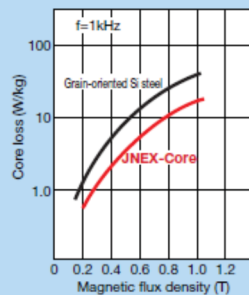
Super Core™ allow the transformer to generate less heat, and provide higher design induction than conventional silicon steel sheets, enabling transformer size to be reduced. This then reduces the quantities of other required transformer materials, such as the copper wire, leading to overall cost reductions.

By taking full advantage of the low magnetostriction characteristics of JNEX-Core, it is also possible to reduce transformer noise dramatically.

● Examples of noise and size reduction for high-frequency transformers (for fixed core loss)



● High-frequency transformer noise and core loss comparison



Motors & Generators

Because of its superior low core loss characteristics, Super Core™ has many advantages in high-speed motors and power generator applications -- stator, rotor, and yoke -- and contributes greatly to efficiency.

It is also effective in reducing noise that is caused in part by magnetostriction.

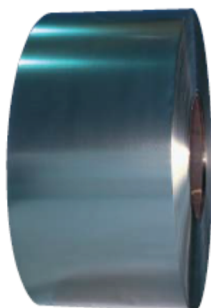
Super Core™ has attracted the attention for its use in electric and hybrid car motors, power generators, as well as the motors for OA devices.

Other applications

Applications are diverse, including magnetic shields, which take advantage of the excellent permeability into high-frequency ranges, magnetic yokes used at high-frequencies, heating equipment inductors, and CT(Current Transformer). Other applications include inductors and filters that reduce high-frequency noise.

PRODUCTS

■ Base Coil



*The base coil is made on a continuous production line with a siliconizing process.

■ Slit Coil



*The base coil goes through a slitter line, slits are cut and the coil is hooped.

*After a paper sleeve is put around its inner circumference, the slit coil is wound with rust-preventing paper used for packaging. It is then placed on skids for shipment.

Product Dimensions and Specifications

Product name	Thickness (mm)	Code number	Core loss (W/kg)	Dimensions (mm)	Space factor (%)	Density (g/cm ³)
JNEX-Core	0.10	10JNEX900	W10/400 9.0 or less	Sheet width 20~600	90 or more	7.49
JNHF-Core	0.10	10JNHF600	W0.5/20k 6.0 or less	Core outer diameter Max 900	90 or more	7.53
	0.20	20JNHF1300	W0.5/20k 13.0 or less	Core inner diameter Std. 508	92 or more	7.57

* W10/50 indicates the core loss at 50 Hz, 1 T (=10kG) when the magnetic flux sine wave is excited. Similarly, W10/400 indicates for 400 Hz, 1 T (=10kG), and W0.5/20k indicates the core loss for 20 kHz, 0.05 T (=500G).

Insulating Coating

A mixture of organic and inorganic type of coating is available.

Substances of Environmental Concern Data

● Analytical method

In JFE's Electrical Steel Sheet products, substances of environmental concern listed below are not detected in the results of analyses conducted by following methods.

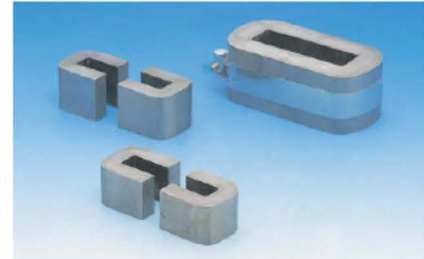
Substance	Preparation	Analytical method	Minimum limit of determination
Hg	Wet digestion	Atomic absorption spectrometric method after reduction-generation as Mercury gas	1ppm
Cd	Wet digestion (dissolved completely)	Atomic absorption spectrometric method	10ppm
Pb	Wet digestion (dissolved completely)	Atomic absorption spectrometric method	10ppm
Cr ⁶⁺	Extraction in boiling water	Diphenylcarbazide spectrophotometric method	0.01µg/cm ²

Note: 1. Insulation coating contains Cr³⁺. Please pay attention when heating in the oxidizing atmosphere or using in the high temperature conditions.
2. Chemical substances such as PBB and PBDE are neither intentionally added nor used in our production processes.

Processed Goods

● Wound Cores (C-core and Toroidal core)

- ▶ After the steel coil is formed and annealed, it is soaked in varnish and fixed.
- ▶ The sheet thickness is 0.05 mm or 0.1 mm.
- ▶ Please contact us regarding the available size.



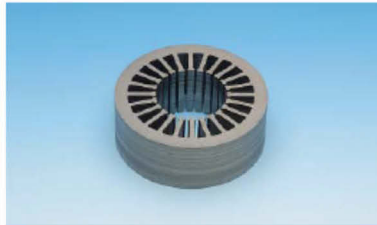
● Laminated Cores

- ▶ A core produced with a stamping-lamination process to take full advantage of the features of non-oriented Super Core™.
- ▶ Unlike products using conventional 3% Si electrical steel sheets, these can be used up to high-frequency ranges.
- ▶ Please contact us regarding the available size.



■ Block Core

- Block cores are small and medium sized cores for reactors and transformers. They are highly effective for reducing costs when mass-producing such equipment.
- The standard lamination fixing method is adhesive fixation.



■ Adhesive-Laminated Core for Motors

- A core that has been adhesive-laminated and solidified
- Provide significant reduction in high-frequency core loss due to high-speed rotation

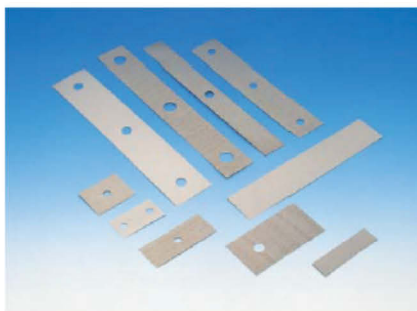


■ Block Core with Rounded Corners

- A laminated core made in virtually the same shape as a cut core, so that it is possible to use the same washers and clamp bands

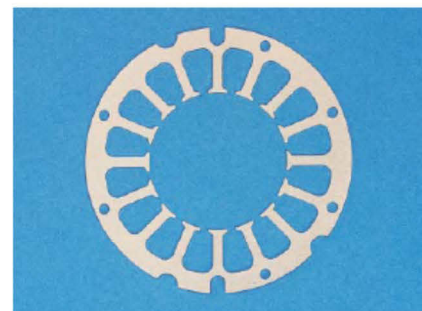
● Stacked Cores

- ▶ These cores are used mainly with medium- and large-sized transformers and reactors. The user stacks the strips and affixes them using bolts.
- ▶ The possible range of production varies somewhat depending on the processing maker, so check before proceeding.
- ▶ Please contact us regarding the available size.



● Cores for Motors and Power Generators

- ▶ Motors and power generators using Super Core™, the best non-oriented magnetic steel sheets available, demonstrate superior performance.
- ▶ The core manufacture is determined separately in consultation with each customer according to their design plans.



■ For inquiries or orders, contact the office listed below or your nearest JFE Steel Corporation office.

2-2-3 Uchisaiwaicho, Chiyoda-ku, Tokyo 100-0011 (Hibiya Kokusai Bldg)
 Electrical Steel Section TEL +81-3-3597-4099 FAX +81-3-3597-4779
 URL : <http://www.jfe-steel.co.jp/en/supercore>

Appendix C

1. Basic sizing matlab code

```
>> % Khurram shahzad, MS Thesis
>> % Oct 2016
% Program: pm1basic
% Program performs basic sizing and parameter calculations
% for generators.
%%%%%%%%%%%%%%%%%%%%%%%%%%%%%%%%%%%%%%%%%%%%%%%%%%%%%%%%%%%%%%%%%%%%%%%%
%%%%%%%%%%%%%%%%%%%%%%%%%%%%%%%%%%%%%%%%%%%%%%%%%%%%%%%%%%%%%%%%%%%%%%%%
% Definition of variables
% Name Variable
% General variables
% Pwr Required power
% rpm Speed (RPM)
% psi Power factor angle
% f Electrical frequency (Hz)
% omega Electrical frequency (rad/sec)
% vtip Tip speed (m/s)
% LovD L/D ratio
% stress Gap shear stress (psi)
% Rotor variables
% R Rotor radius (m)
% D Rotor diameter (m)
% Lst Rotor stack length (m)
% p Number of pole pairs
% Bg Expected air gap flux density (T)
% Stator variables
% Kz Surface current density (A/m)
% Jz Current density (A/m2)
% hs Slot height (m)
%%%%%%%%%%%%%%%%%%%%%%%%%%%%%%%%%%%%%%%%%%%%%%%%%%%%%%%%%%%%%%%%%%%%%%%%
%%%%%%%%%%%%%%%%%%%%%%%%%%%%%%%%%%%%%%%%%%%%%%%%%%%%%%%%%%%%%%%%%%%%%%%%
```

```

clear;
% Constants & conversion factors

hs = .015; % Assume slot depth of 15 mm
lams = 0.5; % Assume slot fill fraction
conv1 = 9.81; % 9.81 W per Nm/s
conv2 = 703.0696; % 703.0696 N/m2 per psi
%%%%%%%%%%%%%%%%%%%%%%%%%%%%%%%%%%%%%%%%%%%%%%%%%%%%%%%%%%%%%%%%%%%%%%%%
%%%%%%%%%%%%%%%%%%%%%%%%%%%%%%%%%%%%%%%%%%%%%%%%%%%%%%%%%%%%%%%%%%%%%%%%
% INPUTS
%%%%%%%%%%%%%%%%%%%%%%%%%%%%%%%%%%%%%%%%%%%%%%%%%%%%%%%%%%%%%%%%%%%%%%%%
%%%%%%%%%%%%%%%%%%%%%%%%%%%%%%%%%%%%%%%%%%%%%%%%%%%%%%%%%%%%%%%%%%%%%%%%
Pwr = 660000; % Required power
vtip = 200; % Max tip speed (m/s)
LovD = 2.51; % Wound rotor usually 0.5-1.0, PM 1.0-3.0
% Shear stress usually 1-10 psi small machines, 10-20 large liquid
% liquid cooled machines
stress = 15;
p = 2; % Pole pairs
Bg = 0.8; % Tesla
%%%%%%%%%%%%%%%%%%%%%%%%%%%%%%%%%%%%%%%%%%%%%%%%%%%%%%%%%%%%%%%%%%%%%%%%
%%%%%%%%%%%%%%%%%%%%%%%%%%%%%%%%%%%%%%%%%%%%%%%%%%%%%%%%%%%%%%%%%%%%%%%%
% Calculations
% Size
% Initially use  $Pwr = 2 * \pi * R * Lst * stress * vtip$ 
%  $Lst = 2 * LovD * R$ 
hscm = hs * 100;
R = sqrt(Pwr / (2 * pi * (LovD * 2) * vtip * stress * conv1 * conv2));
D = 2 * R;
Lst = LovD * D;
% Speed

```

```

omega = (p*vtip)/R;
f = omega/(2*pi);
rpm = (60*f)/p;
% Current densities
Kz = (stress*conv2)/(Bg*100);
Ja = 10*Kz/(hscm*lams);

% Output
fprintf('Basic Machine Design\n');
fprintf('Input Parameters:\n');
fprintf('Power = %10.1f kW Shear Stress = %10.1f psi\n',Pwr/1e3,stress);
fprintf('L/D Ratio = %10.2f Tip Speed = %10.1f m/s\n',LovD,vtip);
fprintf('Pole Pairs = %10.1f Air Gap Bg = %10.1f T\n',p,Bg);
fprintf('Output:\n');
fprintf('Rotor Radius = %10.3f m Stack Length = %10.3f m\n',R,Lst);
fprintf('Speed = %10.0f RPM Frequency = %10.1f Hz\n',rpm,f);
fprintf('Ja = %10.2f A/cm2\n',Ja)

```

2. Detailed sizing matlab code

```
>> % Khurram shahzad, MS Thesis
% Oct 2016
% Program: pmlinput
% Program used as input file for pmlcalc
% All necessary input parameters entered here.
clear;
%%%%%%%%%%%%%%%%%%%%%%%%%%%%%%%%%%%%%%%%%%%%%%%%%%%%%%%%%%%%%%%%%%%%%%%%
%%%%%%%%%%%%%%%%%%%%%%%%%%%%%%%%%%%%%%%%%%%%%%%%%%%%%%%%%%%%%%%%%%%%%%%%
% Definition & Entry of variables
% General variables
Pwr = 660000; % Required power (W)
rpm = 60000; % Speed (RPM)
psi = 0; % Power factor angle
% Rotor variables
R = 0.032; % Rotor radius (m)
hm = 0.025; % Magnet thickness (m)
Lst = 0.160; % Rotor stack length (m)
p = 2; % Number of pole pairs
Br = 1.2; % Magnet remnant flux density (T)
thm = 50; % Magnet physical angle (deg)
thsk = 10; % Magnet skew angle (actual deg)
% Stator variables
q = 3; % Number of phases
Ns = 24; % Number of slots
Nsp = 1; % Number of slots short pitched
g = .004; % Air gap (m)
```

```

tfrac = 0.5; % Peripheral tooth fraction
hs = .025; % Slot depth (m)
hd = .0005; % Slot depression depth (m)
wd = 1e-6; % Slot depression width (m)
syrat = 0.7; % Stator back iron ratio (yoke thick/rotor radius)
Nc = 1; % Turns per coil
lams = 0.5; % Slot fill fraction
sigst = 6.0e+7; % Stator winding conductivity
% Densities
rhos = 7700; % Steel density (kg/m3)
rhom = 7400; % Magnet density (kg/m3)
rhoc = 8900; % Conductor density (kg/m3)
% Khurram Shahzad
% Oct 2016
% Program: pm1calc
% MUST RUN pm1input PRIOR TO RUNNING pm1calc
%%%%%%%%%%%%%%%%%%%%%%%%%%%%%%%%%%%%%%%%%%%%%%%%%%%%%%%%%%%%%%%%%%%%%%%%
%%%%%%%%%%%%%%%%%%%%%%%%%%%%%%%%%%%%%%%%%%%%%%%%%%%%%%%%%%%%%%%%%%%%%%%%
% Definition of variables
% Name Variable
% General variables
% Pwr Required power (W)
% rpm Speed (RPM)
% psi Power factor angle
% f Electrical frequency (Hz)
% omega Electrical frequency (rad/sec)
% vtip Tip speed (m/s)
% lambda Flux linkage

```

```

% Ea RMS Internal voltage (V)
% Rotor variables
% R Rotor radius (m)
% hm Magnet thickness (m)
% Lst Rotor stack length (m)
% p Number of pole pairs
% Br Magnet remnant flux density (T)
% thm Magnet physical angle (deg)
% thsk Magnet skew angle (actual deg)
% Stator variables
% q Number of phases
% m Slots per pole per phase
% Ns Number of slots
% Nsp Number of slots short pitched
% g Air gap (m)
% ge Effective air gap (m)
% tfrac Peripheral tooth fraction
% hs Slot depth (m)
% hd Slot depression depth (m)
% wd Slot depression width (m)
% syrat Stator back iron ratio (yoke thick/rotor radius)
% Nc Turns per coil
% lams Slot fill fraction
% sigst Stator conductivity
% Kc Carter coefficient
% Loss Models
% P0 Base power for core losses
% F0 Base frequency for core loss
% B0 Base flux density
% epsb Flux density exponent
% epsf Frequency exponent
% rhos Steel density

```


% rhom Magnet density

% rhoc Conductor density

%%
%%

% Constants to be used

mu0 = 4*pi*1e-7; % Free space permeability

tol = 1e-2; % Tolerance factor

cpair = 1005.7; % Specific heat capacity of air (J/kg*C)

rhoair = 1.205 ; % Density of air at 20 C (kg/m3)

nuair = 1.5e-5; % Kinematic viscosity of air at 20 C (m2/s)

P0 = 36.79; % Base Power Losss, W/lb

F0 = 1000; % Base freuency, 60 Hz

B0 = 1.0; % Base flux density, 1.0 T

epsb = 2.12;

epsf = 1.68;

% Generate geometry of machine

% Number of slots/pole/phase

m = Ns/(2*p*q);

% Number of armature turns (each slot has 2 half coils)

Na = 2*p*m*Nc;

% Tooth width

wt = 2*pi*(R+g+hm+hd)*tfrac/Ns;

% Slot top width (at air gap)

wst = 2*pi*(R+g+hm+hd)*(1-tfrac)/Ns;

% Slot bottom width

wsb = wst*(R+g+hd+hs)/(R+g+hm+hd);

% Stator core back iron depth (as p increases, dc decreases)

dc = syrat*R/p;

% Full-pitch coil throw

Nsfp = floor(Ns/(2*p));

% Actual coil throw

Nsct = Nsfp - Nsp;

```

% Estimate end turn length
% End turn travel (one end)
laz = pi*(R+g+hm+hd+0.5*hs)*Nsct/Ns;
% End length (half coil)
le2 = pi*laz;
% End length (axial direction)
le1 = 2*le2/(2*pi);
% Calculate electrical frequency & surface speed
f = p*rpm/60;
omega = 2*pi*f;
vtip = R*omega/p;
% Winding & skew factors
gama = 2*pi*p/Ns;
alfa = pi*Nsct/Nsfp;
kp = sin(pi/2)*sin(alfa/2);
kb = sin(m*gama/2)/(m*sin(gama/2));
kw = kp*kb;
ths = ((p*thsk)+1e-6)*(pi/180); % skew angle (elec rad)
ks = sin(ths/2)/(ths/2);
% Calculate magnetic gap factor
Rs = R+hm+g;
Ri = R;
R1 = R;
R2 = R+hm;
kg = ((Ri^(p-1))/(Rs^(2*p)-Ri^(2*p)))*((p/(p+1))*(R2^(p+1)-R1^(p+1))...
+(p*Rs^(2*p)/(p-1))*(R1^(1-p)-R2^(1-p)));
% Calculate air gap magnetic flux density
% Account for slots, reluctance, and leakage
ws = (wst+wsb)/2; % Average slot width
taus = ws + wt; % Width of slot and tooth
Kc = 1/(1-(1/((taus/ws)*((5*g/ws)+1))));
ge = Kc*g;

```



```

Cphi = (p*thm)/180; % Flux concentration factor
Kl = 0.95; % Leakage factor
Kr = 1.05; % Reluctance factor
murec = 1.05; % Recoil permeability
PC = hm/(ge*Cphi); % Permeance coefficient
Bg = ((Kl*Cphi)/(1+(Kr*murec/PC)))*Br;

% Calculate magnetic flux and internal voltage
thmrad = thm*(pi/180);
B1 = (4/pi)*Bg*kg*sin(p*thmrad/2);
lambda = 2*Rs*Lst*Na*kw*ks*B1/p;
Ea = omega*lambda/sqrt(2); % RMS back voltage

% Calculation of inductances/reactances

% Air-gap inductance
Lag = (q/2)*(4/pi)*(mu0*Na^2*kw^2*Lst*Rs)/(p^2*(g+hm));

% Slot leakage inductance
perm = mu0*((1/3)*(hs/wst) + hd/wst);
Las = 2*p*Lst*perm*(4*Nc^2*(m-Nsp)+2*Nsp*Nc^2);
Lam = 2*p*Lst*Nsp*Nc^2*perm;
if q == 3
Lslot = Las + 2*Lam*cos(2*pi/q); % 3 phase equation
else
Lslot = Las - 2*Lam*cos(2*pi/q); % multiple phases
end

% End-turn inductance (Hanselman)
As = ws*hs; % Slot area
Le = ((Nc*mu0*(taus)*Na^2)/2)*log(wt*sqrt(pi)/sqrt(2*As));

% Total inductance and reactance
Ls = Lag+Lslot+Le;
Xs = omega*Ls;

% Lengths, Volumes, and Weights

% Armature conductor length
Lac = 2*Na*(Lst+2*le2);

```

```

% Armature conductor area (assumes form wound)
Aac = As*lam/(2*Nc);
% Mass of armature conductor
Mac = q*Lac*Aac*rhoc;
% Overall machine length
Lmach = Lst+2*le1;
% Core inside radius
Rci = R+hm+g+hd+hs;

% Core outside radius
Rco = Rci+dc;
% Overall diameter
Dmach = 2*Rco;
% Core mass
Mcb = rhos*pi*(Rco^2-Rci^2)*Lst; % Back iron
Mct = rhos*Lst*(Ns*wt*hs+2*pi*R*hd-Ns*hd*wd); % Teeth
Mc = Mcb + Mct;
% Magnet mass
Mm = 0.5*(p*thmrad)*((R+hm)^2-R^2)*Lst*rhom;
% Shaft mass
Ms = pi*R^2*Lst*rhos;
% 15% service fraction
Mser = 0.15*(Mc+Ms+Mm+Mac);
% Total mass
Mtot = Mser+Mc+Ms+Mm+Mac;
% Stator resistance
Ra = Lac/(sigst*Aac);
% Core Loss Calculations
% Tooth Flux Density
Bt = Bg/tfrac;
% Back iron flux density (Hanselman)
Bb = Bg*R/(p*dc);
% Core back iron loss

```

```

Pcb = Mcb*P0*abs(Bb/B0)^epsb*abs(f/F0)^epsf;
% Teeth Loss
Pct = Mct*P0*abs(Bt/B0)^epsb*abs(f/F0)^epsf;
% Total core loss
Pc = Pcb + Pct;
% Start loop to determine terminal voltage and current
notdone = 1;
i = 0;
Ia = Pwr/(q*Ea);
while notdone ==1
i = i + 1;
xa = Xs*Ia/Ea;
% Conductor losses
Pa = q*Ia^2*Ra;
% Gap friction losses
% Reynold's number in air gap
omegam = omega/p;
Rey = omegam*R*g/nuair;
% Friction coefficient
Cf = .0725/Rey^.2;
% Windage losses
Pwind = Cf*pi*rhoair*omegam^3*R^4*Lst;
% Get terminal voltage
Va = sqrt(Ea^2-((Xs+Ra)*Ia*cos(psi))^2)-(Xs+Ra)*Ia*sin(psi);
Ptemp = q*Va*Ia*cos(psi)-Pwind;
error = Pwr/Ptemp;
err(i) = error;
if abs(error-1) < tol
notdone = 0;
else
Ia = Ia*error;
end

```

```

end
% Remaining performance parameters
% Current density
Ja = Ia/Aac;
% Power and efficiency
Pin = Pwr+Pc+Pa+Pwind;
eff = Pwr/Pin;
pf = cos(psi);
fprintf('pmlcalc complete: Ready.\n');
% Khurram Shahzad, MS Thesis
% Oct 2016
% MUST RUN pmlinput and pmlcalc PRIOR TO RUNNING pml output

% Variables for output display
Pout = Pwr/1e3;
Jao = Ja/1e4;
Pco = Pc/1e3;
Pwindo = Pwind/1e3;
Pao = Pa/1e3;
wso = ws*1000;
hso = hs*1000;
wto = wt*1000;
dco = dc*1000;
Lso = Ls*1000;
hmo = hm*1000;
go = g*1000;

```

```

% Output Section:
fprintf('\nPM Machine Design, Version 1: Surface Magnet, Slotted Stator\n');
fprintf('Machine Size:\n');
fprintf('Machine Diameter = %8.3f m Machine Length = %8.3f m\n',Dmach,Lmach);
fprintf('Rotor radius = %8.3f m Active length = %8.3f m\n',R,Lst);
fprintf('Slot Avg Width = %8.3f mm Slot Height = %8.3f mm\n',wso,hso);
fprintf('Back Iron Thick = %8.3f mm Tooth Width = %8.3f mm\n',dco,wto);
fprintf('Machine Ratings:\n');
fprintf('Power Rating = %8.1f kW Speed = %8.0f RPM\n', Pout,rpm);
fprintf('Va (RMS) = %8.0f V Current = %8.1f A\n', Va,Ia);
fprintf('Ea (RMS) = %8.0f V Arm Resistance = %8.5f ohm\n',Ea,Ra);
fprintf('Synch Reactance = %8.3f ohm Synch Induct = %8.3f mH\n',Xs,Lso);
fprintf('Stator Cur Den = %8.1f A/cm2 Tip Speed = %8.0f m/s\n', Jao,vtip);
fprintf('Efficiency = %8.3f Power Factor = %8.3f\n', eff,pf);
fprintf('Phases = %8.0f Frequency = %8.1f Hz\n',q,f);
fprintf('Stator Parameters:\n');
fprintf('Number of Slots = %8.0f Num Arm Turns = %8.0f\n',Ns,Na);
fprintf('Breadth Factor = %8.3f Pitch Factor = %8.3f\n', kb,kp);
fprintf('Tooth Flux Den = %8.2f T Back Iron = %8.2f T\n', Bt,Bb);
fprintf('Slots/pole/phase = %8.2f\n',m);
fprintf('Rotor Parameters:\n');
fprintf('Magnet Height = %8.2f mm Magnet Angle = %8.1f degm\n',hmo,thm);
fprintf('Air gap = %8.2f mm Pole Pairs = %8.0f\n',go,p);
fprintf('Magnet Remanence = %8.2f T Aig Gap Bg = %8.2f T\n',Br,Bg);
fprintf('Magnet Factor = %8.3f Skew Factor = %8.3f\n',kg,ks);
fprintf('Machine Losses:\n');
fprintf('Core Loss = %8.1f kW Armature Loss = %8.1f kW\n', Pco,Pao);
fprintf('Windage Loss = %8.1f kW Rotor Loss = TBD kW\n', Pwindo);

```

```
fprintf('Machine Weights:\n');  
fprintf('Core = %8.2f kg Shaft = %8.2f kg\n',Mc,Ms);  
fprintf('Magnet = %8.2f kg Armature = %8.2f kg\n',Mm,Mac);  
fprintf('Services = %8.2f kg Total = %8.2f kg\n',Mser,Mtot);  
pm1calc complete: Ready.
```


7 Bibliography

- Ahmad, R.A., Pan, Z. & Saban, D. 2007, 'On-Board Electrical Network Topology Using High Speed Permanent Magnet Generators', *2007 IEEE Electric Ship Technologies Symposium*.
- Arkkio, A., Jokinen, T. & Lantto, E. 2005, 'Induction and permanent-magnet synchronous machines for high-speed applications', *2005 International Conference on Electrical Machines and Systems*, vol. 2, IEEE, pp. 871-6.
- Arnold, D.P., Das, S., Park, J.-W., Zana, I., Lang, J.H. & Allen, M.G. 2006, 'Microfabricated high-speed axial-flux multiwatt permanent-magnet generators&# 8212; part II: Design, fabrication, and testing', *Journal of microelectromechanical systems*, vol. 15, no. 5, pp. 1351-63.
- Bianchi, N. & Lorenzoni, A. 1996, 'Permanent magnet generators for wind power industry: an overall comparison with traditional generators', *Opportunities and Advances in International Electric Power Generation, International Conference on (Conf. Publ. No. 419)*, IET, pp. 49-54.
- Binder, A. & Schneider, T. 2007, 'High-speed inverter-fed AC drives', *Electrical Machines and Power Electronics, 2007. ACEMP'07. International Aegean Conference on*, IEEE, pp. 9-16.
- Binder, A., Schneider, T. & Klohr, M. 2006, 'Fixation of buried and surface-mounted magnets in high-speed permanent-magnet synchronous machines', *IEEE Transactions on Industry Applications*, vol. 42, no. 4, pp. 1031-7.
- Binns, K. & Shimmin, D. 1995, 'The relationship between performance characteristics and size of permanent magnet motors', *Electrical Machines and Drives, 1995. Seventh International Conference on (Conf. Publ. No. 412)*, IET, pp. 423-7.
- Binns, K. & Shimmin, D. 1996, 'Relationship between rated torque and size of permanent magnet machines', *IEE Proceedings-Electric Power Applications*, vol. 143, no. 6, pp. 417-22.
- Caricchi, F., Crescimbeni, F., Mezzetti, F. & Santini, E. 1996, 'Multistage axial-flux PM machine for wheel direct drive', *IEEE Transactions on Industry Applications*, vol. 32, no. 4, pp. 882-8.
- Celera Motion, m.t. 2016, *comparison of slotted and slotless stators*, viewed 01/09 2016, <http://www.celeramotion.com/sites/default/files/TN-2001_Comparison_of_Slotless_and_Slotted_Motors.pdf>.
- concentrated winding*, <<http://www.electrical4u.com/winding-factor-pitch-factor-distribution-factor/>>.
- Corporation, J.S., *Electrical steel sheets for high-frequency*, <http://www.jfe-steel.co.jp/en/products/electrical/catalog/fl_e-002.pdf>.
- Curiac, P., Jeong, Y.H. & Jung, S.J. 2003, 'Prospects for magnetization of large PM rotors: conclusions from a development case study', *IEEE Transactions on Energy Conversion*, vol. 18, no. 3, pp. 409-16.

- Dorrell, D., Staton, D., Kahout, J., Hawkins, D. & McGilp, M. 2006, 'Linked electromagnetic and thermal modelling of a permanent magnet motor', *Power Electronics, Machines and Drives, 2006. The 3rd IET International Conference on*, IET, pp. 536-40.
- Dorrell, D.G. 2007, 'Design requirements for brushless permanent magnet generators for use in small renewable energy systems', *Industrial Electronics Society, 2007. IECON 2007. 33rd Annual Conference of the IEEE*, IEEE, pp. 216-21.
- Dorrell, D.G., Hsieh, M.-F., Popescu, M., Evans, L., Staton, D.A. & Grout, V. 2011, 'A review of the design issues and techniques for radial-flux brushless surface and internal rare-earth permanent-magnet motors', *IEEE Transactions on Industrial Electronics*, vol. 58, no. 9, pp. 3741-57.
- El-Hasan, T.S., Luk, P.C., Bhinder, F. & Ebaid, M. 2000, 'Modular design of high-speed permanent-magnet axial-flux generators', *IEEE Transactions on magnetics*, vol. 36, no. 5, pp. 3558-61.
- El Shahat, A. & El Shewy, H., 'High speed pm synchronous motor basic sizing neural regression function for renewable energy applications', *Paper ID X*, vol. 304, pp. 28-30.
- El Shahat, A. & El Shewy, H. 2009a, 'Generating basic sizing design regression neural function for hspmsm in aircraft', *EP-127, 13th International Conference on Aerospace Science & Aviation Technology*.
- El Shahat, A. & El Shewy, H. 2009b, 'High Speed Synchronous Motor Basic Sizing Neural Function for Renewable Energy Applications', *MDGEN05, The International Conference on Millennium Development Goals (MDG): Role of ICT and other technologies December*, pp. 27-9.
- El Shahat, A. & El Shewy, H. 2010, 'High fundamental frequency PM synchronous motor design neural regression function', *Journal of Electrical Engineering*, vol. 10.
- El Shahat, A., Keyhani, A. & El Shewy, H. 2010a, 'Sizing a High Speed PM Generator for Green Energy Applications', *Journal of electrical systems*, vol. 6, p. 16.
- El Shahat, A., Keyhani, A. & El Shewy, H.M. 2010b, 'Optimized Sizing of High Speed PM Generator for Renewable Energy Applications', *Fourteenth International Middle East Power Systems Conference, MEPCON*, pp. 19-21.
- Fengxiang, W., Wenpeng, Z., Ming, Z. & Baoguo, W. 2002, 'Design considerations of high-speed PM generators for micro turbines', *Power System Technology, 2002. Proceedings. PowerCon 2002. International Conference on*, vol. 1, IEEE, pp. 158-62.
- GAŠPARIN, L. & FIŠER, R. 2013, 'Sensitivity of cogging torque to permanent magnet imperfections in mass-produced PM synchronous motors'.
- George P. Gogue & Joseph J. Stupak, J., *Theory & Practice of Electromagnetic Design of DC Motors & Actuators*, <<http://www.consult-g2.com/course/chapter7/chapter.html>>.
- Gieras, J.F. 2002, *Permanent magnet motor technology: design and applications*, CRC press.

- Gieras, J.F. 2008, *Advancements in electric machines*, Springer Science & Business Media.
- Goss, J., Mellor, P., Wrobel, R., Staton, D. & Popescu, M. 2012, 'The design of AC permanent magnet motors for electric vehicles: A computationally efficient model of the operational envelope'.
- Guda, S.R., Wang, C. & Nehrir, M. 2005, 'A simulink-based microturbine model for distributed generation studies', *Proceedings of the 37th Annual North American Power Symposium, 2005.*, IEEE, pp. 269-74.
- Hamdi, E.S. 1994, *Design of small electrical machines*, John Wiley & Sons, Inc.
- Hanselman, D.C. 2003, *Brushless permanent magnet motor design*, The Writers' Collective.
- Hendershot, J.R. & Miller, T.J.E. 1994, *Design of brushless permanent-magnet motors*, Magna Physics Pub.
- Hendershot, J.R. & Miller, T.J.E. 2010, *Design of brushless permanent-magnet machines*, Motor Design Books.
- Hosseini, S.M., Agha-Mirsalim, M. & Mirzaei, M. 2008, 'Design, prototyping, and analysis of a low cost axial-flux coreless permanent-magnet generator', *IEEE transactions on magnetics*, vol. 44, no. 1, pp. 75-80.
- Huang, S., Luo, J., Leonardi, F. & Lipo, T.A. 1998, 'A general approach to sizing and power density equations for comparison of electrical machines', *IEEE Transactions on Industry Applications*, vol. 34, no. 1, pp. 92-7.
- Huynh, C., Zheng, L. & Acharya, D. 2009, 'Losses in high speed permanent magnet machines used in microturbine applications', *Journal of Engineering for Gas Turbines and Power*, vol. 131, no. 2, p. 022301.
- Hwang, C., Chang, C., Cheng, S., Chan, C., Pan, C. & Chang, T. 2004, 'Comparison of performances between IPM and SPM motors with rotor eccentricity', *Journal of magnetism and magnetic materials*, vol. 282, pp. 360-3.
- Hwang, C., Tien, C. & Chang, H. 2007, 'Performance and applications of a small PM generator', *physica status solidi (c)*, vol. 4, no. 12, pp. 4635-8.
- Jang, S.-M., Cho, H.-W. & Jeong, Y.-H. 2006, 'Influence on the rectifiers of rotor losses in high-speed permanent magnet synchronous alternator', *Journal of applied physics*, vol. 99, no. 8, p. 08R315.
- Jensen, C.C., Profumo, F. & Lipo, T.A. 1992, 'A low-loss permanent-magnet brushless DC motor utilizing tape wound amorphous iron', *IEEE transactions on industry applications*, vol. 28, no. 3, pp. 646-51.
- Keyhani, A., Marwali, M.N. & Dai, M. 2009, *Integration of green and renewable energy in electric power systems*, John Wiley & Sons.

- Kolehmainen, J. & Ikaheimo, J. 2008, 'Motors with buried magnets for medium-speed applications', *IEEE Transactions on Energy Conversion*, vol. 23, no. 1, pp. 86-91.
- Kolondzovski, Z., Arkkio, A., Larjola, J. & Sallinen, P. 2011, 'Power limits of high-speed permanent-magnet electrical machines for compressor applications', *IEEE transactions on Energy Conversion*, vol. 26, no. 1, pp. 73-82.
- Leicht, J., Castro, N., Silva, E., Landgraf, F., Moses, A. & Yonamine, T. 2008, 'Magnetic properties of 6.5% silicon content non-oriented electrical steel under sine and PWM excitation', *Journal of Magnetism and Magnetic Materials*, vol. 320, no. 14, pp. e385-e8.
- Lesani, H., Monsef, H. & Darabi, A. 2007, 'Design considerations of high speed axial flux permanent magnet generator with coreless stator', *2007 International Power Engineering Conference (IPEC 2007)*, IEEE, pp. 1097-102.
- Li, J., Choi, D.-W., Son, D.-H. & Cho, Y.-H. 2012, 'Effects of MMF harmonics on rotor eddy-current losses for inner-rotor fractional slot axial flux permanent magnet synchronous machines', *IEEE Transactions on Magnetics*, vol. 48, no. 2, pp. 839-42.
- Marques, B.R.d.F., *Virtual Prototyping of a Brushless Permanent Magnet AC Motor - Electromagnetic and Thermal Design using CAD Software*, <<https://fenix.tecnico.ulisboa.pt/downloadFile/395145026134/dissertacao.pdf>>.
- Mellor, P., Wrobel, R. & Holliday, D. 2009, 'A computationally efficient iron loss model for brushless AC machines that caters for rated flux and field weakened operation', *Electric Machines and Drives Conference, 2009. IEMDC'09. IEEE International*, IEEE, pp. 490-4.
- Mellor, P.H., Burrow, S.G., Sawata, T. & Holme, M. 2005, 'A wide-speed-range hybrid variable-reluctance/permanent-magnet generator for future embedded aircraft generation systems', *IEEE transactions on industry applications*, vol. 41, no. 2, pp. 551-6.
- Miller, T. 2002, 'SPEED's Electric Machines', *University of Glasgow, Department of Electronics and Electrical Engineering*, vol. 2011.
- Mlot, A., Lukaszyn, M. & Korkosz, M. 2015, 'Magnet eddy-current loss reduction in a high-speed permanent magnet machine with concentrated windings'.
- Moros, O. & Gerling, D. 2015, 'New flexible harmonic cost effective concentrated winding topology', *Industrial Electronics Society, IECON 2015-41st Annual Conference of the IEEE*, IEEE, pp. 000427-32.
- Nagorny, A.S., Dravid, N.V., Jansen, R.H. & Kenny, B.H. 2005, 'Design aspects of a high speed permanent magnet synchronous motor/generator for flywheel applications', *IEEE International Conference on Electric Machines and Drives, 2005.*, IEEE, pp. 635-41.
- Paulides, J.J., Jewell, G.W. & Howe, D. 2004, 'An evaluation of alternative stator lamination materials for a high-speed, 1.5 MW, permanent magnet generator', *IEEE transactions on magnetics*, vol. 40, no. 4, pp. 2041-3.

- Pavlik, D., Garg, V., Repp, J. & Weiss, J. 1988, 'A finite element technique for calculating the magnet sizes and inductances of permanent magnet machines', *IEEE transactions on energy conversion*, vol. 3, no. 1, pp. 116-22.
- Pillay, P. & Freere, P. 1989, 'Literature survey of permanent magnet AC motors and drives', *Industry Applications Society Annual Meeting, 1989., Conference Record of the 1989 IEEE*, IEEE, pp. 74-84.
- Polikarpova, M., Ponomarev, P., Lindh, P., Petrov, I., Jara, W., Naumanen, V., Tapia, J. & Pyrhönen, J. 2015, 'Hybrid Cooling Method of Axial-Flux Permanent-Magnet Machines for Vehicle Applications', *IEEE Transactions on Industrial Electronics*, vol. 62, no. 12, pp. 7382-90.
- Rahman, M. & Slemon, G. 1985, 'Promising applications of neodymium boron iron magnets in electrical machines', *IEEE transactions on Magnetics*, vol. 21, no. 5, pp. 1712-6.
- Rippy, M. 2004, 'An Overview Guide for the Selection of Lamination Materials, Proto Laminations', Inc.
- Rucker, J.E., Kirtley, J. & McCoy, T.J. 2005, 'Design and analysis of a permanent magnet generator for naval applications', *IEEE Electric Ship Technologies Symposium, 2005.*, IEEE, pp. 451-8.
- Sahin, F. & Vandenput, A. 1999, 'Design considerations of the flywheel-mounted axial-flux permanent-magnet machine for a hybrid electric vehicle', *Eighth European conference on power electronics and applications. EPE*, vol. 99.
- Sahin, F. & Vandenput, A. 2003, 'Thermal modeling and testing of a high-speed axial-flux permanent-magnet machine', *COMPEL-The international journal for computation and mathematics in electrical and electronic engineering*, vol. 22, no. 4, pp. 982-97.
- Sarumol, G. & Reeba, S. 2015, 'Minimisation of losses in permanent magnet synchronous generator for high speed applications', *2015 International Conference on Control Communication & Computing India (ICCC)*, IEEE, pp. 200-5.
- Scridon, S., Boldea, I., Tutelea, L., Blaabjerg, F. & Ritchie, A.E. 2005, 'BEGA-A biaxial excitation generator for automobiles: Comprehensive characterization and test results', *IEEE transactions on industry applications*, vol. 41, no. 4, pp. 935-44.
- Sitapati, K. & Krishnan, R. 2001, 'Performance comparisons of radial and axial field, permanent-magnet, brushless machines', *IEEE Transactions on Industry Applications*, vol. 37, no. 5, pp. 1219-26.
- Slemon, G.R. 1994, 'On the design of high-performance surface-mounted PM motors', *IEEE Transactions on Industry Applications*, vol. 30, no. 1, pp. 134-40.
- Staunton, R., Nelson, S., Otaduy, P., McKeever, J., Bailey, J., Das, S. & Smith, R. 2004, *PM motor parametric design analyses for a hybrid electric vehicle traction drive application*, United States. Department of Energy.

- Tassi, A., Zanolchi, G. & Staton, D. 2006, 'Fem and lumped circuit thermal analysis of external rotor motor', *IECON 2006-32nd Annual Conference on IEEE Industrial Electronics*, IEEE, pp. 4825-8.
- Van der Veen, J., Offringa, L. & Vandenput, A. 1997, 'Minimising rotor losses in high-speed high-power permanent magnet synchronous generators with rectifier load', *IEE Proceedings-Electric Power Applications*, vol. 144, no. 5, pp. 331-7.
- Wiak, S., Krawczyk, A., Dolezel, I. & Kolondzovski, Z. 2008, 'Determination of critical thermal operations for high-speed permanent magnet electrical machines', *COMPEL-The international journal for computation and mathematics in electrical and electronic engineering*, vol. 27, no. 4, pp. 720-7.
- Winding Factor | Pitch Factor | Distribution Factor*, <<https://www.electrical4u.com/winding-factor-pitch-factor-distribution-factor/>>.
- Xing, J.Q., Chen, L., Zhang, Q. & Ma, Y.F. 2012, 'Design and Analysis of Fan-Cooling for High Speed Permanent Magnet Machine Rotor', *Advanced Materials Research*, vol. 591, Trans Tech Publ, pp. 3-6.
- Zarei, A.H., Abbaszadeh, K. & Safari, K. 2012, 'The Analytical Analysis of the Rotor Losses in the PMSM Motors', *Proceedings of the World Congress on Engineering and Computer Science*, vol. 2.